



HAL
open science

Analysis and control of acid sites in zeolites

Ana Palčić, Valentin Valtchev

► **To cite this version:**

Ana Palčić, Valentin Valtchev. Analysis and control of acid sites in zeolites. Applied Catalysis A : General, 2020, 606, pp.117795. 10.1016/j.apcata.2020.117795 . hal-03035450

HAL Id: hal-03035450

<https://normandie-univ.hal.science/hal-03035450>

Submitted on 2 Dec 2020

HAL is a multi-disciplinary open access archive for the deposit and dissemination of scientific research documents, whether they are published or not. The documents may come from teaching and research institutions in France or abroad, or from public or private research centers.

L'archive ouverte pluridisciplinaire **HAL**, est destinée au dépôt et à la diffusion de documents scientifiques de niveau recherche, publiés ou non, émanant des établissements d'enseignement et de recherche français ou étrangers, des laboratoires publics ou privés.

Analysis and control of acid sites in zeolites

Ana Palčić^{a*}, Valentin Valtchev^{b,c*}

^aRuđer Bošković Institute, Division of Materials Chemistry, Laboratory for Synthesis of New Materials, Bijenička cesta 54, Zagreb, Croatia

^bQingdao Institute of Bioenergy and Bioprocess Technology, Chinese Academy of Sciences 189 Song Ling Rd Qingdao, Shandong 266101, P.R. China

^cNormandie Univ, ENSICAEN, UNICAEN, CNRS, Laboratoire Catalyse et Spectrochimie, 6 Boulevard Maréchal Juin, Caen, France

E-mail: ana.palcic@irb.hr; valentin.valtchev@ensicaen.fr

CONTENTS

1	Introduction	2
2	Structure - properties relationship in zeolites	3
3	Analysis of acid sites in zeolites	3
3.1	Acid sites in zeolites	3
3.2	Experimental methods for zeolites' acidity evaluation	6
3.3	Zeolites' acidity assessment by probe molecules	8
3.4	Theoretical methods for zeolites' acidity evaluation.....	13
4	In situ control of acid sites in zeolites	15
4.1	In situ controlling the Al location in the zeolite framework.....	16
4.1.1	MFI-type materials	16
4.1.2	FER-type materials	4
4.1.3	CHA	6
4.1.4	MOR	9
4.1.5	Zeolite Beta (BEA@BEB).....	11
4.1.6	Other framework type materials	13
4.2	Post-synthesis aluminium incorporation	16
4.3	Al zoning	21
4.4	Controlling the zeolite acidity by incorporating heteroatoms in the zeolite framework	22
4.4.1	Boron-containing zeolites.....	22
4.4.2	Germanium-containing zeolites.....	25
4.4.3	Tin-containing zeolites	25
5	Summary and outlook.....	31

Abstract

The exceptional catalytic performance of zeolites is due to the presence of active sites in a shape-selective environment, i.e., in micropores with molecular dimensions. The present review provides a comprehensive analysis of active sites in zeolite frameworks. It is focused on the active sites generated by the Al incorporation in the framework. The inclusion of other heteroatoms in the zeolite framework is also addressed. After the introduction of zeolite-type materials and a discussion of the structure-properties relationship in zeolites the central part of the review is devoted to i) the analytical methods and their complementarity for the evaluation of the number, strength, and position of active sites and ii) the *in situ* and post-synthesis methods of acid sites assessment and control. The data presented herein provide guidelines for making zeolite materials by design in terms of acidity.

Keywords: zeolites, acid sites, *in situ* and post-synthesis methods, aluminum location

1 Introduction

Zeolites are defined as crystalline aluminosilicate microporous materials. The designation microporous denotes material comprising pores smaller than 2 nm based on the IUPAC convention [1]. In the past decades, the term zeolite has been extended to designate materials having a more diverse chemical composition, for instance, there are (silico)aluminophosphate, germanosilicate, zincosilicate, gallosilicate, etc., zeolite-type (zeotype) materials. Presently, the key feature which is taken as an essential criterion to classify a material as “zeolitic” is its structure. A zeolite is built of tetrahedra having a central T atom (T = Si, Al, Ge, Ga, P, B, ...) and oxygen at the vertices [2]. The tetrahedra connected by sharing vertex oxygen atoms build a three-dimensional system of voids and channels (Figure 1). Considering the possible building units, T–O–T angles and distances, over two million hypothetical zeolite structures have been predicted [3]. However, the zeolite crystallization is a rather complex process (Figure 1), and presently, there are solely about 250 known zeolite framework types approved by the Structure Commission of the International Zeolite Association [4]. The number of new framework types is continuously increasing, yet there is a big gap between predicted and obtained materials. On the other hand, a framework can be synthesized with different compositions, thus increasing the diversity of zeolite properties and potential applications.

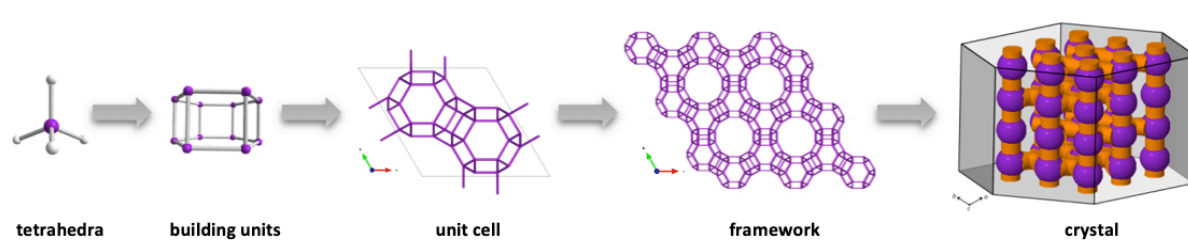


Figure 1. Schematic representation of zeolite structure formation.

Zeolites are technological materials with diverse applications that range from heterogeneous catalysis, ion and molecular separations to drug delivery and sensing [5,6]. The selection of a zeolite for a particular use is decided on the grounds of its pore system, chemical composition, hydrophobicity/hydrophilicity, acidic properties, and (hydro)thermal stability. The industrial impact of zeolites in the field of heterogeneous catalysis is enormous. Firstly, they are used in fluid catalytic cracking (FCC) and hydrocracking technology, a vital process in the oil-refining industry based on FAU-type zeolite [7]. Furthermore, they are used in a number of petrochemical processes. A sound example is the methanol-to-olefins (MTO) technology, where CHA-type and MFI-type zeolites compete as the principle part of the catalyst [8]. It is worth noting the production capacity of olefins of currently the largest MTO unit in the world is 833,000 metric tons per year [9]. Since 2010 Cu-SSZ-13 (CHA-type zeolite) is commercially employed as an emission control catalyst in diesel automotive exhaust after-treatment systems [10]. The significance of synthetic zeolites in the global market is reflected through the production of above 3000 kilotons per year (data 2014), which continues to grow [11]. The synthetic zeolite market value in 2017 was USD 13.67 billion, and the global zeolite market will reach USD 33.8 billion by 2022 [12].

The acidic properties of zeolites largely determine their success as heterogeneous catalysts. Namely, the conversion degree of the reaction, product yield, selectivity, catalyst lifetime, susceptibility to coking, and regeneration potential is directly related to the nature, number, and distribution of acid sites within the zeolite crystals. In turn, the acidity of zeolites is a function of their structure type and the chemical composition of a particular material. In aluminosilicate zeolites, acid sites are associated with the aluminium present in the zeolite material. Aluminium can occupy different positions in the framework, which impacts zeolite acidity. Furthermore, zoning in the aluminium distribution throughout the crystal is observed,

which can influence the catalytic performance of a particular material due to the difference in the effective diffusion path of reactants prior to reaching the active site [13]. Hence, the preparation of the materials having well-defined Al siting is of paramount importance for controlling zeolite acidity. Besides aluminium, we have included boron and germanium substitutions in zeolite framework, which are largely used to generate new zeolite structures. The Sn-containing zeolites were included in the review to exemplify the importance of Lewis sites in catalytic reactions. We limit our review to Sn since the Lewis acidity is a vast topic, which cannot be fully covered in the framework of the present review.

Our objective is to present a comprehensive overview of the advances in zeolite acid sites controls with an accent on the recent developments of the *in situ* and post-synthesis methods. The zeolite acidity control would not be possible without an advanced analysis of acid sites. Therefore, the methods of analysis of active zeolite sites will be revised as well. The ultimate objective of our review is to provide practical guidance for tuning zeolite acidity.

2 Structure - properties relationship in zeolites

The structure of zeolites can be represented by various building units, the most common way is by rings having a different number of central tetrahedral (T) atoms. The oxygen atoms are neglected in this kind of depiction. Connecting of building units leads to the formation of the framework with a defined array of voids and channels within the structure. Materials comprising 8-membered ring (8MR) as limiting pore opening are defined as small pore zeolites. The pore openings of medium pore zeolites are restricted by 10-membered rings (10MR), while large pore zeolites constitute a 12-membered ring (12MR). In extra-large pore zeolites, the pore openings are larger than 12MRs. Furthermore, the zeolites are sub-divided to materials with one-, two- and three-dimensional channel systems.

As mentioned, zeolites with the same framework type, but different composition exhibit different properties. For instance, pure silica materials have an electrically neutral framework and hydrophobic properties. Introducing other T atoms such as trivalent aluminium changes the charge of the framework to negative and makes the material more hydrophilic. In this case, the presence of charge-compensating cations in the cavities is required. The charge-compensating alkali and alkali-earth cations are exchangeable, which makes zeolites important ion exchangers used for water softening, removal of heavy metal ions, radioactive waste storage, etc. When proton is the charge-compensating cation, the zeolite exhibits acidic properties that are largely explored in the heterogeneous catalysis. Furthermore, the diversity in the dimensions and the shape of voids in zeolite frameworks enables the separation of molecules based on size exclusion – molecular sieving effect. Two parameters determine zeolite (hydro)thermal stability, the framework type, and the chemical composition. In general, high silica zeolites exhibit relatively high (hydro)thermal stability. On the contrary, the zeolites become less thermally stable as the Al content in the framework increases.

The widespread application of zeolites is a direct consequence of their properties, and by tuning their features, zeolites become accessible to exhibit the desired performance in a specific application. The possibilities of zeolite usage in catalysis and gas separation with novel substrates are intensively investigated, and every several years a new process is reported [14-16]. Hence, zeolites are undoubtedly going to continue to be broadly employed and, accordingly, improving their properties to enhance their performance is imperative.

3 Analysis of acid sites in zeolites

3.1 Acid sites in zeolites

In the IUPAC Gold book, a Brønsted acid is defined as “a molecular entity capable of donating a hydron (proton) to a base (i.e., an acid is a “hydron donor”) or the corresponding chemical species” [17]. On the other hand, Lewis acid is “a molecular entity, and the

corresponding chemical species, that is an electron-pair acceptor and therefore able to react with a Lewis base to form a Lewis adduct, by sharing the electron pair furnished by the Lewis base.” Both types of acid sites may be present in zeolites; hence they are solid acid materials. Purely siliceous zeolite framework is electrically neutral, and its surface is not acidic. Nevertheless, in such a lattice, the acid sites may arise at structural defects. Isomorphous substitution of Si^{4+} with trivalent cations such as Al^{3+} results in the development of Brønsted acid sites since Al^{3+} generates negative charge in the framework, which is then compensated by the presence of a proton. Generally, the Brønsted sites in zeolites ensue at oxygen atoms of a hydroxyl group bonded to a metal atom of one type coordinating to an atom of another type, which acts as the Brønsted base – the bridging hydroxyls [18]. Recently, in amorphous silica-alumina was observed an interaction of penta-coordinated Al with adjacent silanols, which act as Brønsted acid sites [19]. Lewis acid sites are related to coordinatively unsaturated cations that can accept electrons. In zeolites, Lewis acid sites may develop at the external surface or extra-framework moieties, for instance, extra-framework aluminium (EFAl) [20]. Also, a recent study suggests that Lewis sites can occur at framework tetrahedral Al atoms [21]. Another explanation of framework Al possibly acting as Lewis acid site could be the existence of Al(OH)Si bridge in the $\text{Si}-\text{O}^-(\text{H}^+)-\text{Al}^-$ or $\text{SiOH} \rightarrow \text{Al}$ resonance form [22,23]. In this case, the aluminium coordination is not complete, and the base can be adsorbed on this site.

Most zeolite materials applied as catalysts have both Brønsted and Lewis acid sites. Besides, the conversion between Brønsted and Lewis acid sites can sometimes take place in zeolites. Namely, at high temperatures, the dehydroxylation of zeolite Brønsted sites may occur, and Lewis acid sites with Si and Al of coordination number three can be formed [24]. Moreover, during high-temperature treatment, the framework dealumination often occurs, thus generating octahedral aluminium species, which act as Lewis acid sites [25]. Accordingly, in such a case, the Brønsted acidity decreases. Likewise, upon ammonia adsorption, the aluminium coordination can be reversed to tetrahedral [26].

The upper limit of the number of protonic sites in zeolites is the number of framework Al atoms, more precisely ratio of the framework atoms $\text{T}^{4+}/\text{T}^{3+}$ [27]. According to Lowenstein's rule, the maximal Si/Al ratio in zeolites equals 1, hence the highest number of protons possibly present in zeolites is $8.3 \text{ mmol H}^+ \text{ g}^{-1}$ zeolite [28]. However, usually, the number of protons is lower because of the dealumination of zeolite framework during the high-temperature treatment.

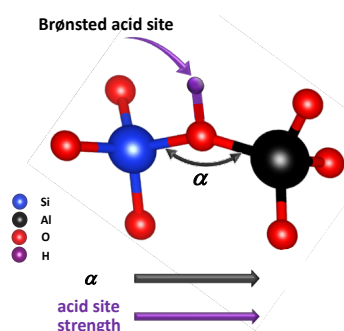


Figure 2. Zeolite Brønsted acid sites strength as a function of the T–O–T bond angle.

Zeolite solid acids exhibit similar behavior as acids in a solution, and the strength of zeolite Brønsted acid sites is comparable to sulfuric acid [29,30]. In general, the strength of a Brønsted acid is defined via deprotonation energy (DPE) required to dissociate the proton from conjugate anion to an infinite distance [31]. DPE values of zeolites can be estimated via computational chemistry methods, yet the results vary depending on the used model. In practice, the Brønsted acid strength is indirectly observed using adsorbed probe molecules

able to interact with acid sites. For instance, the chemical shifts of the carbonyl group of acetone adsorbed on the zeolite in ^{13}C NMR spectrum is related to the acid strength as the higher chemical shift corresponds to stronger site [32]. Further, in comparison to amorphous aluminosilicates of similar chemical composition, crystalline protonic zeolites exhibit stronger acidity. The explanation stems from their structure, notably geometric constraints imposed on T–O–T bond angles (Figure 2) [22]. Namely, an increase in the bond angles leads to higher acidity per acid site since the deprotonation of bridging OH groups requires less energy [33]. For this reason, the acid sites of H-MOR (bond angle range of $143\text{--}180^\circ$) and H-MFI ($133\text{--}177^\circ$) zeolites are stronger than of H-FAU ($133\text{--}147^\circ$). *Ab initio* models of aluminosilicate clusters revealed the most stable angles for protonated and deprotonated bridging hydroxyls are 134° and 179° , respectively [34]. In amorphous materials, the lattice can relax, resulting in bond angles with less related strain, and consequently, they possess weaker acid sites.

Another framework-related effect is that the strength of each proton site decreases with increasing Al content, more specifically when there are more aluminum atoms in the next nearest neighbor position (NNN) of this particular atom. Hence, the proton attached to isolated Al with no close Al neighbor is the stronger acid site [35]. The bridging hydroxyl group has higher ionic character and hence a stronger acidity. Further, for the certain chemical composition of the zeolite, the polarity of the lattice becomes more significant as the framework density reduces. In general, the electronegativity of the T atom is affecting the zeolite acid strength and it is decreasing in series $\text{Al}(\text{OH})\text{Si} > \text{Ga}(\text{OH})\text{Si} > \text{Fe}(\text{OH})\text{Si} > \text{In}(\text{OH})\text{Si} > \text{B}(\text{OH})\text{Si}$ [36,37].

On account of the complexity of zeolite synthesis systems, the distribution of aluminium may vary from crystal to crystal and even can differ within a single crystal; presenting regions of higher or lower Al concentration [38,39]. The Al atoms sitting within the individual zeolite framework T sites can be considered in terms of its location in the network of channels and cages. The position of Al tetrahedron determines the accessibility of the active sites and metal counter cations. Moreover, the location of Al directs the formation of reaction intermediates in the enclosing void volume of the charge balancing cations. The two most frequent types of Al arrangements are paired (sequence $\text{Al-O}(-\text{Si-O})_x-\text{Al}$, $x = 1, 2$), and single Al atoms (sequences $\text{Al-O}(-\text{Si-O})_x-\text{Al}$, $x \geq 3$) [40,41]. Particularly noteworthy is the location of Al pairs in the six-membered rings (6MRs) (Figure 3). Various studies reported that the siting and distribution of Al atoms in the zeolite lattice are neither random nor statistically controlled [42–44]. It was found that the Al distribution over the T-sites is kinetically controlled and markedly changes depending on the synthesis conditions [42,43].

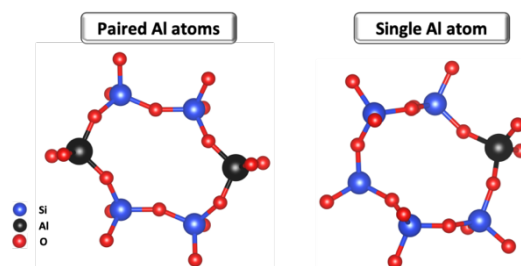


Figure 3. Depiction of the most common distributions of Al atoms in zeolite 6MRs.

The protonic forms of aluminosilicate zeolites have found more extensive use as solid acid catalysts than any other materials. In catalysis by Brønsted acids, the protonation is the crucial step, where the activation energy barrier is reduced [45]. In Lewis acid catalysis, the activation energy is lowered by polarising molecules, thus making them more reactive. The main reason for the broad usage of zeolites lies in the fact that in their frameworks, the number, nature, position, and the strength of the acid sites can be precisely adjusted. Besides,

they represent stable and environment-friendly solid catalysts that can be prepared at a large scale with a high degree of reproducibility. The following sections will address the recent results of controlling the siting of Al atoms in zeolites by employing various synthesis approaches. It should be noted that papers reporting procedures of zeolite acid sites control by *in situ* and post-synthesis methods are revised. First, the basics of the experimental and theoretical methods for zeolite acidity assessment are addressed. Further, the strategies of controlling the acid sites location within the zeolite framework by direct synthesis approach as well as by post-synthesis isomorphous substitution with Al are reviewed. The possibilities of tailoring of zeolites with specific acidic properties are exemplified on industrially relevant materials, as well as some promising new framework types. In addition, altering the acidity of zeolites in the presence of several T atoms other than Al is demonstrated.

3.2 Experimental methods for zeolites' acidity evaluation

Since Al is related to the acid sites in zeolites, information on its position and distribution, as well as its coordination number, gives an indication of the nature and distribution of acid sites within the studied materials. Thus, the initial estimation of the acidity of zeolites can be made on the grounds of the elemental analysis of the materials, which provides the Si/Al ratio of the material. Inductively coupled plasma-emission spectroscopy (ICP-ES), X-ray fluorescence (XRF) and X-ray photoelectron spectroscopy (XPS) are the most common methods applied for this purpose. Further, the spectroscopic techniques based on the interactions of the sample with the X-rays generated by various sources (synchrotron, electron microscope, etc.) afford data on the metals present in the sample. X-ray absorption spectroscopy (XAS) probes the local structure and Al coordination. The Al–O–Si bridging angle affects the Al K-edge absorption spectra and thus in a recent study was possible to determine the local Al structure associated with the Brønsted acid sites by EXAFS (extended X-ray absorption fine structure) analysis [46]. Moreover, EXAFS made possible the analysis of scattering from atoms up to 6 Å away from the absorbing Al. Besides, in this study the quantification of both framework and extraframework aluminium species has been performed [47]. Similarly, the Al K-edge X-ray absorption near edge structure (XANES) spectra exhibits features that indicate the elongation of one of the four Al–O bonds about the Al induced by the formation of Si(OH)Al species upon the dehydration of hydronium ions [48]. In addition, micro X-ray diffraction (μ XRD) crystallography imaging study of ZSM-5 single crystal uncovered differences in aluminium concentration [39], while scanning transmission X-ray microscopy (STXM) at a resolution of 30 nm enabled the distinction among different Al coordination environments and determination of regions rich in more highly coordinated aluminium atoms [49]. Various other methods, which are addressed in the following sections, afford information on the acid properties from different perspectives. In conjunction, they allow a rather clear assessment of zeolite acid sites' nature, strength, and distribution over the framework positions.

The natural abundance of ^{27}Al nucleus is nearly 100%, and thus ^{27}Al NMR spectra with high signal-to-noise ratios can be acquired within a short period of time [50]. Generally, approximate chemical shifts in zeolites in ^{27}Al magic angle spinning (MAS) NMR spectra are at 50–60 ppm for tetrahedral oxygen-coordinated aluminium, at 30–50 ppm for tetrahedral non-framework Al species, 30 ppm for five-fold coordinated species and 0 ppm for octahedral aluminium in experiments where $[\text{Al}(\text{H}_2\text{O})_6]\text{NO}_3$ is employed as a reference (Figure 4) [51]. The quadrupolar character of the ^{27}Al nucleus ($I = 5/2$) results in broader peaks than those obtained for ^{29}Si due to the interactions with the external magnetic field as well as with the electric field gradient generated by its surrounding environment. In zeolite science, often, the issue of “invisible” or “hidden aluminium” is put forward. Namely, highly distorted low symmetry sites can give rise to very broad signals, which often is completely unobservable

[51]. Recent technological progress combined with higher magnetic fields, faster magic angle spinning rates, and newly developed measurement techniques (sequences) was found efficient

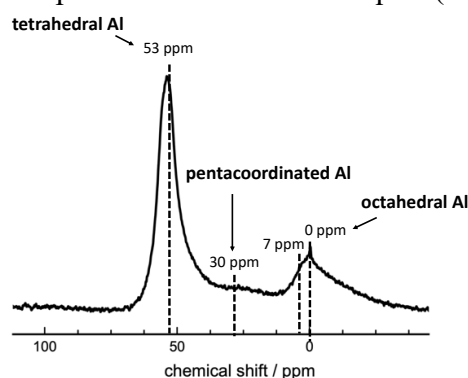


Figure 4. ^{27}Al MAS NMR spectrum of MFI-type zeolite material which possesses Al atoms of various coordination environments.

to circumvent this problem [52–54]. Sample hydration is also a useful approach in reducing the contribution of the invisible Al to the overall ^{27}Al MAS NMR [55].

^{29}Si NMR spectra afford information on the zeolite acidic properties in terms of the connectivity within the zeolite framework, i.e., on the types of $\text{Si}(n\text{Al})$ sites, and on the mean T–O–T angles. ^{29}Si nucleus has a spin $\frac{1}{2}$ and owing to rather low natural abundance ($< 5\%$) and slow relaxation, long acquisition times are necessary to collect resolved spectra. ^{29}Si MAS NMR spectra of all-silica zeolites consist of resonances at different chemical shift values which stem from crystallographically non-equivalent tetrahedrally bonded Q^4 Si atoms, $\text{Si}(\text{OSi})_4$ [56]. Q^3 Si atoms appear at structural defects. They are connected to one silanol group and three other tetrahedra. Their resonances in ^{29}Si MAS NMR spectra are shifted downfield in comparison to Q^4 species. In the case when Al is present within the zeolite framework, the signals in ^{29}Si MAS spectra become broadened, resulting in overlapping of the Q^4 Si resonances. Besides, this generates different environments of Si since it may have different numbers of Si and Al atoms in their second coordination sphere. Each Al atom in the next coordination shell causes an additional downfield chemical shift, thus enabling the calculation of the framework Si/Al ratio [56]. The technique of cross-polarization (CP) is based on the exciting spin system by transferring the magnetization from another nucleus. This approach is used for identifying some NMR signals. For instance, in the case of $\{^1\text{H}\}^{29}\text{Si}$ CP MAS NMR, the signal of Q^3 silicon atoms attached to a hydroxyl group, $(\text{SiO})_3\text{SiOH}$, is enhanced over Q^4 Si atoms and/or $\text{Si}(3\text{Si},1\text{Al})$ peak in comparison to the signal intensity in the standard ^{29}Si MAS NMR spectrum.

^1H MAS NMR spectroscopy of dehydrated zeolite materials is one of the techniques which can provide information on the hydroxyl groups. The signals of hydroxyl groups arise in a range of chemical shifts of $\delta_{1\text{H}} = 0\text{--}16$ ppm. The metal (cation) OH groups, e.g., AlOH , LaOH , and MgOH groups located in the large cages of dehydrated zeolites or at the outer surface of solid particles display the chemical shifts ranging from -0.5 to 1.0 ppm. The resonances of the terminal silanol SiOH groups at the external surface of the zeolite particles and framework defects appear at $1.3\text{--}2.2$ ppm [57]. The signals with chemical shifts up to 16 ppm originate from the silanol groups forming strong hydrogen bonds. In dealuminated zeolites are frequently present signals at $\delta_{1\text{H}} = 2.4\text{--}3.6$ ppm, which are assigned to the hydroxyl protons at extra-framework aluminum species (AlOH) [58]. The bridging $\text{Al}(\text{OH})\text{Si}$ groups exhibit signals at $3.6\text{--}5.5$ ppm, whereas the resonances at chemical shifts of $5\text{--}7$ ppm indicate these groups are involved in the hydrogen bonding with neighboring framework oxygens. Methods such as $^1\text{H}\text{--}^1\text{H}$, $^{27}\text{Al}\text{--}^{27}\text{Al}$ and $^{31}\text{P}\text{--}^{31}\text{P}$ double-quantum (DQ) magic-angle spinning (MAS) NMR spectroscopy techniques as well as $^1\text{H}\text{--}^{27}\text{Al}$ DQ MAS NMR have been

developed to study the spatial proximity between different acid sites in zeolite samples. An example of 2D NMR spectra of zeolite materials is given in Figure 5.

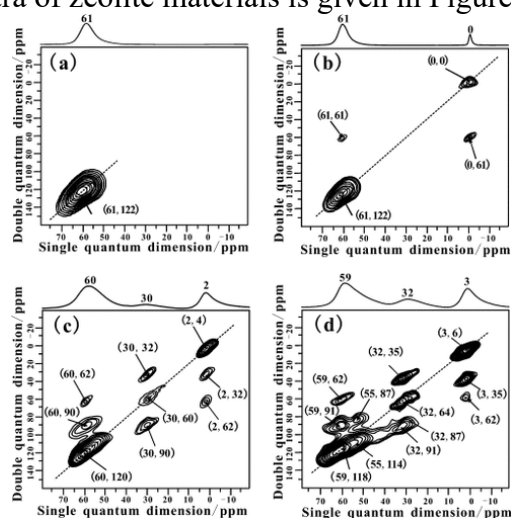


Figure 5. ^{27}Al MAS and double-quantum MAS NMR spectra of zeolite Y (a) before and after calcination in air at (b) 500, (c) 600, and (d) 700 °C. One-dimensional ^{27}Al MAS spectra are plotted on the top of 2-dimensional spectra. Reproduced with permission from reference [59].

Infrared spectroscopy provides valuable information on the acidic properties of materials. In the spectral region ($3800\text{--}3000\text{ cm}^{-1}$), which corresponds to stretching vibrations of hydroxyl groups, typical infrared spectra of activated (calcined *in vacuo*) zeolites feature several bands. The bands corresponding to the silanol groups appear at $3710\text{--}3760\text{ cm}^{-1}$ (Figure 6), as the contributions of isolated silanols at the external surface, weakly interacting internal silanols possibly near structural defects (intracrystalline Si–OH), and internal silanols in zeolite channels vary in a particular sample [60]. The stretching mode of the bridging hydroxyl groups gives rise to a band at $3600\text{--}3650\text{ cm}^{-1}$, while the broad band at about 3500 cm^{-1} arises due to silanol nests [61].

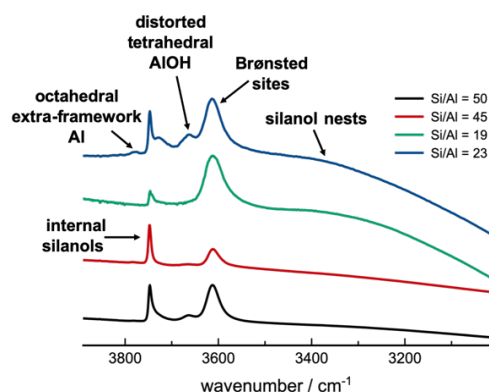


Figure 6. FTIR spectra in the OH region of the ZSM-5 materials of different Si/Al ratios.

3.3 Zeolites' acidity assessment by probe molecules

The very definition of the acids involves the exchange of H^+ or electrons between the acid-base pair, therefore employing molecules that get adsorbed and interact with acid sites is a standard method to get insight on the acidic properties of the zeolites. The perturbations of the spectra of both the zeolite surface groups and probe molecule upon the interaction can provide qualitative and quantitative information on the acid site. This approach is particularly

convenient for the investigations of Lewis acid sites as they cannot be directly detected by IR since a coordinatively unsaturated site does not undergo vibration [62].

Pyridine is a commonly employed probe molecule for zeolite acidity assessing since it interacts with both Brønsted and Lewis acid sites. The band at $\approx 1540\text{ cm}^{-1}$ is associated with pyridine on Brønsted acid sites, whereas that at $\approx 1450\text{ cm}^{-1}$ arises from pyridine adsorbed on Lewis acid sites. Furthermore, the multi-bands in the region $1580\text{--}1660\text{ cm}^{-1}$ can be useful to make a distinction between pyridine adsorbed on different acid sites [63]. Pyridine can penetrate pores of most catalytically important zeolites as its kinetic diameter is 0.57 nm. Bulkier molecules have limited access to micropores and are used to probe acid sites on the external surface of the zeolite crystals. E.g., the kinetic diameters of methyl-substituted

Table 1. Common basic probe molecules used for the evaluation of the acidity of zeolite materials by infrared spectroscopy. Their kinetic diameter and typical band region in the spectrum of a probe molecule adsorbed on the zeolite corresponding to interactions with acid sites are also presented.

probe molecule		reference	
H₂			
kinetic diameter/Å	2.9		
band position/cm ⁻¹	4150–4090		[64,65]
interaction with site	cations		
N₂			
kinetic diameter/Å	3.6		
band position/cm ⁻¹	2360–2345	2335–2330	[66]
interaction with site	Lewis	Brønsted	
CO			
kinetic diameter/Å	3.8		
band position/cm ⁻¹	2240–2190	2180–2155	[67,68]
interaction with site	Lewis	Brønsted	
d₃-acetonitrile			
kinetic diameter/Å	3.8–4.2		
band position/cm ⁻¹	2335–2325	2300–2295	[69,70]
interaction with site	Lewis	Brønsted	
NH₃			
kinetic diameter/Å	2.6		
band position/cm ⁻¹	1630–1620	1450–1410	[71,72]
interaction with site	Lewis	Brønsted	
Pyridine			
kinetic diameter/Å	5.7		
band position/cm ⁻¹	1545	1450	[73]
interaction with site	Brønsted	Lewis	
2,6-dimethylpyridine (lutidine)			
kinetic diameter/Å	6.7		
band position/cm ⁻¹	1650–1625	1620–1595	[74,75]
interaction with site	Brønsted	Lewis	
2,4,6-trimethylpyridine (collidine)			
kinetic diameter/Å	7.4		
band position/cm ⁻¹	1650–1635	1633	[76,77]
interaction with site	Brønsted	Lewis	
di-tert-butylpyridine			
kinetic diameter/Å	7.9		
band position/cm ⁻¹	1615	1450	[78]

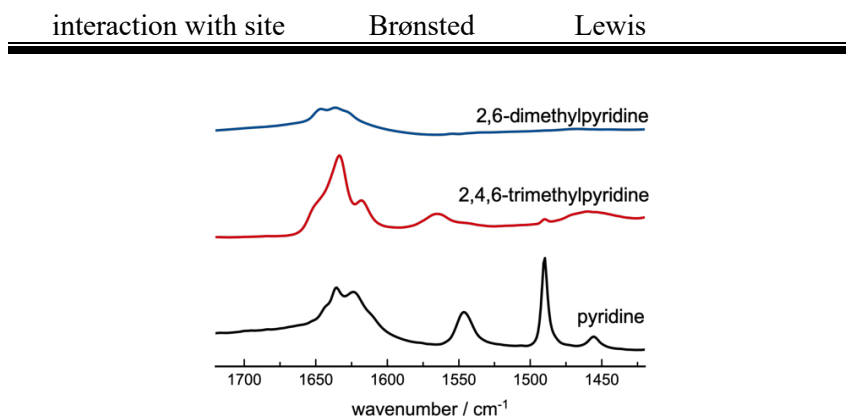


Figure 7. FTIR spectra of ZSM-5 zeolite in the region 1720–1420 cm^{-1} with adsorbed pyridine, 2,6-dimethylpyridine, and 2,4,6-trimethylpyridine.

pyridines 2,6-lutidine (2,6-dimethylpyridine) and 2,4,6-collidine (2,4,6-trimethylpyridine), are 0.67 nm and 0.74 nm, respectively, and thus their penetration ability to some micropores is reduced (Figure 7) [62]. Accordingly, they are used to distinguish the silanols located inside or outside the micropores and consequently to establish their accessibility [79,80]. Other probe molecules used to evaluate the zeolite acidity are CO, NO, CO₂, N₂, H₂, O₂, NH₃, CH₃CN, benzene, alkanes, etc. (Table 1). These probe molecules have different basicities and can be used under various experimental conditions providing information on the nature and strength of the acid sites in the zeolite framework. Table 1 summarizes the most frequently employed basic probe molecules for the assessment of the acidity of zeolitic materials by infrared spectroscopy. The kinetic diameter of the probe molecule and typical band region in the spectrum of a zeolite material with adsorbed particular probe molecule is presented too. In the past years, many comprehensive reviews on probing zeolites by infrared spectroscopy have been published, and it is recommended to consult them when looking for more details on the matter [62,79,81,82].

Phosphine molecules have been proved to be particularly useful to probe acid sites investigated by NMR (Figure 8) [83]. The MAS-NMR spectra of trimethylphosphine (TMP) adsorbed on zeolites enables clear distinguishing between the acid sites. Acidic protons react with the strong Lewis base forming $[(\text{CH}_3)_3\text{P}-\text{H}]^+$ adducts that exhibit a ³¹P chemical shift of

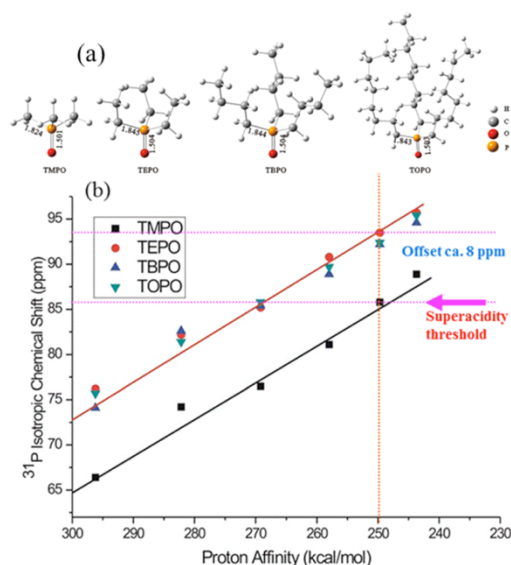


Figure 8. (a) Optimized structures of trialkylphosphine oxide (TMPO, TEPO, TBPO, and TOPO – trioctylphosphine oxide) probe molecules. (b) A plot of calculated ³¹P chemical shift of adsorbed R₃POH⁺ complexes and proton affinity envisaged on the grounds of the 8MR

zeolite cluster model. Reprinted with permission from reference [83]. Copyright (2017) American Chemical Society.

ca. -3 ppm and a J_{P-H} coupling constant of ca. 500 Hz. The TMP bonded to Lewis sites has resonances at notably higher fields (-30 to -70 ppm), and when Al is present, a J_{P-Al} coupling of ca. 300 Hz may result in a multiplet of six lines [84]. Employing trimethylphosphine oxide (TMPO) and tributylphosphine oxide (TBPO) facilitates distinction among the acid sites located in the internal voids and on the external surfaces of zeolites. The kinetic diameter of TMPO (ca. 0.55 nm) is smaller than the pore opening of the ten-membered ring (ca. 0.60 nm) of zeolite ZSM-5; hence TMPO can diffuse in the channels and pores of the zeolite and get bonded to both the internal and external acid sites. On the other hand, TBPO of a kinetic diameter of ca. 0.82 nm is too large to penetrate into the channels. Only the acid sites located on the external surface of the zeolite crystals are accessible to TBPO [85].

Isotopic labeling was also found to be useful in distinguishing various acid sites in zeolite materials. For instance, ^{17}O NMR resonance from oxygen directly bound to the Brønsted acid site has been observed in ^{17}O -enriched zeolite NH_4Y [86]. Measuring of the adsorbed ^{15}N -pyridine by ^{15}N MAS NMR spectroscopy enabled assessing the strength and number of isolated framework metal sites (Sn, Ti, Zr, Hf, Nb, Ta, B, Ga, and Al) in Beta zeolite materials [87]. Similarly, H/D isotope exchange was utilized to quantify the total number of Brønsted acid sites as well as their distribution throughout zeolite crystals of different sizes [88]. Besides, the hopping of protons (limited delocalization – moving of protons in regions wider than over the surrounding four lattice oxygen atoms) at temperatures above 300 °C was confirmed by the H/D isotope exchange between acidic OD groups of several zeolites (CHA, MFI, MOR) and methane [89]. The isotope exchange between acidic OD groups and H in ethane provided information on the strength of acid sites in various zeolites [90]. Further, the addition of 99.69% ^{29}Si enriched $^{29}SiO_2$ in the SAPO-34 synthesis system resulted in a material with present Si islands as detected by ^{29}Si NMR [91]. In SAPO materials, Si is associated with Brønsted acidity and shows a direct relationship with the coke deposition.

The UV/Vis spectroscopy is another method used to account for the acid sites in heterogeneous catalysts. Measuring the UV/Vis spectrum of pyridine interacting with the zeolite was found to be a promising tool for investigating zeolites acidic properties [92]. The technique relies on the fact that the electronic properties of pyridine get altered upon the interaction with acid sites, and thus pyridine bonded to various sites can be distinguished. One of the most notable advantages of this method is the possibility to discriminate the different surface OH groups. Namely, the UV/Vis bands position is mostly affected by the species

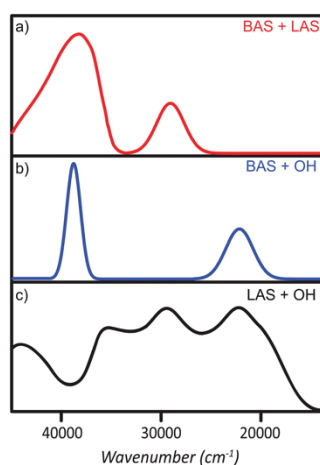


Figure 9. UV/Vis spectra after pyridine adsorption on hypothetical solid acids possessing (a) Brønsted and Lewis acid sites, (b) Brønsted acid sites and hydroxyl surface groups, and (c)

Lewis acid sites and hydroxyl surface groups. Reproduced from reference [92] with permission from the PCCP Owner Societies.

adjacent to the hydroxyl group. In addition, the study of the acidic strength of the hydroxyl groups is attainable as well (Figure 9). Also, a staining method employing thiophene to visualize the zeolite particulates, FCC catalyst components, was developed. On the grounds of the fluorescence microscopy images, the maps of Brønsted acid sites in a single zeolite particle were created. The method is based on the thiophene oligomerization catalysed by Brønsted acid sites [93]. Similarly, the liquid-phase oligomerisation of styrene monitored by UV/Vis spectroscopy enables the investigation of the Brønsted acid sites in zeolite constituent of the FCC particles. Besides, the usage of the styrenes of different reactivity allows the determination of the zeolite Brønsted acid sites strength within the FCC particle [94].

In temperature-programmed desorption (TPD) experiments, the sample is heated while the pre-adsorbed probe molecules get gradually desorbed [95]. Ammonia is the most frequently used probe molecule in TPD technique (NH_3 -TPD), yet the usage of CO, amines, alcohols, acetonitrile, has also been reported [96-100]. The desorption curve is plotted as the rate of the gas desorption versus the temperature [101]. Generally, the desorption peak maximum position is a function of the acid site strength, whereas the peak area is correlated with the amount of acid sites. One should note that the experimental conditions may influence the peak positions. Besides, the TPD profiles may comprise multiple overlapping peaks. In such a case, the curve deconvolution is applied to attain information on the total quantity of the acid sites as well as the amount of the particular acidic site [102]. The major disadvantage of the TPD method is that Brønsted and Lewis acid sites cannot get distinguished. Besides, the desorbed probe molecules can get re-adsorbed while they are coming out of the pores and thus can affect the final results [103]. TPD technique has been upgraded by developing an NH_3 IRMS-TPD (infrared/mass spectroscopy TPD) method based on the *operando* instrumentation set-up, which allowed to ascertain the nature of acid sites (Figure 10) [104].

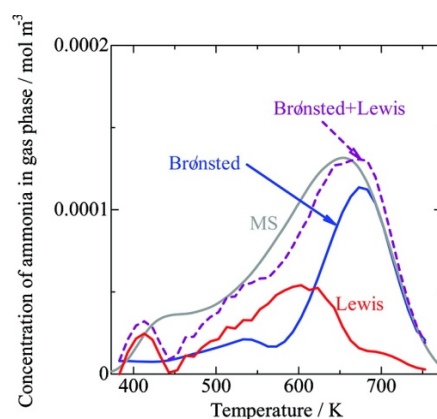


Figure 10. NH_3 IRMS-TPD spectrum of SSZ-13 zeolite. Reprinted with permission from reference [105]. Copyright (2011) American Chemical Society.

Microcalorimetry is a direct method for measuring the heat of adsorption of probe molecules on zeolites. The experiment is performed by dosing the aliquots of the probe molecule onto the sample held at the chosen temperature until reaching full surface coverage. Indeed, a large variety of probe molecules such as NH_3 , pyridine, amines, H_2O , N_2O , etc. has been studied [106–108]. The results are plotted as the adsorption enthalpy as a function of the coverage. Usually, in the case of high-silica zeolites that possess strong Brønsted acid sites, the higher differential adsorption enthalpy at low coverage is measured. The microcalorimetry results of the ammonia adsorption at 150 °C have shown a marked influence of the local geometry of

bridging hydroxyl groups within the zeolite framework (bond angles and distances) on their acid strength. Namely, zeolites of similar Si/Al ratio, yet different structure types present differences in adsorption heats up to $\approx 50 \text{ kJ mol}^{-1}$ [109]. However, one should be aware of many limitations this method is facing. From a practical point of view, it takes a long period of time to achieve the complete equilibrium. Also, similar differential heats of adsorption can be measured from the strong Lewis centers and strong Brønsted sites. Finally, the adsorption could be limited by diffusion [110]. Still, it is a powerful technique for zeolite acidity evaluation.

Recently, a new method for measuring Brønsted acid site densities based on reactive gas chromatography has been developed [111]. The technique relies on alkylamine decomposition to selectively count the Brønsted acid sites within zeolite lattice. The molecule decomposition occurs within the inlet of gas chromatograph, and a flame ionization detector quantitatively measures the products. The values on the Brønsted acid site densities obtained by the reactive gas chromatography are in good agreement with the acidity results collected by the conventional TPD mass spectrometry as well as with the *in situ* pyridine titration of isopropanol dehydration. The technique allows reliable measurement of the Brønsted acid site densities of siliceous materials as low as $\approx 1.0 \mu\text{mol g}_{\text{cat}}^{-1}$.

The proposed method to assess the distance between the Al atoms that are facing the same channel and have a cooperative effect on the charge-balancing cation site occupation is related to the zeolite exchange capacity for the divalent metal hexa-aqua-complex cation, $[\text{Co}(\text{H}_2\text{O})_6]^{2+}$ [112]. Namely, there are three cation sites in the six-membered rings (α -, β - and γ -types) of the MOR, FER, MFI, and BEA zeolite frameworks. The α -type 6MR comprises two 5MRs and is twisted, β -type site is planar, whereas γ -type 6 MRs build a complex boat-shaped structure. Upon ion exchange with the $[\text{Co}(\text{H}_2\text{O})_6]^{2+}$, the cations occupy the 6MRs with paired Al atoms, and the bands in the UV/Vis spectra of a specific sample can be decomposed to get the concentration of the Co^{2+} at a particular cation site. The sum of the molar concentrations of Co^{2+} at the individual sites is directly proportional to the concentration of the paired Al sites. The concentration of the unpaired sites is calculated indirectly as a difference between the concentration of the Co^{2+} needed for complete ion exchange and the concentration of Co^{2+} at the α -, β - and γ -type cationic sites of mordenite, ferrierite, ZSM-5 and Beta zeolites [42]. Recently, this approach has been applied to CHA-type materials, as well [113].

3.4 Theoretical methods for zeolites' acidity evaluation

The theoretical methods have developed substantially in the past years and are now commonly used in zeolite science. They provide a complementary viewpoint that helps to get insight into zeolite properties in general, addressing them from different perspectives. In terms of zeolite acidity, it allows studying the Al distribution and proton sitting in the zeolite framework. Various approaches have been employed to simulate the active zeolite sites in many cases neglecting the confinement effects [114–116]. In general, the calculated spectra fit well with the experimentally measured spectra [47,117]. In addition, a plethora of theoretical studies dealing with modeling interactions/adsorption of molecules of different character and zeolite materials have been conducted [118]. For example, the shifts in the stretching frequencies in the IR spectra of zeolite materials with adsorbed CO have been calculated [119]. The results are in fair agreement with the experimental findings. Furthermore, the heats of ammonia desorption from zeolite materials measured by the TPD frequently coincide with the theoretical calculations using different functionals [120,121].

Deprotonation energy (i.e., the proton affinity) of the Brønsted acid sites is a feature denoting the zeolite acidity. Often the computational approach is more convenient for the determination of deprotonation energy than complicated experimental methods. Thus

embedded cluster systems have been used to model zeolites H-Y and H-ZSM-5 and study the deprotonation energy differences between the structures. No matter the exchange-correlation functional, the deprotonation energy of FAU zeolite is the lowest followed by ZSM-5 acid sites located in the sinusoidal channel, in the intersections, and finally in the straight channel [122]. Besides, the local geometry around the acid site (bond lengths and angles among atoms), which determines its acid strength, can be correlated with energy parameters. DFT investigation on cluster models of Brønsted acid of FAU, BEA, MFI, FER, MWW, and MOR frameworks suggests that when the Si(OH)Al unit is pushed from both sides, the acid strength becomes higher because the Al–O distance is shorter [123]. Namely, the stronger acid sites are generated when the Al–O bond is shorter, and the Si–O–Al angle larger [124]. On the other hand, it was calculated by QM-Pot approach (Table 2) that the difference in the deprotonation energies of zeolites having different frameworks is within a range of $<30 \text{ kJ mol}^{-1}$ [125]. Further, in 2015 Jones and Iglesia used a periodic DFT method and reported that in MFI, BEA, MOR, FER, CHA, and FAU zeolite frameworks the ensemble-averaged deprotonation energies are invariable on the Al location [126]. These energies reveal that conjugated anions are similarly stable independently on both Al siting as well as zeolite framework type, i.e., O–H bond lengths and Si–O–Al angles. For that reason, the acid strength is determined only by the type of the T-atom incorporated within the framework regardless of its position, number, and distribution. Ergo, the catalytic activity of the zeolite materials is determined by the confinement effects that stabilize the transition states and adsorbed intermediates through dispersion forces. Further, in a recent study, Rybicki and Sauer proposed the decomposition of the deprotonation energy into two components: intrinsic deprotonation energy and a proton “solvation” energy, which is a function of the dielectric constant of the material. Namely, the *ab initio* studies have shown a linear correlation of the deprotonation energies of zeolites with the reciprocal value of the average dielectric constant [127]. Again the intrinsic deprotonation energies of most of the zeolites have very similar values, and thus, in line with the conclusion of Jones and Iglesia, all zeolites present almost identical acid strength regardless of their structure.

As already mentioned, in practice, the acidity of zeolites is estimated on the grounds of their interactions with various probe molecules. However, from a theoretical chemistry point of view, this is a complex matter, and there is a distinction between the results of the acidity quantification using a simulation of the probe molecules adsorption and calculations of the deprotonation energies [128]. The simulations indicate that in this case not only intrinsic acidity should be taken into account, but also the stabilization of the adsorbed molecule or its conjugated acid confined within the zeolite voids by dispersion forces. The concept of the effect of confinement in zeolite rests on the long-range attractive van der Waals interactions and contributes to the adsorption energy of a molecule on a surface [129]. Initial results indicated the enhancement of the (van der Waals) adsorption energy on concave surfaces, while further studies showed there is a surface barrier to sorption into cylindrical pores in the zeolite channels. Indeed, the computational methods facilitated quantitative assessment of the confinement effects in zeolite materials and led to a better understanding of adsorption and catalysis processes in zeolites by modeling sites with high adsorption affinity for certain gases [130], active site structures [131], the reaction coordinates [132,133], transition states and intermediates [134,135], encapsulated particles/clusters [136], reaction barrier predictions [137], etc. Besides, as OSDA molecule may be considered as a physisorbed sorbate molecule, this approach enabled a better understanding of zeolite synthesis and even designing the transition state mimicking OSDA, which yielded target zeolite with improved catalytic performance in the target reaction [138]. Finally, the most recent trend in computational chemistry is developing *operando* theoretical methods which describe the catalytic processes [139].

Table 2. Deprotonation energies of different T sites in some zeolite structures calculated using the QM-Pot approach. Adapted from reference [140] - Published by The Royal Society of Chemistry.

zeolite	FAU	MFI	CHA	FER	FAU
site	O1H	O7-H	O1H	O7-H	O3-H
$E_{dp} / \text{kJ mol}^{-1}$	1206	1235	1225	1218	1203

4 In situ control of acid sites in zeolites

The two avenues of incorporating Al into zeolite framework positions are the *in situ* synthesis route and the post-synthesis modification. The two different approaches are illustrated in the next sections of the paper through examples of directing the Al sitting within the zeolite framework by changing the synthesis or post-synthesis treatment parameters. Further, the essential aspects of zeolite synthesis procedure are given in the light of preparing materials of required properties.

The post-synthesis treatment is discussed in detail since there are a plethora of conditions under which the post-synthesis treatment of zeolites can be performed. For instance, the choice of the treating agent, pH, temperature, duration of the procedure, and the number of the treatment steps are provided. All these parameters impact the properties of the final material, and the outcome of the post-synthesis treatment of zeolite in terms of chemical composition, the number of introduced Al, and its position may vary to a large extent. Briefly, the post-synthesis Al incorporation is sensitive to the micro/macroscale properties of the initial material or minor fluctuations in the treatment conditions.

Generally, the zeolite synthesis mixture contains a few essential elements. Each chemical containing silicon or aluminum can be considered as a potential T atom source. The physicochemical properties and solubility of the initial T atom source affect the overall reaction kinetics and crystal growth process. Moreover, different zeolite types or crystal morphologies can be obtained when the T atom source is changed [141]. Water is the most common solvent in zeolite preparation, but other solvents such as ionic liquids and ethylene glycol have also been successfully employed, providing new opportunities in the zeolite syntheses [142,143]. Hydroxide and fluoride anions are used as mineralizers (mobilizers) in preparing of zeolites. Mineralizer solubilizes the reactants forming complexes of various polycondensation degrees depending on the mineralizer concentration. Crystals prepared in hydroxide media have more defects than fluoride route materials [61]. Furthermore, all-silica counterparts of some zeolite materials have been prepared in fluoride systems [144]. Also, when fluoride ions have been used, several previously unknown zeolite frameworks have been discovered [145,146].

Structure directing agents are moieties that assemble the array of zeolite voids and channels. They are confined within the zeolite framework, yet not a part of it. Inorganic cations such as alkali and alkali-earth cations with their hydration spheres are considered as structure-directing agents for natural and low-silica synthetic zeolites. It was found that particular cations prefer certain positions within the framework [147]. Accordingly, they can yield different structure types, thus exhibiting the structure-directing effect [148]. The inorganic cations present within the voids are exchangeable, whereas the organic species in the final product are occluded within the pores and are predominantly decomposed by calcination. Certain efforts have been made towards designing of degradable and recyclable organic structure-directing agents (OSDAs), thus eliminating the combustion step [149]. The

aftermath of using OSDAs was the increase of the Si/Al ratio of the zeolites due to their larger size, which limits the amount of OSDA molecules that can be confined inside the zeolite. Hence, less Al is incorporated into the framework. Finally, the geometry (size and shape), electronic properties, rigidity, polarity, and hydrophobicity of the organic molecules will exhibit an effect on the final zeolite formed [150].

The initial zeolite synthesis reaction mixture is prepared when the reaction components get admixed. Two main events take place during any new solid phase formation – nucleation and (crystal) growth. The nucleus is the smallest entity within a system that brings structural information and can yield the final product at given reaction conditions. As the nutrient pool determines the reaction kinetics and, subsequently, its termination, the number of viable nuclei directly affects the final size of the crystals. Zeolite synthesis system is particularly complex, and the distribution of the species mainly depends on the starting compounds, pH, and reaction temperature [151–153]. In such a heterogeneous system, many possible processes may occur: condensation of silicate species, polymerization, depolymerization, dissolution, gel formation, gel reorganization, etc. Most of these reactions, equilibria, and interactions are correlated and can change as the reaction advances [154,155]. The outcome of the process is a result of small differences in the thermodynamic parameters of the competing processes and kinetic barriers [156].

4.1 In situ controlling the Al location in the zeolite framework

4.1.1 MFI-type materials

MFI-type material is a medium pore zeolite possessing a three-dimensional channel system of intersected straight and sinusoidal 10MR channels with the diameter of the intersection cavity of about 9 Å. There are 12 crystallographic non-equivalent T-sites (Figure 11), and the aluminium atoms can occupy a range of T-sites within the MFI framework, hence affecting the material's performance in a particular application. The materials with Si/Al ratio ranging from infinity to 10 have been synthesized in the presence of various OSDAs (tetraethylammonium, di-n-propylamine, 1,5-diaminopentane, tripropylamine, ethyldiamine, morpholine, propanolamine, ethanolamine, dipropylamine, triethylenetetramine, diethylenetetramine, glycerol, n-propylamine, hexanediol, di-n-butylamine, propylamine, etc. [157]), but generally, the tetrapropylammonium (TPA) cation is utilized. In addition, there are many reports on OSDA-free syntheses of ZSM-5, very often in the narrow range of composition of the starting reaction mixtures with rather long crystallisation times and with stirring [158-161].

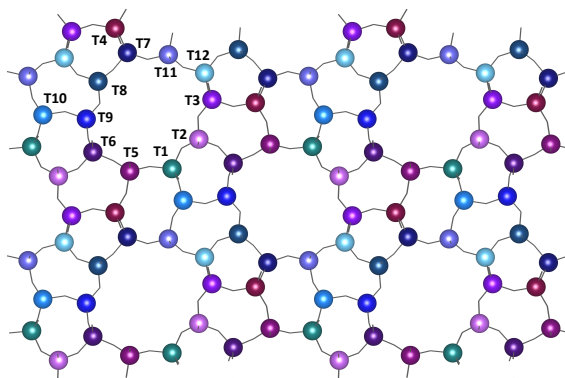


Figure 11. MFI zeolite framework with labels of crystallographically non-equivalent T sites.

Furthermore, MFI-type materials have been prepared from OSDA-free synthesis mixtures with added seed crystals [162-166]. It is necessary to note that all silica MFI-type material is

termed silicalite-1, while the Al-containing materials are referred to as ZSM-5. Besides Al, heteroatoms such as Ti, B, Fe, Sn, V, Zn, Ga, As, Mn, etc. have been introduced into the MFI zeolite framework [167-175].

To account for the acidic properties of ZSM-5, Yokoi et al. used tetrapropylammonium hydroxide (TPAOH), dipropylamine (DPA), cyclohexylamine (Cha) and hexamethylenimine (HMi) with or without Na cations as summarized in Table 3. The prepared materials have nearly equal Si/Al ratio (≈ 50) and, thus, a similar number of acid sites [176]. Nevertheless, the activities of these ZSM-5 materials in 3-methylpentane cracking and catalyst lifetimes in methylcyclohexane cracking differ noticeably. Such behaviour was reasoned by constraint index analysis, and it was concluded that the bimolecular cracking in the 3-methylpentane cracking proceeds via a bulky transition state over the acid sites located at the channel intersections. Consequently, it has been estimated that in the sample prepared using TPA^+ in the presence of Na^+ the number of acid sites in the intersection positions is very low. On the other hand, when Na^+ is not present in the TPA containing reaction mixture, the acid sites in the obtained ZSM-5 material mostly reside in large spaces, i.e. in the channel intersections. Likewise, ZSM-5 zeolites synthesized in the DPA, Cha, and HMi systems with Na^+ possess the acid sites predominantly located at the channel intersections [176]. Accordingly, Pashkova et al. established that the addition of Na^+ ions to the initial zeolite synthesis mixture does not affect the location of Al at the intersection, but does influence its distribution over single isolated Al (increased fraction) and paired Al sites (reduced number) [177].

Yokoi et al. further investigated the topic by the use of pentaerythritol with Na^+ in the ZSM-5 synthesis. The product contained Al atoms predominantly situated at straight and sinusoidal channels in the MFI framework (Figure 12) [178]. This work was further extended by using a series of straight- and branched-chain alcohols (1,3-propanediol (PDO), 1,6-hexanediol (HDO), glycerol (GLY), diethylene glycol (DEG), triethylene glycol (TEG), tert-butanol (TBO), trimethylolethane (TME) and pentaerythritol (PET)) in the ZSM-5 synthesis. The Al atoms in the ZSM-5 prepared with bulky and branched-chain alcohols such as TBO, TME, and PET combined with Na^+ were located in narrow straight and/or sinusoidal channels [179].

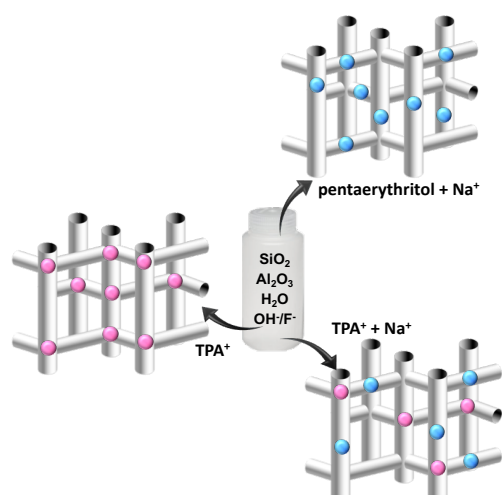


Figure 12. Schematic representation of the Al sitting within the final MFI-type material prepared from the zeolite synthesis mixtures containing TPA, TPA with Na^+ , and pentaerythritol with Na^+ .

TPA/Na ZSM-5 material was the least stable in the n-hexane cracking. In this reaction, the highest yield of propane was measured for TME/Na and PET/Na samples. Two tested ZSM-5 materials prepared with the bulky OSDAs, TME/Na and PET/Na, were the most stable catalysts in the MTO reaction. The deactivation took place as a consequence of the coke

deposition; thus, the improved endurance of TME/Na- and PET/Na-derived catalysts to coking is ascribed to the acid sites occupying the channel positions, thus posing steric constraints on the formation of the coke precursors [179]. In the following study of the PET/Na system, the Al in the prepared ZSM-5 material was again primarily located within the 10 MR channels presenting a higher number of acid sites than ZSM-5 synthesized with the aid of TPA [180]. Moreover, the Brønsted sites acid are stronger, and Lewis sites weaker in comparison with the material yielded in the TPA system. In n-octene cracking reaction, PET/Na-ZSM-5 was more active catalyst with longer lifetime and lower hydrogen transfer coefficient than the TPA-ZSM-5 [180]. In another set of experiments, ZSM-5 materials have been synthesized in the presence of TPAOH, pentaerythritol, and n-butylamine. Once again, the acid sites reside in the MFI framework channels when PET is used and in the channel intersections in the case of TPAOH, while the n-butylamine yielded material that possesses Al distributed in both of these environments [181]. Upon modification with Pt, the samples with acid sites in the channel intersections produced more aromatic compounds and less methane in the reaction of ethane aromatization than that of a ZSM-5 with acid sites located in the channels.

Two sets of ZSM-5 zeolites having Si/Al ratio ranging from 13 to 30 and with the distribution of framework Al as paired and single atoms were prepared by Bernauer et al. employing various Si and Al sources [182]. The protons on the paired Al atoms are regarded as close protons while the isolated protons are bonded to distant single Al atoms. In these ZSM-5 samples, most of the acid sites are positioned at the channel intersections. The authors had found that the oligomerization process over close protons is about 2–10 times higher in turnover rates per acid site than over the ZSM-5 zeolites with isolated protons located at the channel intersection as well [182]. The additional study revealed that the presence of Na⁺ in the initial zeolites synthesis mixture results in a high population of single Al atoms in the final material's framework due to the stabilization effect of Na⁺ on single SiAlO₄⁻ species in the amorphous precursor [183]. On the other hand, the Al pairs get incorporated in the 6MRs due to the impact of the positive charge of TPA⁺ that can be polarized by anions. The polarization ability of anions together with OH⁻ on the N atom charge decreases in the order OH⁻ > Cl⁻ > PO₄³⁻ > NO₃⁻: the lower the positive charge on the N atom, the lesser population of Al pairs and higher incorporation of single Al atoms sited in the vicinity of TPA⁺.

Two ZSM-5 samples of similar Si/Al ratio (≈ 15) were prepared from dry amorphous aluminosilicate precursors with the assistance of TPAOH as OSDA [184]. Silica sol was employed as the Si source, and in the sample ZSM-5_(p) Al source was aluminium butoxide while in the ZSM-5_(s) polyaluminium chloride PAX-18 was used. Prior to the hydrothermal treatment, both dried aluminosilicate precursors were mixed with water, ethanol, NaOH, and NH₃ with the addition of 1 wt% of ZSM-5 seeds. In order to account for the Al position within the zeolite framework ²⁷Al 3Q MAS NMR spectra of the studied materials together with UV/Vis spectra of the samples ion-exchanged with [Co(H₂O)₆]²⁺ were recorded. It was concluded that the majority of Al is facing the channel intersections in both samples, yet the dominant Al distribution in ZSM-5_(p) is as single atoms (83%) whereas the paired Al atoms are prevalent in the ZSM-5_(s) (70%). In addition, the samples are similar in terms of the quantity of Brønsted and Lewis acid sites, containing mainly Brønsted and a few Lewis type sites. Likewise, these acid sites have nearly equal strength. The authors investigated the ethanol transformation to hydrocarbons in the presence of the prepared materials. Based on the FTIR and *operando* experiments, it was found that the ethanol adsorption on the protonic sites is faster on isolated Al than on the paired sites. At 250 °C the conversion degree is lower for the paired Al sites, but both catalysts exhibit high selectivity towards ethene. The paired Al atoms stabilize the ethanol molecule by forming an additional hydrogen bond, thus promoting the ethanol-ethoxy-mediated dissociative pathway. Besides, the adjacent Brønsted sites facilitate

the dimerization and hydrogen-transfer reactions. The data suggest that the regeneration of Brønsted acid sites at higher temperatures takes place via releasing of ethane [184]. Another study reports the synthesis of two series of ZSM-5 zeolite materials with silica sol and tetraethylorthosilicate (TEOS) as the silicon source. Both series of materials present similar properties in terms of their acidity, morphology, and textural properties. Nevertheless, they differ with respect to aluminium location in the framework, as in the silica sol series prevails the Al position in the sinusoidal and straight channels, while in the samples prepared in TEOS systems Al is dominantly sited in the channel intersections. Consequently, they exhibit different performance as catalysts in methanol to olefins reaction. The results suggest the Al in the channel intersections favours the aromatic cycle reaction pathway while the Al in the channels promotes the alkene cycle in MTO reaction [185].

In terms of their performance in a specific application, nanosized materials may exhibit strikingly different behavior than their micron-sized counterparts. Keeping this in mind, researchers have devoted special attention to design nanosized zeolites presenting particular properties. For instance, nanosized ZSM-5 materials were synthesized in a system with varying H₂O/Al ratio from 200 to 2600. Decreasing the Al content in the synthesis mixture yielded samples with Al distributed at the rim of the crystals. In addition, these acid sites were more abundant and stronger. However, testing these materials as catalysts in methanol to hydrocarbon (MTH) reaction showed they are less stable and have lower catalyst capacity than the samples prepared with higher Al concentration [186]. In another study, nanosized ZSM-5 materials were prepared at 100, 120, 150, and 170 °C [187]. The materials present similar Si/Al ratio (≈ 30), but the particle size, the number of acid sites, and their strength increase with the increase of synthesis temperature. Further, in the samples that crystallized at lower temperatures (100 and 120 °C), deposition of amorphous aluminosilicate species within the zeolite particles was observed, suggesting that under such synthesis conditions, the incorporation of aluminum in the zeolite framework is reduced. Upon testing in MTO reaction, the ZSM-5 material prepared at the lowest temperature (100 °C) showed the most extended catalyst lifetime, highest propene selectivity, and light olefins yield. On the other hand, on the materials synthesised at higher temperatures (150 and 170 °C), the aromatics cycle pathway of the MTO became more expressed, resulting in more ethene produced. The high-temperature samples present more than the double quantity of coke in the spent catalyst than do the samples prepared at 100 and 120 °C. Further, in the materials obtained at 150 and 170 °C are present alkylated polycyclic aromatic compounds, whereas in the chromatograms of the spent 100 °C ZSM-5 were detected partially hydrogenated oxygen-containing species. The reason for such different behaviour of the ZSM-5 sample prepared at 100 °C is the lower acid site density, lower acid strength, and shorter diffusion path. The larger external surface area of this sample also contributes to better performance in the MTO reaction [187].

Aggregated nanosized MFI-type crystals with size from 30 to 2000 nm were prepared using different quantities of sodium bromide by a two-step heating hydrothermal synthesis. The decrease of NaBr content resulted in lowering the crystal size and higher ratio of weak to strong acid sites, as well as in the higher number of Brønsted acid sites at the external surface as determined by di-tert-butylpyridine titration. Moreover, the total number of Brønsted acid sites, as well as the ratio of Brønsted to Lewis acid sites, is decreasing [188]. Testing of these materials as catalysts in methanol to hydrocarbon reaction showed that the samples with

Table 3. Gel composition and initial silica and alumina sources in the starting zeolite synthesis mixture; Si/Al ratio and preferred Al location in the final high silica zeolite products yielded from respective synthesis mixtures.

molar oxide composition with OSDA*	Al source	Si source	zeolite framework	preferred Al location	Si/Al	reference
1 SiO ₂ : 0.01 Al ₂ O ₃ : 0.5 TPAOH : 8.3 H ₂ O	Al(NO ₃) ₃ [‡]	40 wt% SiO ₂ [†]	MFI	intersections	53	[176]
1 SiO ₂ : 0.01 Al ₂ O ₃ : 0.25 TPAOH : 0.1 NaCl : 8.3 H ₂ O	Al(NO ₃) ₃	40 wt% SiO ₂	MFI	channels + intersections	52	[176]
1 SiO ₂ : 0.01 Al ₂ O ₃ : 0.4 Dpa : 0.1 Na ₂ O : 25 H ₂ O	Al(NO ₃) ₃	40 wt% SiO ₂	MFI	intersections	42	[176]
1 SiO ₂ : 0.01 Al ₂ O ₃ : 0.4 Cha : 0.1 Na ₂ O : 25 H ₂ O ⁺	Al(NO ₃) ₃	40 wt% SiO ₂	MFI	intersections	51	[176]
1 SiO ₂ : 0.01 Al ₂ O ₃ : 0.5 HMi : 0.1 Na ₂ O : 25 H ₂ O : 0.07 H ₂ SO ₄	Al(NO ₃) ₃	40 wt% SiO ₂	MFI	intersections	48	[176]
OSDA: TPA ⁺ + Na ⁺	Al(NO ₃) ₃		MFI	single Al	13	[177]
OSDA: TPA ⁺ + Na ⁺	Al(NO ₃) ₃		MFI	single Al	20	[177]
OSDA: TPA ⁺ + Na ⁺	AlCl ₃		MFI	single Al	30	[177]
1 SiO ₂ : 0.02 Al ₂ O ₃ : 0.5 PET : 0.125 Na ₂ O : 25 H ₂ O	Al(NO ₃) ₃	40 wt% SiO ₂	MFI	channels	24	[178]
1 SiO ₂ : 0.02 Al ₂ O ₃ : 0.25 TPAOH : 0.1 NaCl : 8.3 H ₂ O	Al(NO ₃) ₃	40 wt% SiO ₂	MFI	channels + intersections	24	[178]
1 SiO ₂ : 0.02 Al ₂ O ₃ : 0.25 TPAOH : 8.3 H ₂ O	Al(NO ₃) ₃	40 wt% SiO ₂	MFI	intersections	24	[178]
1 SiO ₂ :0.02 Al ₂ O ₃ : 0.25 TPAOH : 60 H ₂ O : 0.25 HF	Al(NO ₃) ₃	40 wt% SiO ₂	MFI	intersections	26	[179]
1 SiO ₂ : 0.02 Al ₂ O ₃ : 0.25 NaCl : 0.25 TPAOH : 60 H ₂ O	Al(NO ₃) ₃	40 wt% SiO ₂	MFI	channels + intersections	28	[179]
1 SiO ₂ : 0.02 Al ₂ O ₃ : 0.5 PDO : 0.125 Na ₂ O : 27 H ₂ O	Al(NO ₃) ₃	40 wt% SiO ₂	MFI	channels + intersections	23	[179]
1 SiO ₂ : 0.02 Al ₂ O ₃ : 0.5 HDO : 0.125 Na ₂ O : 27 H ₂ O	Al(NO ₃) ₃	40 wt% SiO ₂	MFI	channels + intersections	22	[179]
1 SiO ₂ : 0.02 Al ₂ O ₃ : 0.5 GLY : 0.125 Na ₂ O : 27 H ₂ O	Al(NO ₃) ₃	40 wt% SiO ₂	MFI	channels	23	[179]
1 SiO ₂ : 0.02 Al ₂ O ₃ : 0.5 DEG : 0.125 Na ₂ O : 27 H ₂ O	Al(NO ₃) ₃	40 wt% SiO ₂	MFI	channels + intersections	21	[179]
1 SiO ₂ : 0.02 Al ₂ O ₃ : 0.5 TEG : 0.125 Na ₂ O : 27 H ₂ O	Al(NO ₃) ₃	40 wt% SiO ₂	MFI	channels	21	[179]
1 SiO ₂ : 0.02 Al ₂ O ₃ : 0.5 TBO : 0.125 Na ₂ O : 27 H ₂ O	Al(NO ₃) ₃	40 wt% SiO ₂	MFI	channels	21	[179]
1 SiO ₂ : 0.02 Al ₂ O ₃ : 0.5 TME : 0.125 Na ₂ O : 27 H ₂ O	Al(NO ₃) ₃	40 wt% SiO ₂	MFI	channels	22	[179]
1 SiO ₂ : 0.02 Al ₂ O ₃ : 0.5 PET : 0.125 Na ₂ O : 27 H ₂ O	Al(NO ₃) ₃	40 wt% SiO ₂	MFI	channels	22	[179]
1 SiO ₂ : 0.02 Al ₂ O ₃ : 0.125 Na ₂ O : 27 H ₂ O	Al(NO ₃) ₃	40 wt% SiO ₂	MFI	channels	19	[179]
1 SiO ₂ : 0.025 Al ₂ O ₃ : 0.25 TPA : 27 H ₂ O	Al(NO ₃) ₃	40 wt% SiO ₂	MFI	intersections	20	[180]
1 SiO ₂ : 0.020 Al ₂ O ₃ : 0.50 PET : 0.025 NaOH : 27 H ₂ O	Al(NO ₃) ₃	40 wt% SiO ₂	MFI	channels	28	[180]
1 SiO ₂ : 0.033 Al ₂ O ₃ : 0.5 TPAOH : 50 H ₂ O	Al(NO ₃) ₃	40 wt% SiO ₂	MFI	intersections	31	[181]
1 SiO ₂ : 0.033 Al ₂ O ₃ : 0.5 PET : 0.125 Na ₂ O : 25 H ₂ O	Al(NO ₃) ₃	40 wt% SiO ₂	MFI	channels	29	[181]
1 SiO ₂ : 0.033 Al ₂ O ₃ : 0.98 NBA : 0.08 Na ₂ O : 10 H ₂ O	NaAlO ₂	fumed SiO ₂	MFI	channels + intersections	27	[181]
1 SiO ₂ : 0.025 Al ₂ O ₃ : 0.5 TPAOH : 50 H ₂ O	Al(NO ₃) ₃	40 wt% SiO ₂	MFI	intersections	39	[181]
1 SiO ₂ : 0.025 Al ₂ O ₃ : 0.5 PET : 0.125 Na ₂ O : 25 H ₂ O	Al(NO ₃) ₃	40 wt% SiO ₂	MFI	channels	39	[181]
1 SiO ₂ : 0.025 Al ₂ O ₃ : 0.98 NBA : 0.08 Na ₂ O : 10 H ₂ O	NaAlO ₂	fumed SiO ₂	MFI	channels + intersections	37	[181]
OSDA: TPA ⁺	Al-butoxide [‡]	30 wt% SiO ₂ [†]	MFI	intersections, paired Al	15	[184]
OSDA: TPA ⁺	poly-AlCl ₃ [‡]	30 wt% SiO ₂	MFI	intersections, single Al	15	[184]
0.94 SiO ₂ : 0.03 Al ₂ O ₃ : 0.54 PYR: 0.48 HF : 4.6 H ₂ O	Al-isopropoxide [‡]	TEOS	FER	T3 site	-	[202]
0.94 SiO ₂ : 0.03 Al ₂ O ₃ : 0.06 TMA : 0.48 PYR : 0.48 HF : 4.6 H ₂ O	Al-isopropoxide	TEOS	FER	T1 site	-	[202]

SiO ₂ : 0.033 Al ₂ O ₃ : 0.54 PYR : 0.5 HF : 5 H ₂ O	alumina	40 wt% SiO ₂	FER	8MR	13	[204]
SiO ₂ : 0.033 Al ₂ O ₃ : 0.06 TMAOH : 0.48 PYR : 0.5 HF : 5 H ₂ O	alumina	40 wt% SiO ₂	FER	8MR	17	[204]
SiO ₂ : 0.033 Al ₂ O ₃ : 0.06 TMAOH : 0.48 HMI : 0.5 HF : 5 H ₂ O	alumina	40 wt% SiO ₂	FER	10MR	17	[204]
SiO ₂ : 0.133 Al ₂ O ₃ : 0.5 TMAdaOH : 44 H ₂ O	Al(OH) ₃	40 wt% SiO ₂	CHA	single Al	15	[217]
SiO ₂ : 0.067 Al ₂ O ₃ : 0.5 TMAdaOH : 44 H ₂ O	Al(OH) ₃	40 wt% SiO ₂	CHA	single Al	25	[217]
SiO ₂ : 0.033 Al ₂ O ₃ : 0.5 TMAdaOH : 44 H ₂ O	Al(OH) ₃	40 wt% SiO ₂	CHA	single Al	26	[217]
1 SiO ₂ : 0.133 Al ₂ O ₃ : 0.3 TMAdaOH : 0.2 NaOH : 44 H ₂ O	Al(OH) ₃	40 wt% SiO ₂	CHA	increased fraction of paired Al	15	[217]
1 SiO ₂ : 0.133 Al ₂ O ₃ : 0.4 TMAdaOH : 0.1 NaOH : 44 H ₂ O	Al(OH) ₃	40 wt% SiO ₂	CHA	increased fraction of paired Al	25	[217]
1 SiO ₂ : 0.133 Al ₂ O ₃ : 0.21 TMAdaOH : 0.29 NaOH : 44 H ₂ O	Al(OH) ₃	40 wt% SiO ₂	CHA	increased fraction of paired Al	13	[217]
1 SiO ₂ : 0.033 Al ₂ O ₃ : 0.25 TMAdaOH : 0.25 KOH : 44 H ₂ O	Al(OH) ₃	40 wt% SiO ₂	CHA	small fraction of paired Al	15	[220]
1 SiO ₂ : 0.033 Al ₂ O ₃ : 0.125 TMAdaOH : 0.375 KOH : 44 H ₂ O	Al(OH) ₃	40 wt% SiO ₂	CHA	single Al	14	[220]
1 SiO ₂ : 0.033 Al ₂ O ₃ : 0.024 TMAdaOH : 0.476 KOH : 44 H ₂ O	Al(OH) ₃	40 wt% SiO ₂	CHA	single Al	10	[220]
1 SiO ₂ : 0.0125 Al ₂ O ₃ : 0.35 TMAdaOH : 18 H ₂ O	Al(OH) ₃	40 wt% SiO ₂	CHA	single Al	30	[221]
1 SiO ₂ : 0.0125 Al ₂ O ₃ : 0.35 TMAdaOH : 18 H ₂ O	FAU [‡]	FAU [†]	CHA	increased fraction of paired Al	36	[221]
1 SiO ₂ : 0.0125 Al ₂ O ₃ : 0.45 TMAdaOH : 12.3 H ₂ O	FAU	FAU	CHA	increased fraction of paired Al	40	[221]
20.5–21 SiO ₂ : 1 Al ₂ O ₃ : 1.8 Na ₂ O : 1 TEOH : 15.2 H ₂ O	NaAlO ₂	SiO ₂ spheres [†]	MOR	8MR	10	[233]
120 SiO ₂ : 1 Al ₂ O ₃ : 8.6 Na ₂ O : 12 TBAOH : 1420 H ₂ O	NaAlO ₂	40 wt% SiO ₂	MEL	10MR	121	[271]
120 SiO ₂ : 0.5 Al ₂ O ₃ : 8.6 Na ₂ O : 12 TBAOH : 1420 H ₂ O	NaAlO ₂	40 wt% SiO ₂	MEL	10MR	213	[271]
80 SiO ₂ : Al ₂ O ₃ : 46.4 TBAOH : 1280 H ₂ O	Al(NO ₃) ₃	TEOS	MEL	increased fraction at intersections, paired Al	35	[272]
80 SiO ₂ : Al ₂ O ₃ : 32 TBAOH : 1280 H ₂ O : NaCl	Al(NO ₃) ₃	TEOS	MEL	intersections, paired Al	34	[272]
80 SiO ₂ : Al ₂ O ₃ : 32 TBAOH : 1280 H ₂ O : NaCl : 0.07 LiCl	Al(NO ₃) ₃	TEOS	MEL	intersections, increased fraction of paired Al	35	[272]
1 SiO ₂ : 0.0025 Al ₂ O ₃ : 0.125 B ₂ O ₃ : 0.1 Na ₂ O : 0.5 PMP : 2 EDA : 100 H ₂ O	Al ₂ (SO ₄) ₃	fumed SiO ₂	RTH	T1, T2 and/or T3	207	[273]
1 SiO ₂ : 0.0025 Al ₂ O ₃ : 0.125 B ₂ O ₃ : 0.1 Na ₂ O : 0.5 MP : 2 EDA : 100 H ₂ O	Al ₂ (SO ₄) ₃	fumed SiO ₂	RTH	T1, T2 and/or T3	190	[273]

*OSDA: pyrrolidine – PYR; tetramethylammonium cation – TMA⁺; hexamethyleneimine – HMI; tetrapropylammonium cation – TPA⁺; dipropylamine – DPA; cyclohexylamine – Cha; pentaerythritol – PET; 1,3-propanediol – PDO; 1,6-hexanediol – HDO; 1,6-hexanediol – HDO; glycerol – GLY; diethylene glycol – DEG; triethylene glycol – TEG; tert-butanol – TBO; trimethylolthane – TME; n-butylamine – nBA; N,N,N-trimethyl-1-admantylammonium cation – TMAda⁺; 1,2,2,6,6-pentamethylpiperidine – PMP; 1-methylpiperidine – MP; ethylenediamine – EDA

[‡]Al(NO₃)₃ · 9H₂O; Al-butoxide – aluminium butoxide; poly-AlCl – polyaluminium chloride PAX-18; Al-isopropoxide – aluminium isopropoxide; FAU – FAU-type zeolite

[†]40 wt% SiO₂ – 40 wt% colloidal SiO₂; 30 wt% SiO₂ – 30 wt% colloidal SiO₂; FAU – FAU-type zeolite; SiO₂ spheres – porous silica spheres

crystal size in the range 80-200 nm and fewer internal Brønsted acid sites promote the selectivity to propylene as well as extend the zeolite catalyst lifetime.

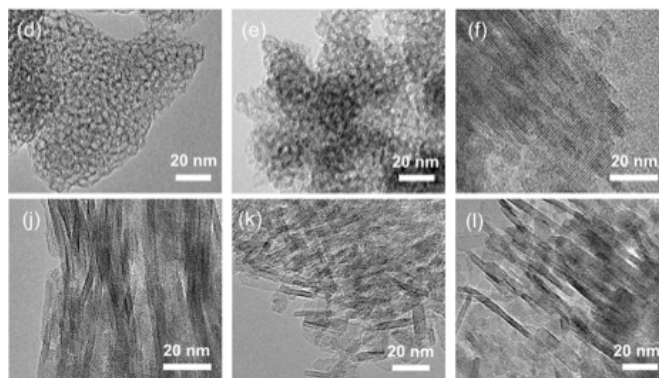


Figure 13. TEM images of nanolayered ZSM-5 materials synthesized using $C_{22}H_{45}-N^+(CH_3)_2-C_6H_{12}-N^+(CH_3)_2-R$ ($R = \text{hexyl or propyl}$). Reproduced with permission from reference [189].

Nanolayered ZSM-5 zeolites of $Si/Al = 19-27$ were synthesized using $C_{22}H_{45}-N^+(CH_3)_2-C_6H_{12}-N^+(CH_3)_2-R$ ($R = \text{hexyl or propyl}$) as structure-directing agents (Figure 13) [189]. Upon using the propyl group instead of hexyl, the crystallization was accelerated due to the mitigated occupation of the MFI channel intersections by quaternary ammonium moieties. When NaF was added to the reaction system, a nanolayered ZSM-5 zeolite of high crystallinity was formed. However, not all Al atoms were incorporated into the zeolite framework, which affects the Brønsted acidity of the prepared materials – the acid sites concentration is lower when compared with a ZSM-5 reference synthesized in the absence of bulky OSDA. The acid site density was found to be a function of the material's crystallinity. Still, the Brønsted acid sites of all the nanolayered ZSM-5 samples were of comparable strength to that of the reference ZSM-5 zeolite. Further, more Lewis acid sites were measured in the nanolayered ZSM-5 zeolites than in the bulk ZSM-5 due to the presence of extra-framework Al species. The prepared materials were tested as catalysts in n-heptane hydroisomerization and methanol-to-hydrocarbons reaction. Their performance correlates well with the Brønsted acid site density of the ZSM-5 zeolites. Yet, the nanolayered ZSM-5 zeolites exhibit similar catalytic performance as the bulk ZSM-5 reference. The higher isomers' selectivity and the selectivity to di-branched isomers of the nanolayered ZSM-5 was attributed to the shorter diffusion pathway. In methanol-to-hydrocarbons reaction, the nanolayered materials showed higher propylene to ethylene ratio than the reference ZSM-5 sample. Furthermore, the turnover number was higher for the nanolayered ZSM-5 zeolites suggesting that all the existing Brønsted acid sites are accessible [189].

4.1.2 FER-type materials

Ferrierite is a medium-pore zeolite which possesses four crystallographically distinct tetrahedral sites in its structure (Figure 14). The sites are distributed over two different channel systems, 10 MR (parallel to the [001] direction) and 8 MR (parallel to the [010] direction) channels. At the intersection of the 8 MR and 10 MR channels, the so-called ferrierite cage is formed. Comprehensive investigations of the Al location within the FER framework have shown that it can be directed by utilizing a particular OSDA. Moreover, heteroatoms such as B, Ga, Ti, and Fe have been successfully incorporated in the FER framework [190-195]. FER-type materials have been obtained in the presence of a range of OSDAs (tetramethylammonium (TMA), pyridine, pyrrolidine (Pyr), choline, piperidine, 2,4-pentandione, etc.) [196]. Besides, very often dual-templating concept is applied for FER

preparation (tetramethylammonium + trimethylamine, tetramethylammonium + 1,3-diaminopropane, pyridine + propylamine, tetramethylammonium + 1-benzyl-1-methylpyrrolidinium (BMP), piperidine + cetylmethylpiperidinium [197–201]). Furthermore, it is possible to prepare ferrierite materials in the absence of OSDAs. In this case, a cooperative effect of Na^+ and K^+ cations was established [202].

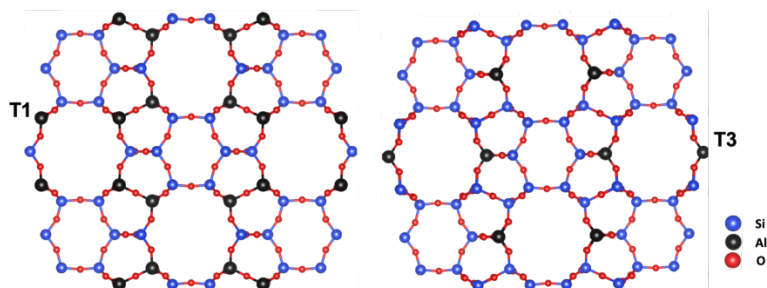


Figure 14. A *c*-axis view on the FER-type framework in the hypothetical case when Al atoms occupy all T1 (left) and T3 (right) sites.

An extensive structural study of FER-type zeolite material of $\text{Si}/\text{Al} = 16$ synthesized using a combination of tetramethylammonium (TMA) and pyrrolidine (Pyr) as OSDAs has shown that TMA^+ species occupy the ferrierite cage solely, whereas Pyr is present in both the ferrierite cage and the 10MR channels (see Table 3). In the latter case, the arrangement of Pyr is slightly different in the sample prepared with pyrrolidine exclusively. The results suggest that in the FER sample prepared in the presence of TMA and Pyr, aluminum tends to populate the T1 site in the 8MR and the cage. As shown in Table 3, in the material prepared solely with Pyr, Al exhibits preference for the T3 site located in the ferrierite cage [203]. The authors surmised that the organic molecules with protons able to form hydrogen bonds with oxygen atoms present a stronger effect on the Al distribution than the quaternary ammonium cations. Namely, in the latter system, the organic moieties shield the positive charge of the N atom, thus disabling the cation to establish strongly directed interactions with the Al-containing species in the zeolite synthesis mixture. Accordingly, Al is not incorporated into a specific position within the zeolite framework. In the case of FER-type materials prepared in the presence of fluoride ions using 1-benzyl-1-methylpyrrolidinium, Pyr, and TMA, the aluminium occupation of T positions depends on the OSDA employed [204].

Using a combination of TMA cations with cyclic amines having different dimensions (pyrrolidine and hexamethyleneimine (HMI)) FER-type zeolites of low Si/Al ratio (< 20) and various Al distributions have been synthesized. When Pyr was used, either in the presence or absence of TMA cations, materials with the majority of the acid sites within the 8MR channels were produced. On the other hand, HMI, together with TMA, resulted in materials having acid sites predominantly located within the 10MR channels [205]. It was suggested that there are very strong electrostatic interactions between the cyclic amines used as OSDAs and the zeolite framework. The change of the acid site distribution depends on the physicochemical properties of the amine and its relative position/orientation within the lattice. Further, the addition of ferrierite seeds to the FER synthesis reaction mixture without the presence of OSDAs yielded material denoted as FER@FER having enhanced crystallinity compared to seed crystals. Such material exhibited a lesser amount of defect sites, i.e., extra-framework Al species yielding Lewis sites, and an increased amount of Brønsted acid sites assigned to stable T2 sites. The highly crystalline FER@FER showed high methyl acetate productivity and selectivity in gas-phase carbonylation of dimethyl ether (DME). Besides, its deactivation rate in this reaction is lower. Tetrahedral Al sites, especially the T2 sites, were found to be the active sites required for the selective formation of hydrogen-bonded DME intermediates by suppressing a competitive water absorption generated by the methanol

dehydration on the Brønsted acid sites [206]. On the other hand, the addition of 3 wt% of FER seeds with respect to silica in the pyrrolidine-based synthesis gel resulted in a FER-type material with lower number of Brønsted acid sites and higher number of Lewis acid sites than the non-seeded synthesis gel [207]. When sodium lauryl sulfate (SLS) surfactant was added to the synthesis gel, a ferrierite material with a substantially higher number of Lewis acid sites than in the materials obtained in the seeded and un-seeded systems. Abundant Lewis acid sites in SLS-derived FER make it inappropriate as a catalyst for the vapor-phase dehydration of methanol to DME since they promote the formation of by-products [207].

Catizzone et al. synthesised FER-type materials using pyrrolidine (Pyr), ethylenediamine (En), tetrahydrofuran (THF) as well as 1,8-diaminooctane (DAO) as OSDAs [195]. Moreover, SLS was used to control the crystal size of the FER-type material prepared with Pyr as OSDA. The obtained crystals were different in size, morphology, and the agglomeration level. At the same time, the addition of SLS to the pyrrolidine mixture resulted in the formation of notably smaller crystals with the longest dimension < 500 nm, than in the absence of SLS. The ^{27}Al MAS NMR data indicate THF produced FER-type materials with all Al built into zeolite framework. Further, in Pyr, En, and DAO samples, there is less than 10% octahedral extra-framework Al. NH_3 -TPD profiles are nearly identical for the Pyr-FER and SLS-Pyr-FER, demonstrating that the surfactant molecules alter the crystal morphology rather than acidic properties. According to IR spectra of the samples studied with adsorbed deuterated acetonitrile, the En-FER and DAO-FER possess the highest concentration of Lewis acid sites ($\approx 40\%$). In THF-FER there is 15% of Lewis acid sites with respect to total acidity. The fraction of strong Lewis acid sites in this series of samples follows the order DAO-FER > En-FER > Pyr-FER (\approx SLS-Pyr-FER) > THF-FER. THF-FER was the least efficient catalyst in methanol to dimethyl ether reaction, which was attributed to the larger size of the crystals. For the same reason, Pyr-FER is less active at 180 °C than nanosized SLS-Pyr-FER, but at higher temperatures, the samples DAO-FER, En-FER, Pyr-FER, and SLS-Pyr-FER display similar performance. In terms of DME selectivity at 180 °C, the yield is 100% over THF-FER and DAO-FER. At higher temperatures, the DME selectivity gradually decreases. THF-FER sample continuously loses its activity during the reaction at 240 °C with the most significant quantity of deposited carbonaceous species. The highest concentration of Brønsted acid sites, as well as the largest size of the crystals, may cause fast deactivation of the THF-FER material. Further, the samples Pyr-FER and SLS-Pyr-FER have similar acidic properties, yet less coke is formed on smaller SLS-Py-FER [195].

4.1.3 CHA

CHA-type zeolite is a small pore material. The CHA framework is a member of both the D6R-only and ABC-6 zeolite structures families. Namely, its structure can be represented by stacking planes of non-connected 6MRs following the AABBC sequence. Further, the CHA-type framework can be represented by the assembling of exclusively D6Rs. *Cha* cage is a part of the three-dimensional pore system, and the CHA-type lattice comprises one unique inequivalent T site. The synthesis of low-silica aluminosilicate CHA-type materials is usually conducted by employing zeolite Y as both Si and Al source in potassium hydroxide reaction media [208]. In order to prepare a CHA material having $\text{Si}/\text{Al} > 5$ (SSZ-13), the presence of an OSDA like N-methyl-3-quinuclidinol iodide, N,N,N-trimethyl-2-ammoniumxonorborane, choline and benzyltrimethyl-ammonium hydroxide in a reaction mixture is required. Still, the N,N,N-trimethyl-1-adamantammonium hydroxide (TMAdaOH) is the most common OSDA for SSZ-13 synthesis [209]. All siliceous CHA material has been attained in the fluoride medium [210]. Recently, efforts have been made in reducing chabazite synthesis costs and finding more environment-friendly preparation routes such as by using TEAOH and/or adding CHA seeds to the reaction mixture [211,212]. Besides well-known silicoaluminophosphate

CHA-type analog SAPO-34, the acidity of CHA-type aluminosilicate zeolites can be tuned by the framework incorporation of heteroatoms. Thus B-, Ge-, Zn-, Sn-, Zr-, In-, Ga- and Ti-containing CHA materials have been prepared, often with the addition of seed crystals to the preparation mixture [213-217].

Recently, Lusardi et al. prepared a series of SSZ-13 materials with varied aluminium content, and hence the materials presented framework Si/Al ratio ranging from 9 to 35 [218]. As the Al amount increased, both the number of Brønsted acid sites and extra-framework Al sites increased too. SSZ-13 of Si/Al = 10 together with MOR- and FER-type materials of similar Si/Al ratio were tested in the reaction of carbonylation of dimethyl ether (DME) to methylacetate (MA). MOR was found to be the most active in the initial stage of the reaction but slowly lost its activity as the carbonaceous deposits formed within the 12MRs channel. FER-type material was a notably less active catalyst, whereas CHA is comparable to MOR selectivity-wise and remains active for a longer time. Further, SSZ-13 materials of lower Al amount yielded less MA because the surface coverage of methoxy groups is broader for materials with more Al; hence the probability for the successful collision with CO is higher. The fact that this relation is not linear is owing to the highest methylacetate production rates on methoxy groups residing in the 8MRs. The lowest carbonylation rates are attained for the methoxy groups in the CHA cage above the 6MR, as predicted by the DFT calculations [218]. In order to tune their acidic properties, Di Iorio et al. synthesized CHA-type zeolite materials (Si/Al = 15–30) in hydroxide media in the presence of TMAda⁺ cations. The samples contained only isolated framework Al sites (see Table 3). The addition of Na⁺ to the zeolite preparation reaction mixture, at the same time, maintaining the concentration of cations ((Na⁺ + TMAda⁺)/Al) and other reaction parameters, yielded SSZ-13 zeolites of a fixed Si/Al ratio but with paired Al sites (Figure 15). The amount of paired sites was found to be a linear function of the Na⁺ incorporated into the crystalline solids [199]. This work was extended by involving various Al sources (Al(OH)₃, AlCl₃, Al(NO₃)₃, NaAlO₂, Al₂O₃, Al(O-*i*-Pr)₃) in the

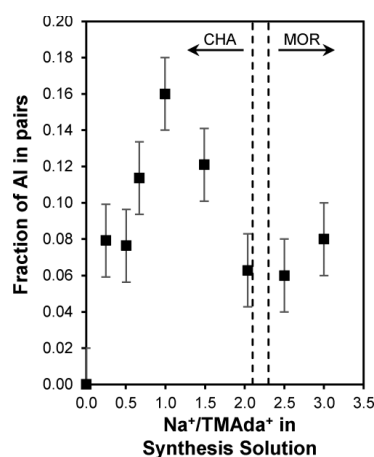


Figure 15. The fraction of paired Al atoms in a series of SSZ-13 zeolites (Si/Al = 15), plotted versus the ratio Na⁺/TMAda⁺ in the initial crystallization mixture of the equivalent total concentration of cations. The dashed field represents the area where a mixture of two phases (CHA and MOR) is formed. Reprinted with permission from reference [219]. Copyright (2016) American Chemical Society.

synthesis. The SSZ-13 material prepared with the aluminium isopropoxide contained a double quantity of the paired Al atoms than the material crystallized using Al(OH)₃. In addition, the CHA-type material prepared from Al(O-*i*-Pr)₃ contained a greater amount of Na⁺ [113]. The data suggest that the Na⁺ is occluded in the extra-framework locations adjacent to the cationic charge of TMAda⁺, consequently directing the formation of paired framework Al atoms. In

methanol dehydration reaction, the samples with paired protons accelerate the turnover rates by order of magnitude compared to the SSZ-13 samples with isolated protons. It seems that the paired protons stabilize surface methoxy species involved in an alternate dehydration mechanism. Interestingly, in the case when K^+ substitutes Na^+ in the otherwise identical reaction conditions, just single 6MR Al atoms are formed in SSZ-13 [220]. This effect was explained by postulating that K^+ competes for TMAda⁺ occlusion within larger void spaces. DFT calculations indicate that in this case, the number of 8MR paired sites might be greater. The ability of paired Al sites in the CHA framework that have high capacity towards divalent cation to get ion-exchanged with Fe^{2+} is convenient for designing catalyst for partial methane oxidation. Namely, the Fe located in the 6MRs with paired Al in the CHA framework are the active sites for this reaction. Inspired by this fact, Devos et al. prepared a series of SSZ-13 samples (Si/Al = 30–45) from amorphous hydrogel precursors and via interzeolite conversion [221]. The materials prepared via interzeolite conversion possessed more paired Al sites and consequently exhibited higher methanol productivity when Fe-modified SSZ-13 materials were employed as catalysts in partial methane oxidation.

In 2018 Nishitoba et al. produced CHA framework-type zeolites with the assistance of TMAdaOH in a system comprising fumed silica, aluminum hydroxide, and the FAU-type zeolite with altering proportions of Al-comprising chemicals – $Al(OH)_3$ and FAU-type zeolite [222]. Besides, 5 wt% of calcined SSZ-13 seed crystals were added to the reaction mixtures. The prepared materials have a similar amount of acid sites, yet the distribution of Al atoms is different. When the proportion of the Al source derived from the FAU-type zeolite was increased, the fraction of Q^4 Si species with two neighboring Al atoms ($Si(OSi)_2(OAl)_2$) was higher as well. The authors correlate the relative population of $Q^4(2Al)$ with the hydrothermal stability of the material since the Al atoms in $Q^4(2Al)$ positions would be easier for dealumination than the ones in $Q^4(1Al)$. A higher fraction of the paired Al sites in the CHA-type materials prepared from the systems with a high quantity of FAU-type zeolite resulted in the formation of a larger amount of aromatic carbonaceous deposits in the material and thus shortened the catalyst lifetime in MTO reaction in comparison to the sample prepared with a lower amount of FAU material [202]. Nanosized SSZ-13 zeolites (Si/Al ratio = 9–25) prepared by steam-assisted synthesis method have been employed in MTO reaction as well. The method involves the preparation of a clear Al-Si precursor sol, followed by water evaporation at 90 °C. The powder was charged in the top part of Teflon-lined autoclave with inserted Teflon vial containing a certain amount of water, avoiding direct contact between liquid water and dried gel. In contrast to SSZ-13 (Si/Al = 14) zeolite prepared by conventional hydrothermal synthesis from amorphous hydrogel precursor, the nanosized vapor-phase synthesized CHA-type material (Si/Al = 15) exhibited 2.6-fold longer catalyst lifetime keeping the 100% conversion. Likewise, the total selectivity towards ethane and propane is higher for the nanosized SSZ-13. This example clearly shows that zeolite downsizing notably contributes to overcoming the diffusion limitations in catalytic processes [223].

Another approach in developing an efficient CHA-type catalyst for MTO is by interzeolite conversion of zeolite L. Different amount of NH_4 -LTL zeolite was added to the system containing fumed silica, TMAdaOH and NaOH providing a series of SSZ-13 materials having Si/Al ratio from 25 to 183. When compared with SSZ-13 prepared from the amorphous hydrogel precursor (Si/Al = 31), the LTL-derived materials have lower peak intensities in the NH_3 -TPD, and the high-temperature desorption peak is shifted towards lower temperatures. Further, the ^{27}Al MAS NMR spectrum of the sample having Si/Al = 47 demonstrates the presence of only tetrahedral Al. The SSZ-13 materials originating from LTL systems present much longer catalyst lifetime and higher selectivities towards ethane and propane in MTO reaction. Maximal catalyst stability and highest ethane and propane yields were achieved for

the SSZ-13 where Si/Al ratio was 96. In this case, the reason for more rapid deactivation of the SSZ-13 obtained from amorphous precursor lies in the higher acid sites density that accelerates coke formation [224]. Lastly, in the Table 4 is demonstrated the effect of zeolite acidic properties on their performance as catalysts in MTO and MTH reactions. In MFI-type material lower amount of Brønsted acid sites favours the formation of propylene, whereas in the case of CHA materials having fewer acid sites ethylene was the main product. In addition, both types of materials deactivate faster if they present a high number of acid sites.

Detailed NMR study of a set of Na-SSZ-13 samples of Si/Al ratio in the range 4–48 prepared with varied Al content in the synthesis gel revealed that in the high silica Na-CHA zeolite, Na⁺ cations are preferentially found at 6MR cationic SIIa0 site corresponding to one Al in the *Cha* cage. As the Al content rises, Na⁺ ions are located at 6MR SIIa1 and 8MR SIII'a1 sites suggesting the presence of Al pairs. In low silica CHA materials, Na⁺ cations occupy all possible ion-exchange sites of the CHA framework due to many Si(2Al) and Si(3Al) moieties [225]. In a recent study, SSZ-13 material was obtained by non-classical attachment growth of nano building blocks mediated by Pickering emulsion in a biphasic water/toluene medium aided by trimethoxy[3-(phenylamino)propyl]silane. 95% of Al present in the solid sample was incorporated into the CHA zeolite framework, and, as observed by NH₃-TPD, it presented acidity comparable to the CHA-type material prepared from a conventional synthesis mixture. Upon ion-exchange with Cu²⁺, this material outperformed the conventional one as a catalyst in NO_x removal by NH₃-SCR under both, low- and high-temperature conditions [226].

Table 4. Impact of MFI- and CHA-type zeolite acidic properties on the MTO and MTH reactions.

Property	Catalytic performance	Reference
MFI-type materials		
Al at channel intersections	aromatic cycle	[185]
channel Al	alkene cycle	[185]
	improved endurance of catalysts to coking	[179]
Al at the rim of the crystals	less stable catalyst of lower capacity	[186]
less Brønsted acid sites	alkene cycle	[187]
lower Brønsted acid site strength	alkene cycle	[187]
fewer internal Brønsted acid sites	higher selectivity to propylene extended catalyst lifetime	[188]
CHA-type materials		
higher fraction of paired Al	shorter catalyst lifetime	[222]
higher acid sites density	shorter catalyst lifetime higher propylene yield	[224]

4.1.4 MOR

MOR-type zeolite framework contains a straight 12 MR channel intersecting with 8 MR side pockets. There are four unique T positions in the MOR-type framework: T1 in the 12 MR channel, T2 and T4 in the intersection between the 12 MR channel and the 8MR pocket, and T3 within the 8MR pocket. It has been found that in mordenite, Al preferentially resides in T3 and T4 sites (Figure 16) [227]. Mordenite occurs as a mineral and with the Si/Al ratio of 5 is the most siliceous natural zeolite. MOR-type materials of Si/Al up to 10 can be prepared without OSDAs (Table 3) [228], whereas the higher Si content has been reached with the assistance of TEA⁺, *n*-butanol, 1-butyl-3-methylimidazolium bromide, etc. [229–232]. It should be noted that all-silica MOR-type material has not been prepared so far. Similar to

other zeolite frameworks, the properties of MOR-type materials have been altered by incorporation of different heteroatoms (B, Ti, Fe, Zn, Ga, Sn, ...) into the framework [233–238].

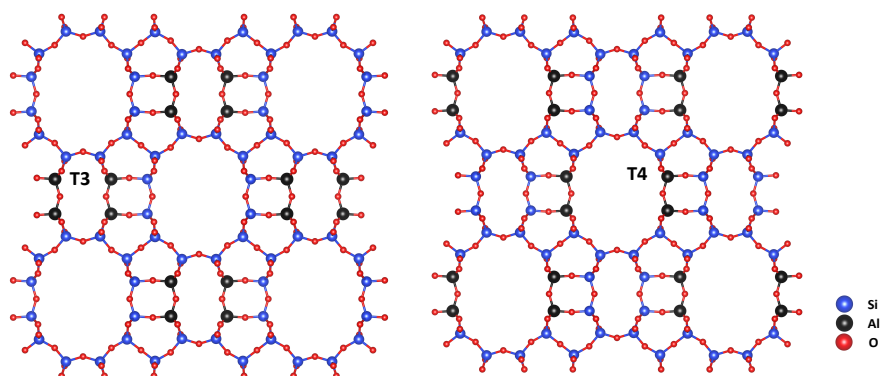


Figure 16. A *c*-axis view on the MOR framework in the hypothetical case when Al atoms occupy all T3 (left) and T4 (right) sites.

Millimeter-sized mordenite (MOR) zeolite spheres (Si/Al = 6–10) with excellent mechanical strength have been prepared via vapor-assisted transformation of Na- and Al-doped SiO₂ spheres in the presence of tetraethylammonium hydroxide (TEAOH), tetramethylammonium hydroxide (TMAOH), hexamethylenimine (HMI) and water (Figure 17) [239]. According to the ¹H MAS NMR spectra and NH₃-TPD analysis, the quantity of Brønsted acid sites in the MOR synthesized from TEAOH-containing system is higher than in commercial mordenite with Si/Al = 6.5 and the similar total amount of acid sites. Moreover, in the TEAOH sample, the number of Brønsted acid sites in the 8MR side pockets is determined to be three times higher than that in the 12MRs (Table 3). As a consequence of the preferential position of acid sites in the 8-MR side pockets, the TEA-MOR material displays superior catalytic activity in the DME carbonylation reaction with a steady DME conversion of 90% in comparison to 23% conversion over the commercial MOR sample. Both samples are highly selective towards methyl acetate (> 95%), yet TEA-MOR catalyst slightly outpaces the commercial one [239]. Nanocrystalline mordenite (nanorods and nanosheets) materials of Si/Al = 30–56 and possessing up to 60% of acid sites located on the external surface have been prepared with the aid of Gemini-type surfactants. On the other hand, conventional MOR crystals in the commercial sample have only 12% of the acid sites at the external surface. Still, all of the

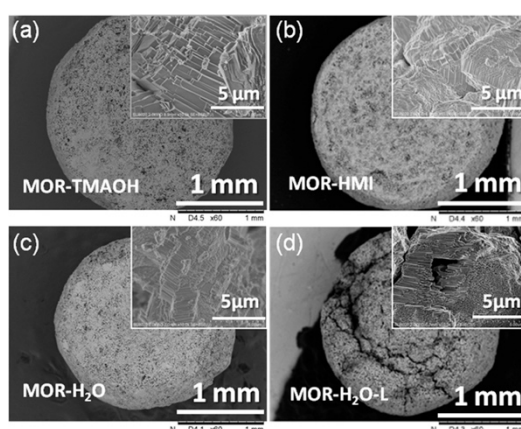


Figure 17. SEM images of MOR spheres synthesized under TMAOH, HMI, and H₂O vapors. Reprinted with permission from reference [239]. Copyright (2018) American Chemical Society.

studied materials, both nanocrystalline as well as micron-sized MOR, exhibit a similar fraction of strong Brønsted and Lewis acid sites [240]. Owing to the improved accessibility of active sites, the nanorod and nanosheet mordenites show higher catalytic activity in acid-catalyzed annulation reaction of 2-naphtol with methylbut-3-en-2-ol than does the commercial zeolite. Furthermore, over the nanorod MOR-type material was achieved the highest yield of dihydronaphthofuranes [240]. In a similar study, Wang et al. prepared a hierarchical MOR, which had acid sites identical in nature, yet more abundant than the conventional MOR-type material synthesized without utilizing Gemini-type surfactant [241]. Both materials are stable and active catalysts for the dehydration of ethanol.

Liu et al. have fabricated hierarchical MOR-type nanosheets by self-assembly of nanocrystals and hexadecyltrimethylammonium bromide (CTAB) combined with polyethylene glycol (PEG) molecules. In comparison to material synthesized in the absence of CTAB and PEG, a higher amount of both Brønsted and Lewis acid sites is present within the hierarchical pore system. Accordingly, nanosheet MOR material exhibits higher activity, xylene selectivity, and longer catalyst lifetime in the toluene disproportionation reaction [242]. The PEG has acted as a mesopore generation agent in the formation of a set of hierarchical MOR catalysts with enhanced crystallinity and a higher quantity of strong acid sites in comparison to the reference zeolite obtained without PEG [243]. The stability and activity of the PEG-MOR-type materials employed as catalysts for DME carbonylation is greatly enhanced with respect to the conventional MOR-type sample. In the course of the reaction, the selectivity towards methyl acetate was always higher than 98.5% for the hierarchical MOR materials. Besides, markedly lower selectivities towards methanol and hydrocarbons are achieved over PEG-MOR than over reference MOR, suggesting that the side-reactions are hindered for the hierarchical catalysts. Clearly, a more significant amount of strong acid sites and improved mass transfer efficiency facilitate the DME conversion over the PEG-MOR-type materials [243].

4.1.5 Zeolite Beta (BEA@BEB)

Zeolite Beta possesses a three-dimensional system of intersecting channels and nine distinct crystallographical T sites. Zeolite Beta is a disordered material, but this does not cause any blocking of the 3D 12MR channel system [4]. The family of zeolite Beta consists of three polymorphs: polymorph A (BEA), polymorph B (BEB), and polymorph C (BEC). Typical zeolite Beta contains polymorphs A and B in a ratio 60:40 [244]. Polymorph A- and polymorph B-enriched materials have been synthesized [245,246], whereas polymorph C has been firstly prepared as Ge-silicate material [227], and subsequently, a pure silica material was obtained [248]. All-silica standard zeolite Beta can be prepared in both fluoride and hydroxide media [210,249]. Further, next to Al, a range of other atoms (Ti, Sn, B, Zr, Hf, Zn, etc.) have been incorporated into zeolite framework in various positions either by *in situ* or post-synthesis methods [244,250–257]. TEOH is a typical OSDA for zeolite Beta synthesis [258], though it can be obtained with numerous organic templates [144,244,259].

The Al atoms in the as-synthesized zeolite Beta samples of Si/Al ratios 9–215 prepared in fluoride medium with TEA as OSDA were found to reside in two crystallographically distinct positions [260]. The site denoted as Td2 becomes more populated with increasing the framework Si content. However, in the calcined materials of Si/Al = 9–56 octahedral Al species appear. In addition, for the calcined materials, the Td1 site is more populated than Td2. In the case of zeolite Beta sample of Si/Al = 215 the Td2 signal in ^{27}Al 3Q MAS NMR resolved into two components. The observed effect is attributed to TEA⁺ cations, which affect the T–O–T angles and shield the Al and Si atoms, thus changing the chemical shifts of some T sites. Noteworthy, the different populations of T sites indicate non-random Al distribution within the zeolite framework. The results suggest that the octahedral Al sites detected upon

calcination are formed by the conversion of tetrahedrally coordinated Al located at specific sites and with another Al site in close proximity needed for the hydrolysis of the Si–O–Al bond [260]. Zhao et al. have prepared high-silica Beta zeolite (Si/Al = 136–340) employing TEAOH as OSDA in the presence of HF. Expectedly, the acid site density in the obtained materials got lower with the increase of the Si content in the framework. The authors varied the HF content (HF/SiO₂ = 0.35–0.65) in the reaction mixture, keeping the ratio between the other reactants constant [261]. The increase of HF content leads to Beta zeolites having similar NH₃-TPD profiles, but a different distribution of tetrahedral Al species, as shown by the ²⁷Al MAS NMR spectra. A broad weak signal in the range -20–0 ppm corresponding to extra-framework octahedral Al becomes more pronounced as the quantity of the HF added to the synthesis mixture is reduced. Furthermore, the sample prepared with the lowest HF amount presents a broad resonance at about 15 ppm, which most probably arises from distorted extra-framework octa- or penta-coordinated Al species, yet in a different environment than the ones around 0 ppm. The ²⁷Al MQ MAS NMR spectra suggest that Al atoms primarily abide T3, T7, T8, and T9 sites in all samples, but the relative population of these sites varies. In all materials, the relative occupancy of the T8 and T9 sites by Al is about 90%. This study unambiguously showed that the HF content of the synthesis mixtures directly impacts the stability of Al species as well as the Al distribution within the ultimate crystalline products. The sample of medium HF/SiO₂ ratio, 0.45, exhibited the longest catalyst lifetime in methanol conversion with propene selectivity of 49.7–58.3 % via the dominantly alkane-based mechanism of the reaction. In this study for the first time, were detected phenol compounds in the spent catalyst. The authors hypothesize that the phenols get strongly adsorbed on the acid sites and thus induce the catalyst deactivation. It was concluded that the cooperative effect of the catalyst acidity and the reaction temperature impact the overall MTO reaction. A small quantity of acid sites facilitates the formation of propene, and high reaction temperatures increase the cracking ability of heavier olefins as well as promote the diffusion of the products [261]. In a series of zeolite Beta samples (Si/Al = 15–230) synthesized in fluoride medium with the quantity of Brønsted acid sites correlates with the Al content. The tetrahedral T atoms present three peaks in ²⁷Al MAS-NMR spectra displaying different environment of the framework Al. The highest fraction of extra-framework Al with respect to the total Al amount was observed in the materials with the Si/Al = 230 due to a lower degree of Al incorporation. When tested as catalysts in aqueous phase cyclohexanol dehydration, samples with a lower number of Brønsted acid sites exhibit longer catalyst lifetime [262].

Uniform nanosized high-silica Beta zeolites (10–20 nm) obtained by Martinez-Franco et al. in OH⁻ and F⁻ media using simple alkyl-substituted flexible dicationic OSDAs (1,10-(pentane-1,5-diyl)bis(1-butylpyrrolidin-1-ium) and 1,10-(pentane-1,5-diyl)bis(1-butylazepan-1-ium)) present Si/Al ratio ranging from 13 to 31 [263]. Almost 80% of the Al species are retained at tetrahedral positions upon the calcination in these nano-sized zeolite Beta samples. The materials of Si/Al ratio 15 synthesized both in hydroxide and fluoride media show the highest number of Brønsted acid sites. In accordance with the lower Al content, the zeolite Beta materials having the Si/Al ratio 30 exhibit lower Brønsted acidity. Nevertheless, these sites are stronger than the ones in the samples of Si/Al=15, as determined by pyridine desorption at 350 °C. The studied materials have been tested as catalysts in the cumene synthesis via alkylation of benzene with propylene. The highest cumene yield as compared to the commercial nano-sized Beta zeolite, as well as reduced catalyst deactivation with time on stream, has been achieved for the samples of Si/Al = 15 due to its higher Brønsted acidity [263]. The same research group prepared a set of nano-sized zeolite Beta with the assistance of N-butyl-N-methylhexamethyleneiminium hydroxide, N-butyl-N,N-dimethylcyclohexylammonium hydroxide and N-butyl-N,N-dimethylcycloheptylammonium hydroxide in hydroxide medium [264]. The Si/Al ratio of the crystalline product was

controlled by variation of the composition of the initial reaction mixture – the gels of Si/Al ratio 15 and 30 produced samples of approximately equal Si/Al ratios, that is 15 and 30, respectively. In each of the pristine Beta zeolites, all the Al species are present in tetrahedral coordination. After the calcination at 580 °C, in the material of Si/Al = 15, 15–20% of Al is released from the framework. However, in the Beta samples having Si/Al ratio 30, only about 5% of Al was released from the framework upon calcination. Similarly to the previously described series of Beta zeolite, the samples with higher Al content exhibited a higher quantity of Brønsted acid sites. Likewise, these materials show enhanced catalytic activity and selectivity towards desired molecules in the industrially relevant reaction of benzene propylation to cumene. The nanosized BEA-type materials are active and stable catalysts for the oligomerization reaction of 1-pentene, with diesel being the most dominant product [264]. Sazama et al. prepared Al-rich zeolite Beta materials (Si/Al = 4.5 and 5.1) in an OSDA-free system using seeds. The materials possess a very low fraction of extra-framework octahedral Al. In comparison to the commercial zeolite Beta (Si/Al = 11) prepared in an OSDA-containing system, the seeded materials present a higher number of acid sites yet of similar strength as the commercial material [265]. In the Al-rich zeolite Beta samples, 40% to 100% of all Al atoms are found in the Al–O–Si–O–Al sequence while in the Si-rich commercial sample, these sequences were not observed. Further, in the Al-rich material, the Al atoms face two different channels, whereas two Al atoms from two different Al–O–Si–O–Al sequences can be oriented towards the same channel denoting close unpaired Al atoms sited in two different rings. Only Al atoms in Al–O–Si–O–Si–O–Al sequences in one ring and a small relative population of Al–O–Si–O–Al sequences face the same channel. It was concluded although the Al- and Si-rich BEA samples exhibit significant differences in the distribution of the Al–O–Si–O–Al sequence, they are similar in terms of the arrangement of Si and Al in the zeolite channels and accordingly are similar in binding counter-ion species [265]. The same group reported that the Al-rich zeolite beta materials with a higher number of Brønsted acid sites are more active in the alkylation of benzene with ethylene. This reaction is not affected by the Lewis sites [266]. Further, a series of hierarchical zeolite Beta was prepared from concentrated amorphous precursors ($H_2O/Si = 2.5–14$) using TEOH as OSDA. As the synthesis time was extended, and the crystallinity degree of the materials increased, the total concentration of medium and strong Brønsted acid sites got higher. Likewise, the ratio of Brønsted and Lewis acid sites in the more crystalline materials increased. These materials were found efficient catalysts in 1-octadecanol conversion [267].

4.1.6 Other framework type materials

FAU-type zeolites represent the bedrock of oil refining with their acidic properties mostly engineered by post-synthesis treatments. Namely, FAU-type zeolites of Si/Al ≈ 2.5 can be obtained from conventional $Na_2O-SiO_2-Al_2O_3-H_2O$ systems. Higher Si/Al ratios are achieved by dealumination, usually by the steaming process, since the *in situ* methods are not very efficient. Hence, a large part of the *in situ* work is devoted to developing organic-free methods of preparing high-silica FAU-type materials. Recently Ferdov et al. obtained a series of zeolite Y materials of Si/Al > 2.5 from the OSDA-free system with higher framework stability than the reference industrial zeolite Y [268]. These materials were less prone to generate extra-framework Al species upon calcination than the commercial zeolite of similar Al content. On the other hand, the commercial zeolite Y maintained a higher crystallinity degree. Nevertheless, both types of materials exhibit comparable activity towards cracking of 1,3,5-triisopropylbenzene. Venkatesan et al. have prepared mesoporous zeolite Y using seeded initial gel and amphiphilic organosilane (3-(trimethoxysilyl)propyl octadecyldimethylammonium chloride) [269]. The resultant material exhibits a higher number of strong external acid sites when compared to the material prepared from a system where

zeolite crystals were added as seeds instead of the seeded gel. Consequently, mesoporous zeolite Y showed high catalytic activity towards decalin cracking owing to the high accessibility of acid sites located on the external zeolite crystal surfaces. In addition, the selectivity to light hydrocarbons was almost four-fold greater than of heavy hydrocarbons being 79% and 20%, respectively.

MEL-type zeolite belongs to the pentasil family of high silica zeolites, which possesses two intersecting 10MR channel systems. In contrast with the MFI-type zeolite, which also has two intersecting 10MR channel systems, the MEL contains only straight channels. Tetrabutylammonium cation is the typical OSDA for the synthesis of MEL-type material, and the aluminium containing materials are denoted as ZSM-11 while the all-silica counterpart as silicalite-2 [270]. A thorough study of ZSM-11 synthesized in a Na^+/TBA^+ system, as presented in Table 3, revealed that Al preferentially occupies sites in the straight 10MR channels of the MEL framework. In the case of ZSM-5 obtained from Na^+/TPA^+ system, the fraction of Al located at the MFI channel intersections was higher. This difference in acid site location is reflected in substantially different performance and mechanisms in the MTO reaction for the two zeolite materials. The intersection acid sites promote the aromatic cycle, whereas the alkene cycle is preferred for the acid sites in the straight channels. Consequently, the accumulation of coke species in ZSM-11 is faster and results in its short catalytic lifetime [271]. Wang et al. further extended this work by investigating the impact of the addition of varied quantities of Na^+ and Li^+ cations to the ZSM-11 preparation mixture with a higher concentration of TBAOH than in the previous study [272]. The prepared materials present bulk $\text{Si}/\text{Al} \approx 35$. Although their acid sites were of similar strength, the data suggest that the presence of Na^+ in the reaction mixture does not have a considerable impact on the Brønsted sites, whereas Li^+ reduces their number. ^{27}Al MAS NMR demonstrated that the ZSM-11 material prepared in an alkali-free system has slightly higher occupancy of Al in the channel intersection positions (54.7%) than in the straight channels. Herein, with the addition of Na^+ and/or Li^+ , Al showed a higher preference for the intersection sites. However, it is necessary to note that in the sample obtained from TBA/Li reaction mixture, 51.2% of Al exists in the Al_2O_3 form. Moreover, the relative population of framework Al is getting lower as the quantity of Li^+ in the TBA/Na/Li mixtures increases. Further, in the TBAOH and TBA/Na MEL-type zeolites was measured a high fraction of paired Al sites (82%). The contribution of paired Al sites becomes lower in the Li^+ -containing systems (67–48). Such action of Li^+ was attributed to strong interactions of the alkali cation with the Al species. Testing the ZSM-11 materials with Al dominantly located at the channel intersection as a catalyst in the MTO reaction revealed that the aromatic cycle is promoted, and more ethene and aromatics are formed. On the other hand, in the sample with an approximately similar fraction of Al in the straight and intersection channels was observed a more noticeable contribution of alkene cycle MTO pathway. As the amount of the extra-framework Al is increasing, and there are fewer Brønsted acid sites, the catalyst lifetime of ZSM-11 materials is shorter. Thus, it is possible to adjust the selectivity and catalyst stability in the MTO reaction by altering the Al position at different zeolite MEL-type framework sites [272].

The framework of RTH-type small pore zeolites is built of *rth* cages with 8MR openings. There are four crystallographically non-equivalent sites. The structure features two channels of non-distorted 8MR pores and distorted 8MRs, which run along with the *a*- and *c*-axis, respectively. As shown in Table 3, Liu et al. have synthesized RTH-type zeolite by using 1,2,2,6,6-pentamethylpiperidine (PMP), N-methylpiperidine (MP) or pyridine (PY) with the addition of ethylenediamine [273]. Moreover, in the scope of the same investigation, the RTH-type zeolite has been prepared without using any OSDA by employing seeds and sodium cations. The obtained results indicate that the use of bulky OSDAs such as PMP and MP leads to the preferential incorporation of Al species at T1, T2 and/or T3 sites (Figure 18).

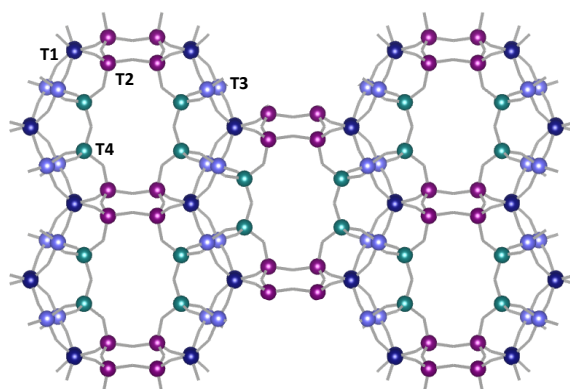


Figure 18. RTH zeolite framework with labels of crystallographically non-equivalent T sites.

On the other hand, in the OSDAs-free synthesis, Al species are uniformly distributed on all T sites. Further, there are weak and strong Brønsted acid sites associated with the framework Al species in the PY-RTH, while PMP-RTH and MP-RTH have just one type of the weak Brønsted acid sites. The order as a function of the strong acid sites is PY-RTH > PMP-RTH \approx MP-RTH. Noteworthy, the weak acid sites in PMP- and MP-RTH samples gave longer lifetime and higher propene selectivity in the MTO reaction than the strong one in PY-RTH.

SSZ-39 is a small pore AEI-type material. Ranson et al. synthesized a series of SSZ-39 samples via interzeolite conversion of FAU-type zeolite from identical synthesis gels with only different amounts of the trans isomer of N,N-dimethyl-3,5-dimethylpiperidinium hydroxide which served as the OSDA [274]. The materials present similar Si/Al ratio 8.6–10. Yet, according to TEM-EDS analysis in the sample made with 28 wt% trans-OSDA, the intergrowths of single crystals have different Si/Al values within different single crystals that form the intergrowth particle. Therefore, there is aluminium zoning in intergrown particles of SSZ-39 prepared with 28 wt% trans-OSDA. Different Al distribution is reflected in different copper uptake during performing ion-exchange under the same conditions. Namely, pure cis isomer yields material with Cu/Al = 0.25 (2.4 wt% Cu) whereas the 28 wt% trans isomer results in Cu-SSZ-39 of Cu/Al = 0.33 (3.0 wt% Cu). When tested in selective catalytic reduction of nitrogen oxides as catalysts, the Cu-SSZ-39 possessing more Cu was more active in the whole temperatures range 150–550 °C. With the purpose of being able to compare the catalytic efficiency of the materials, the sample from cis-OSDA system was additionally ion-exchanged until reaching the same Cu content as with the trans-OSDA. In this case, the activity of the catalyst made with pure cis-OSDA is higher above 350 °C. At elevated flow rate, the Cu-SSZ-39 from the 28 wt% trans-OSDA system is more active at 150 and 200 °C, while the cis-OSDA shows more than 10% higher conversion at higher temperatures. Further, it was found that the Cu-SSZ-39 zeolites synthesized with a different fraction of trans-OSDA display different activity. The authors speculate this behavior arises due to the differences in Al distribution within the studied samples [274].

A medium pore MTT-type material known as ZSM-23 is synthesized with isopropylamine (IPA) and pyrrolidine (PY) as structure-directing agents. These two templates were employed either alone or in ratio IPA/PY = 3 and varying the Al content of the reaction mixture. The usage of the two OSDAs did not affect the total acid site number when compared with the materials prepared with a single template yet did alter their distribution. Upon Pt precipitation on the studied samples, they were evaluated for their efficiency in n-hexadecane hydroisomerization. The samples possessing more weak Brønsted acid sites facilitated the hydroisomerization reaction. Moreover, the highest selectivity of iso-hexadecane was reached over the material with most of Brønsted acid sites [275].

STW-type zeolite, denoted as Al-HPM-1, exhibits chiral framework with helical pores. The material was synthesized by a two-step procedure, referred by the authors as an *in situ* seeds

generation synthesis method [276]. In the study, the all-silica precursor was firstly prepared and treated at 175 °C. After three days, Al(OH)₃ has been added to the reaction mixtures in order to achieve the Si/Al = 15, 25, and 35. The hydrothermal treatment of the synthesis mixture obtained in this way was then continued at 175 °C for 1 day. ²⁹Si and ²⁷Al MAS NMR spectra indicate that the Al occupies both octahedral and tetrahedral positions in the prepared STW materials. Increasing the Si/Al ratio in the reaction mixture resulted in higher amount of Al located in tetrahedral framework positions. All samples were active as catalysts in the reaction of ethanol conversion into ethylene and diethylether, which was conducted to evaluate the acidity of the synthesized STW materials. It was observed that the extra-framework Al inhibited ethanol conversion and diethylether was the preferred product [276]. The presented results indicate that all of the species present in the zeolite synthesis system can exhibit an impact on the crystallization course and hence influence the Al incorporation within the zeolite framework and consequently, their catalytic performance.

4.2 Post-synthesis aluminium incorporation

The *in situ* control of aluminium content and location in the zeolite framework is often challenging. Therefore, numerous studies, employing different methods, have been devoted to the post-synthesis alumination of zeolites. Besides the possibility to introduce Al where the *in situ* method failed, the post-synthesis alumination is cost-effective and provides the opportunities for achieving different Al location. The level of Al insertion and the position it is going to occupy within the zeolite lattice is related to the zeolite framework type, energetics of the particular site and its environment as well as to the nature of the leaving T atom. Some materials have been attained only in all-silica form or in the presence of T atoms other than Al. Moreover, very often, such materials can be synthesized only within a limited range of Si/T ratio, where T is a heteroatom, or in the presence of specific OSDAs. These heteroatoms, particularly Ge and B, were found to be more readily substituted with Al than the framework Si. B and Ge are easily hydrolyzed, which favors their substitution with Al. The following section presents an overview of the approaches applied to incorporate Al into zeolite materials via post-synthesis methods, including vapor phase treatment by Al halides, solution mediated isomorphous substitution as well as by layered atomic deposition. Further, the Al coordination, acidity of the materials, and the benefits attained by the treatment are discussed. Octahedrally and tetrahedrally coordinated Al atoms were introduced into the silicalite-1 sample (Si/Al > 400), which was exposed to AlCl₃ vapour at 400 °C. Pyridine adsorption indicates that the material possesses both Brønsted and Lewis sites [277]. Another study devoted to the alumination of high-silica MFI-type material with aluminium halides showed that the AlCl₃ and AlBr₃ generate both octahedral and tetrahedral Al species. The incorporation of solely tetrahedral Al in ZSM-5 was achieved by hydrothermal treatment using an (NH₄)₃AlF₆ solution of pH 10.5 [278].

Upon treatment of ultrastable zeolite Y (Si/Al = 6.3) with the 0.05 mol dm⁻³ solution of Al(NO₃)₃ FAU-type materials of Si/Al = 5.1 (12 h of treatment) and Si/Al = 4.7 (24 h of treatment) were obtained. Framework Si(OAl) sites have been substituted by Al ions, keeping the crystallinity and micropore volume preserved. The number of Brønsted acid sites and strong Lewis acid sites was higher in aluminated samples, whereas the quantity of weak Lewis acid sites decreased two times, suggesting lowering the concentration of extra-framework Al species [279]. The two FAU-type materials were modified by ruthenium and tested as catalysts in benzene hydrogenation. Aluminated USY zeolite exhibited a higher catalytic activity than the initial zeolite as the reaction rate increased by 5.5 times. Indeed, the enhanced quantity of Brønsted acid sites increases the active site concentration.

The insertion of Al into the zeolite Beta framework was performed by using NaAlO₂ solutions. Si/Al was lowered as a consequence of Al incorporation into structural vacancies

and substituting framework Si atoms. The process was facilitated by increased NaAlO_2 concentration and the temperature of treatment [280]. Further, two dealuminated zeolite Beta materials realuminated by NaAlO_2 showed different tendencies towards Al re-insertion in the framework. The material dealuminated via calcination was realuminated by treatment in mild conditions, and the zeolite acidity was restored to the level of the initial material. On the contrary, the sample dealuminated by acid leaching in HCl could be realuminated only in the presence of TEAOH at 150 °C for 5 days. The framework stability of the realuminated material was not improved with respect to dealuminated samples. In addition, this process generated additional acid sites, mostly weaker than in the parent sample [281]. Similarly, purely siliceous zeolite Beta was treated with aluminium isopropoxide in dry hexane under a nitrogen atmosphere, and Al has been introduced into the zeolite framework. However, only a part of tetrahedral Al atoms present in the aluminated samples is related to the Brønsted acid sites [282]. The same group also treated dealuminated zeolite Beta with aluminium isopropoxide. They obtained tetrahedral aluminium at framework position along with highly distorted extra-framework tetrahedral Al, which was attributed to an amorphous silica-alumina phase. Consequently, the concentration of Brønsted acid sites has increased in the realuminated sample, yet it is associated with approximately 10% of the total Al incorporated into the sample [283].

Silicalite-2 (MEL-type) was stirred for 30 minutes at 60 °C in a solution containing sodium hydroxide, tetrabutylammonium hydroxide, and aluminium nitrate, the final $\text{SiO}_2/\text{Al}_2\text{O}_3$ of the reaction mixtures was 100 and 400. The obtained samples presented more Lewis than Brønsted acid sites revealing the formation of both framework and extra-framework Al species in the course of the alumination treatment [284]. In MTH reaction, the aluminated MEL-type zeolites showed enhanced activity and catalyst lifetime than the Al-MEL-type materials prepared via the conventional zeolite synthesis route.

Martens et al. have introduced Al into ultra-stable zeolite Y, zeolite-4 (ordered mesoporous silica material) and silicalite-1 by atomic layered deposition (ALD) of $\text{Al}(\text{CH}_3)_3$ (Figure 19) [285]. ALD is a technique of thin-film deposition in two cycles where the substrate is exposed to metal compound vapour and subsequently to water vapour at 200 °C and 0.2 Pa base pressure. The authors pinpoint that the advantages of ALD from a practical point of view in comparison to other methods are the automation and the rapidness of the treatment. The materials obtained by this method comprised significant quantities of Al, yet there was a substantial fraction of extra-framework Al species. In ALD-treated USY the number of Lewis acid sites remained unchanged, while the total number of Brønsted acid sites got enhanced. Considering the high amount of EFAl in modified USY, the increase of the concentration of Brønsted sites has been attributed to bridging hydroxyls bonded to distorted Al tetrahedra connected to the framework of oxygen atoms. In decane hydroconversion, the ALD-USY was active at lower temperatures while the selectivity and product yields remained similar to the parent sample. Likewise, ALD-zeolite-4 material presented an increase in the number of acid sites and enhanced catalytic activity in the n-decane hydroconversion reaction with respect to the non-modified sample. On the contrary, there was a small Al uptake and low catalytic

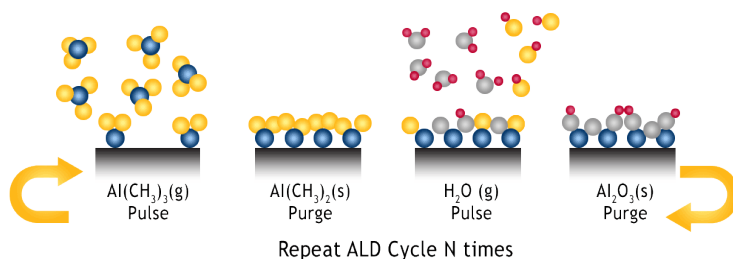


Figure 19. Principle stages of the ALD process. Reproduced with permission from [286].

activity of ALD-silicalite-1, suggesting that the pore openings of the MFI framework are not large enough for transport of $\text{Al}(\text{CH}_3)_3$ [285].

Further, the ALD has been employed to deposit either Si or Al on the pillared MWW (PMWW or MCM-36) and pillared MFI (PMFI) zeolites. The treatment reduced mesopore volume and preserved micropores. In Si-ALD materials, Al exhibited a similar environment as in the initial materials, while in Al-ALD samples, additional Al coordination was generated. The introduction of Si caused the reduction of the total acidity and the number of external acid sites in both pillared materials. In MWW, the total acidity is higher after treatment with Al, yet the external acidity gets lower. In contrast, in pillared MFI material, both total and external acidity got enhanced upon Al-ALD. The obtained materials were tested in ethanol dehydration, alkylation of benzyl alcohol in mesitylene, and direct methane aromatization reactions. The set of experiments showed that the intrinsic catalytic behavior of Brønsted acid sites in PMWW and PMFI was not altered significantly by the ALD treatment. However, a certain selectivity of external acid sites in the alkylation reaction of benzyl alcohol with mesitylene was established [287].

Using the same technique, the group from Leuven introduced Al by ALD into all-silica large pore OKO-type material denoted as -COK-14 [288]. The hyphen denotes an interrupted structure which is stable at room temperature under standard humidity conditions. The fully connected OKO framework can be attained upon heating the all-silica -COK-14 material at a minimal temperature of 300 °C and remains stable in the absence of moisture (COK-14). On the other hand, the ALD-COK-14 material was found to preserve the structure upon storage of 6 months under ambient conditions. 60% of Al introduced into the modified -COK-14 has octahedral coordination and only 21% tetrahedral. The remaining 19% of Al is assigned to distorted tetrahedral and pentacoordinated Al. Although a small quantity of the Al has been incorporated into the framework, the material exhibited certain Brønsted acidity. In addition, the annealing of the structure resulted in the elimination of silanol groups, and thus the pore size widened from 7.2 to 7.9 Å. When modified with Pt nanoparticles, the ALD-COK-14 exhibits remarkable catalytic activity in n-decane hydroconversion in comparison to totally inactive all-silica -COK-14. The marked catalytic performance of ALD-material can be solely assigned to the Brønsted acid sites in spite of their low concentration [288]. Wet ball-milling in the presence of aluminium isopropoxide was recently found as an alternative route to stabilize OKO-type material by introducing Al to the structure. In this case, octahedral Al is the prevailing (77%) specie, whereas 14% of the Al is incorporated into tetrahedral positions. Once again, Brønsted acid sites were generated in the aluminated sample, which is the basis for improved catalytic activity in n-decane hydroisomerization and hydrocracking with respect to ALD-COK-14. In n-decane hydroisomerization reaction remarkably high selectivity of skeletal isomers (72%) was reached, uncommon for large pore zeolites [289].

The alumination of non-calcined germanium-rich zeolite was used to stabilize the zeolite framework [290]. Micron-sized crystals of BEC-type material with $\text{Si}/\text{Ge} = 2.5$ were subjected to a series of post-synthesis treatments with polyaluminium hydroxide chloride solution at 80 °C followed by the extraction of extra-framework Al with hydrochloric acid (Figure 20). The described procedure was repeated twice. Germanium was partially substituted for aluminium, and only the peripheral part of the crystals was aluminated. The process included partial OSDA extraction and incorporation of Al into Ge tetrahedral sites. The partial OSDA extraction is essential for the efficiency of the isomorphous substitution since the remaining molecules stabilize the structure. In order to induce alumination within the whole volume of the crystals, nano-sized BEC-type material of $\text{Si}/\text{Ge} = 3.6$ were employed and subjected to identical post-synthesis treatments as the micron-sized ones [291]. The chemical composition of the resulting material was as follows: $\text{Si}/\text{Al} = 30.8$, $\text{Si}/\text{Ge} = 6.7$. Again the Al was incorporated into the tetrahedral zeolite framework sites replacing the easily

hydrolyzed Ge. The material preserved its crystallinity upon calcination at 600 °C and being exposed to 67% humidity for a month, which demonstrated the significant enhancement of its hydrothermal stability [291].

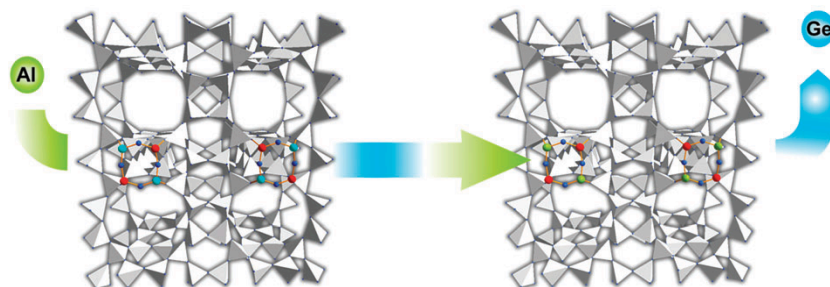


Figure 20. Schematic representation of Ge substitution for Al in the BEC-type framework. Reproduced from [292] by permission of The Royal Society of Chemistry

Germanosilicate ITH zeolite materials having $\text{Si/Ge} = 2.5, 4.4,$ and 5.8 have been subjected to post-synthesis aluminations with an aqueous solution of $\text{Al}(\text{NO}_3)_3$ [293]. Upon aluminations, the samples of $\text{Si/Ge} = 2.5$ and 4.4 presented strong Brønsted and Lewis acid sites as well as additional porosity, which was attributed to the extraction of Ge from D4Rs regularly arranged in the parent ITH materials. On the other hand, additional pores were not formed during the treatment of the zeolite possessing $\text{Si/Ge} = 5.8$. The authors found that the quantity of Al inserted into the ITH framework becomes higher as the Si/Ge ratio of the initial material is decreasing. This effect is related to a higher fraction of Ge–O(Si) bonds prone to hydrolysis, which generates defects that are subsequently condensed with Al. Moreover, the increase of the pore size due to the Ge–O(Si) bonds hydrolysis facilitates the availability of the formed vacancies for Al incorporation. Furthermore, rising the aluminations temperature from 80 to 175 °C leads to the formation of 1.5–2-fold higher number of Brønsted acid sites and a lower quantity of framework Al accessible to pyridine and 2,6-ditert-butylpyridine probe molecules. Aluminated ITH zeolites exhibited catalytic activity in the reaction of tetrahydropyranlation of alcohols while the parent materials containing a small concentration of Lewis sites were almost completely inactive. What's more, solely aimed tetrahydropyranyl ethers were detected as the products in the studied reaction over the Al-ITH materials. Since the lower activity was measured when the size of the substrate alcohol molecule grew larger, the authors point out that, in order to evaluate the catalytic activity of the studied zeolites, is necessary to take into consideration the total concentration of the accessible acid sites [293].

The UTL-type framework can be represented as dense 2D layers connected by D4R. In germanosilicate materials possessing this framework, Ge preferentially occupies the positions in D4Rs [294]. The tendency of germanium for hydrolysis has been the basis of the ADOR (assembly-disassembly-organization-reassembly) method of zeolite synthesis employing UTL-type materials as starting materials. A series of materials (IPC materials) comprising the same 2D layers yet bridged by different linking units has been prepared in this way. Al-IPC (IPC-2, IPC-4, IPC-6, IPC-7) materials have been prepared by the treatment of calcined UTL and Al-UTL materials with the solution of $\text{Al}(\text{NO}_3)_3$, in certain cases in the presence of acetic acid. All Al-IPC materials presented similar and significantly higher amounts of Brønsted and Lewis acid sites than the Al-UTL material. Besides, ^{27}Al NMR indicates there is a certain amount of extra-framework Al entities in the studied samples. Still, these materials exhibited notably different acid sites distribution due to the differences in the channel systems of respective frameworks. Consequently, their performance in the tetrahydropyranlation of bulky 1-decanol changed as a function of the concentration of “external” acid sites. It was found that as the concentration of “external” acid sites becomes higher, the activity of Al-IPC materials in the catalyzed reaction is enhanced [294]. In addition, Al was incorporated in Ge-

containing IPC-2, OKO-type material. The approach involves the preparation of the layered zeolite precursor by acid hydrolysis of Ge-UTL material and subsequent hydrothermal treatment of the layered material with aluminium butoxide in nitric acid solution at 175 °C. The presence of both types of acid sites, i.e. Brønsted and Lewis, indicates that Al was only partially introduced into the framework and there are EFAl species [295].

Germanium containing AFI-type zeolite material of Si/Ge = 8.1 was subjected to de-germanation with HCl prior to the alumination with the solution of Al(NO₃)₃ at 80 °C. The Al introduction did not affect the crystalline structure of the parent materials, yet the material which was firstly de-germanated showed enhanced Al uptake, increased pore-volume, as well as the higher concentration and strength of both Brønsted and Lewis acid sites in comparison to the solely aluminated material. The benefits of the de-germanation step preceding Al treatment are attributed to the creation of hydroxyl nests by removal of germanium atoms from the framework, which are more prone to Al incorporation. In alkylation of toluene with isopropyl alcohol, the AFI-type material modified by two steps procedure exhibited relatively high toluene conversion and selectivity to valuable p-cymene than the catalysts usually used for this reaction such as zeolites Beta and MTW [296].

As-prepared boron-containing zeolite Beta treated with 1 mol dm⁻³ solution of Al(NO₃)₃ at 170 °C was almost entirely aluminated in seven days. NMR data show a decrease of the peak intensity at -11 ppm in ¹¹B MAS NMR spectrum simultaneously with the increase of the peak corresponding to tetrahedral Al in ²⁷Al MAS NMR spectrum indicating the B removal from the BEA framework for Al. It was concluded this isomorphous substitution is a thermally activated process comprising three steps: 1) aluminium insertion in the defect sites near the crystal surface; 2) slow substitution of B by Al in the bulk of the crystals; 3) faster B exchange for Al due to the formation of mesopores in the crystals [297].

B-SSZ-57 (*SFV-type material) contains mostly intersecting intermediate pore channels (10MRs) and a minor area of large pores (12MRs). Boron was selectively substituted in the SSZ-57 framework with aluminium in the large pore region upon treating with the solution of aluminium nitrate. Accordingly, strong Brønsted acid sites were created exclusively in the large pore areas of the zeolite. On the other hand, the Al insertion into B-ZSM-11 with similar 10MRs lattice features was not successful [298]. The alumination of the 12MRs regions in SSZ-57 was substantiated by the constraint index test of n-hexane and 3-methylpentane cracking, as well as the isomerization and disproportionation of 1,3-diethylbenzene. Furthermore, the fact that in hydroisomerization of n-hexane the Pd-modified aluminated SSZ-57 presents similar product selectivities as does the Pd-modified 10-/12-ring zeolite Al-SSZ-56 implies similar transition state selectivities in these materials, which potentially comes from the increased fraction of the Al sites at the intersections of 10- and 12MRs [298]. Zones at al. further extended this work by performing a comprehensive investigation of a series of borosilicate zeolite materials (SSZ-33, SSZ-57, SSZ-70, SSZ-56, SSZ-82, SSZ-24, MEL, Beta) of various framework types possessing intersecting channels of 10- and 12-membered ring channels treated with Al(NO₃)₃ solution [299]. It was found that the first step of Al insertion into a nest “vacancy” is the boron hydrolysis away from the lattice. The process of boron leaving is faster than Al incorporation. NMR analysis shows that the Al is introduced in tetrahedral sites where the boron was located. Besides, different degree of alumination for the studied materials was connected to the higher B occupancy of 4MR positions. Likewise, more boron in the initial zeolite enables achieving higher final Al content since, in this case, a more significant number of B atoms is located in T sites where isomorphous substitution is viable [299].

4.3 Al zoning

Aluminium zoning, i.e., the non-uniform distribution of Al atoms throughout the zeolite crystal, was reported by many researchers [300]. For instance, the spatial distribution of aluminum over ZSM-5 crystals was studied using electron microprobing on large polished crystals [301]. In the crystals prepared from the reaction mixture where TPABr plays the role of the OSDA, Al was concentrated in the crystal rim no matter the initial Al source chemical used. However, the distribution profile was less inhomogeneous in the systems where a source chemical possessing organic functional groups bonded to Al was used. In contrast, in the case of 1,6-hexanediol and OSDA-free synthesis mixtures, crystals with homogeneous aluminium profiles were prepared, while the addition of KNO_3 to the 1,6-hexanediol system leads to an inhomogeneous Al profile. The authors postulate the difference in the Al spatial distribution arises from the interactions between the cations and (alumino)silicate species. Namely, inorganic cations preferably interact with aluminosilicate species, and thus in the 1,6-hexanediol or inorganic systems, the Al is built into the crystals from the early stage of the reaction since Na^+ induces the structure formation. Accordingly, in the presence of inorganic cations, TPA^+ primarily interacts with the silicate species resulting in the Si-rich core MFI-type material with Al incorporated in the later stage of the crystal growth.

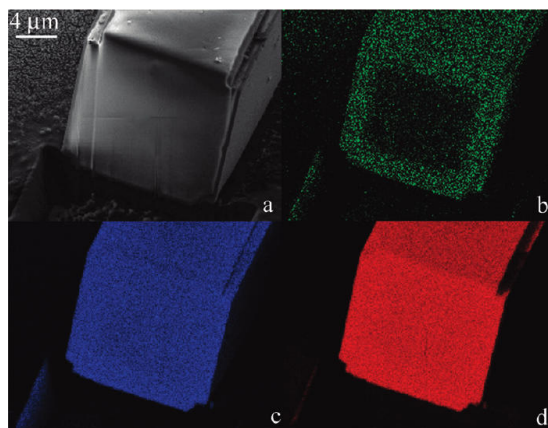


Figure 21. (a) Scanning electron micrograph of the ZSM-5 crystal and EDX maps corresponding to (b) aluminum, (c) silicon, and (d) oxygen. Reprinted with permission from reference [38]. Copyright (2010) American Chemical Society.

EDX mapping of ZSM-5 crystals (bulk Si/Al = 34) displayed in Figure 21 obtained from a reaction mixture of sodium hydroxide, sodium aluminate, silica sol, and tetrapropylammonium bromide revealed the preferential location of Al in the rim of the crystals [38]. Furthermore, crystallographical mapping displayed in Figure 22 confirmed differences in the aluminium concentration within the studied single ZSM-5 crystal [39]. Similar zoning of Al has been also observed in ZSM-5 crystals having different size taken at various stages of synthesis. The authors concluded that the presence of majority of catalytically active sites at the shell of the ZSM-5 crystals arises from the Al deposition during the cooling of the synthesis mixture. Recently Li et al. reported that the level of Al zoning within the crystals becomes higher with the ZSM-5 synthesis advancement. Owing to structural rearrangement in the alkaline reaction medium, the Al migrates towards the rim of the crystals. Besides, it was found that the aluminosilicate species of high Al content are deposited on the growing MFI crystals in the late stage of the reaction [302].

On the contrary, homogeneous distribution of Al has been reported for coffin-shaped large ZSM-5 crystals having a Si/Al ratio of 17 synthesized from Ludox AS-40, tetrapropylammonium bromide, aluminium sulphate, and ammonia [44]. The statistical

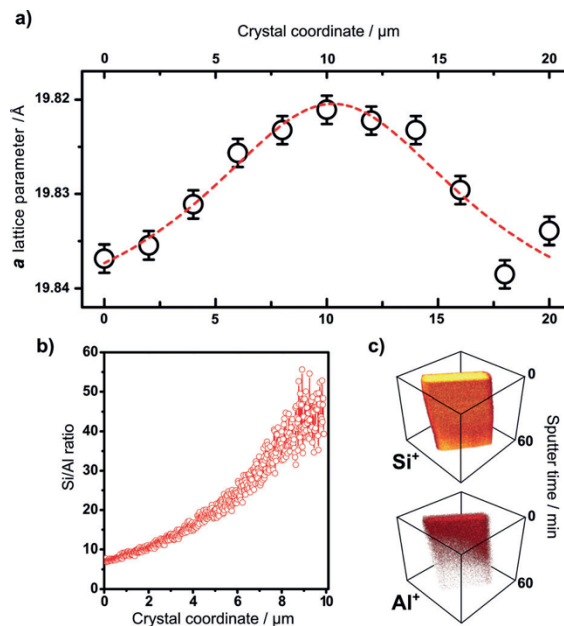


Figure 22. X-rays diffraction intensity maps and time-of-flight secondary ion mass spectrometry sputter-depth profiling analysis of a single ZSM-5 crystal inside orientation demonstrating the Al zoning. (a) Crystal lattice parameter a plotted against the short crystal coordinate (20 μm). (b) Estimated Si/Al ratio within the zeolite ZSM-5 crystal as a function of increasing sputter depth. (c) 3D representation of the depth profiles of Si^+ and Al^+ secondary ions versus sputter time. Reproduced with permission from reference [39].

analysis of atom probe tomography data had shown that Al atoms are uniformly distributed in the ZSM-5 crystals with the most probable Al–Al neighbour distance of 18 ± 6 Å, an average Al density of 0.025 atoms nm^{-3} . Hence, it can be concluded that the synthesis conditions markedly affect the Al distribution within the zeolite crystal.

4.4 Controlling the zeolite acidity by incorporating heteroatoms in the zeolite framework

The incorporation of heteroatoms into zeolite frameworks represents another avenue in tuning their acidity. The framework T^{3+} atoms as B, In, Fe, Ga, provide Brønsted acidity, yet with much lower acid strength and hydrothermal stability than the aluminium counterparts. Other elements such as Ti, Sn, Ge, Zr, Hf, Mo, Nb, W and Ta induce Lewis acid character of the zeolite framework sites that they occupy. In general these materials present higher hydrothermal stability and hydrophobicity than the respective Al-counterparts. Moreover, the heteroatoms present in the zeolite framework alongside Al impact the overall acidity of the material and might display a cooperative effect on its final preformance. Further in text are demonstrated examples how the heteroatoms, both in the presence and absence of framework Al contribute in designing zeolites of novel acidic properties thus expanding the extent of (potential) zeolite applications.

4.4.1 Boron-containing zeolites

Boron is rather easy to get incorporated into zeolite framework sites, and thus, there are many examples where it was employed for the engineering of zeolite acidity. Quantum chemical calculations reveal that the energy difference between the most and least stable Al sitting in the MFI framework is lower than 9 kcal/mol [303]. Contrarily, boron undoubtedly exhibits thermodynamic preference to be located at the T6 position at the channels' intersection,

followed by T10 in the sinusoidal 10MR channel [304]. It seems that boron is more stable at T sites with shorter Si–Si distances, in agreement with the smaller dimensions of the BO₄ tetrahedra in comparison to AlO₄. The preferred boron occupation of T6 and T10 sites is retained in mixed Al-B-ZSM-5 models in which two Al and two B atoms are placed at the same T position, directing the location of Al into the 10MR channels of the MFI lattice. This premise was confirmed experimentally. A series of B-ZSM-5, Al-ZSM-5 and Al-B-ZSM-5 samples having different compositions were prepared from synthesis gels of varied Al and B content [304]. The boron species extracted from the framework during calcination have been washed with the NH₄NO₃ solution. In the cases when Si/(Al+B) < 24 there is competitive incorporation of Al and B at the available positions. All Al present in the synthesis gel is incorporated into the zeolite framework, while just a fraction of the B is inserted in the MFI structure. Nevertheless, the Co²⁺-exchange experiments show the sample of Si/Al = 46 and Si/B = 82 presented a higher quantity of paired Al sites compared to the corresponding Al-ZSM-5 sample having Si/Al = 44 (Table 5). Most probably, the Al atoms get incorporated in the closer framework positions because of the effect of boron already present within the framework. Besides, the amount of paired Al sites in the straight 10MR channels is higher in the B-containing sample. Accordingly, the result of the 1-hexene cracking test reaction gives a higher ratio of mono- to bimolecular cracking for the Al-B-ZSM-5 catalyst denoting a more significant relative population of Al active sites located within the 10MR channels, i.e., boron favours channels intersection positions when competing with Al. In methanol to propene process, this Al-B-ZSM-5 sample showed higher propene selectivity, lower aromatics, and alkanes selectivity and longer catalyst lifetime than the materials prepared without the assistance of boron [304].

Table 5. Results of Co²⁺-exchange experiments on different ZSM-5 samples synthesized with and without boron added to the crystallization media. Reprinted (adapted) with permission from reference [304]. Copyright (2018) American Chemical Society.

Sample	Composition ^a		Co-exchange experiment				
	Si/Al	Si/B	Al _{isol} ^b	Al _{pair} ^c	Al _α ^d	Al _β ^d	Al _γ ^d
Z5-50	44	-	45%	55%	32%	65%	3%
Z5-50-B1	46	82	30%	70%	45%	55%	<1%

^aMeasured by ICP-AES

^bCalculated according to equation $n(\text{Al}_{\text{isol}}) = n(\text{Al}_{\text{total}}) - n(\text{Al}_{\text{pair}})$

^c $n(\text{Al}_{\text{pair}}) = n(\text{Co}^{2+})$

^dMeasured by deconvolution of UV-Vis spectra of dehydrated ZSM-5.

In the case of MFI synthesis systems where TPA and Si/Al ratio were kept constant (≈ 50) and B content varied, 20–40% of Al sites were paired, independently on the boron quantity added [305]. On the other hand, in analogous experiments where a mixture of tetrapropylammonium cations and ethylenediamine (EDA) is used as OSDA, the obtained B-Al-MFI zeolites contain less than 5% of Al in paired configurations, irrespectively of the Si/B ratio. Herein, in the systems with solely TPA⁺, one TPA⁺ moiety gets confined per one channel intersection of the MFI framework while in the crystals formed with EDA/TPA⁺ = 15 and $n(\text{Si}) > n(\text{TPA}^+)$ there is one TPA⁺ per two MFI channel intersections. EDA is located within the voids not occupied by TPA⁺, and as the B content increases, the EDA-B complexes build two B atoms per EDA molecule in the MFI framework. First-order rate constants of methanol dehydration to dimethylether over B-Al-MFI indicate acid sites are confined within smaller voids. Given this, the Al distribution within the zeolite framework is directed by the

widespread impact of the organic molecules over the boron atoms present within the synthesis mixture [305].

The boron-containing zeolite Beta materials were prepared in the presence of seeds ($\text{Si/B} = 4\text{--}38$; $\text{Si/Al} = 170\text{--}90$). The addition of boric acid in the reaction mixture affected the morphology and the size of the crystals compared to the seed crystals. When compared to the Al-BEA sample, the addition of B exhibited two different sites. Namely, boron assumes both tetrahedral and trigonal coordination in the BEA@BAB framework. Trigonal B coordination is related to the weak Brønsted acid sites, while the tetrahedral coordination offered Lewis acid sites. Lowering the boron content in the synthesis gel led to a reduced amount of boron of trigonal coordination while the amount of B in tetrahedral coordination remained the same. The B-samples possessed fewer Brønsted acid sites, more Lewis acid sites, and an increased fraction of weak acid sites than the Al-BEA material. The catalyst with the highest Si/B ratio of 6 was the most active and stable in the methanol to olefins reaction. It reached the highest propylene selectivity of 60%, together with the highest propylene/ethylene ratio of 7 [306].

Al- and B-containing AEI-type zeolite materials have been synthesized from commercial FAU zeolite by using tetraethylphosphonium hydroxide (TEPOH) as OSDA. Solid-state NMR and FTIR confirmed the incorporation of B into the lattice. The samples having $\text{Si/Al} = 13$ and $\text{Si/B} = 260$ displayed a lower quantity of Brønsted acid sites derived from framework Al species compared to the boron-free AEI sample of $\text{Si/Al} = 11$. Yet, the strength of Al acid sites is not affected by the presence of boron in the framework. Accordingly, in B,Al-AEI material, there are Brønsted acid sites related to framework B species, which are weaker than Al-derived acid sites [307]. B,Al-AEI zeolite sample has improved catalytic lifetime in the ethene conversion reaction with respect to B-free material due to the decreased amount of the strong acid sites. Besides, it exhibits high selectivity to butenes. Suppressing the successive reactions of butenes such as their cracking represents another benefit brought about by the introduction of B in the zeolite framework, thus lowering the acid site density. Another study reports the preparation of the CON framework-type zeolite materials ($\text{Si/B} = 22\text{--}37$; $\text{Si/Al} = 87\text{--}196$) by post-synthesis and the direct-synthesis methods [308]. The post-synthesis method involves the deboronation of B-CON sample and subsequent alumination. In the direct synthesis method, B-BEA@BAB seeds were added to the reaction mixture comprising boric acid, aluminum sulfate, sodium hydroxide, fumed silica, and N,N,N-

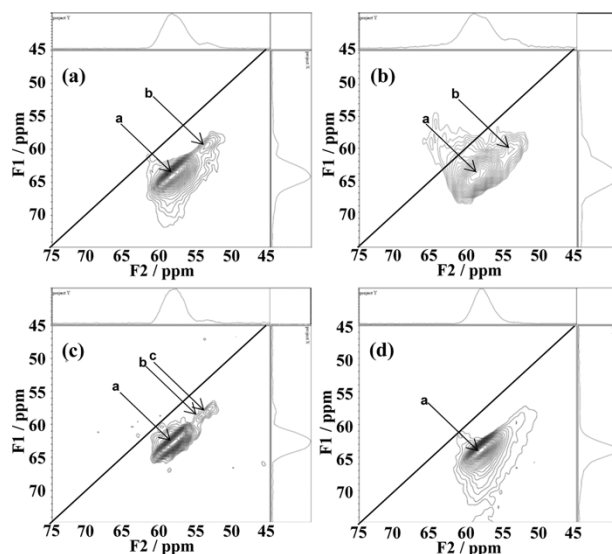


Figure 23. ^{27}Al MQMAS NMR spectra of [Al,B]-CON zeolite materials prepared by direct synthesis under (a, b) static ($\text{Si/Al} = 106$ and 196) and (c) tumbling conditions ($\text{Si/Al} = 134$)

and (d) the material prepared by post-synthesis treatment ($\text{Si}/\text{Al} = 87$). Reprinted with permission from reference [308]. Copyright (2015) American Chemical Society.

trimethyl(-)-cis-myrtanylammmonium hydroxide (TMMAOH). There is a substantial difference between the *in situ* and post-synthesis aluminated CON-type samples in terms of the environment of Al species. Moreover, as indicated by the ^{27}Al MQMAS NMR spectra in Figure 23, there is a marked difference in the Al distribution among the samples prepared *in situ* under the static and tumbling conditions. Besides, the sample prepared by the post-synthesis method has a higher quantity of Lewis acid sites as well as a slightly higher amount of defect sites than the directly prepared CON-type material. Consequently, CON-type aluminosilicate zeolites prepared directly under the tumbling conditions ($\text{Si}/\text{B} = 26$; $\text{Si}/\text{Al} = 134$) exhibited a high propene selectivity, low ethene selectivity, and a very long catalytic life compared to Beta and ZSM-5 zeolite in methanol to olefins (MTO) reaction. Further, it was surmised that in the sample with Si/Al ratio of 87 prepared by post-synthesis aluminated, aluminium occupied the 12MR positions as it showed higher heavy compounds selectivities and the lower propene selectivity [308]. This conclusion is in line with the report of Zones et al. on the SSZ-57 treatment with Al [299].

4.4.2 Germanium-containing zeolites

The positions of Brønsted acid sites in Al-ITQ-21 of a range of $(\text{Si} + \text{Ge})/\text{Al}$ ratios have been evaluated by comparing them with Al-free ITQ-21 [309]. The materials were prepared using N(16)-methylsparteinium cations as OSDA with varying amounts of added aluminium isopropoxide. Germanosilicate ITQ-21 has no Brønsted acid sites, while in Al-ITQ-21, the Brønsted sites are generated due to the isomorphic substitution of Si by Al. The quantity of Brønsted acid sites is nearly proportional to the Al concentration in Al-ITQ-21 material. Almost all of the Al atoms occupied T positions in the Al-ITQ-21 for the samples having $(\text{Si} + \text{Ge})/\text{Al}$ higher than 25. There are three distinct T positions in the ITQ-21 structure. Germanium has a preference for the T1 site, while the Al atoms mainly occupied T1 positions at high $(\text{Si} + \text{Ge})/\text{Al}$ and then began to populate T2 positions when $(\text{Si} + \text{Ge})/\text{Al}$ became lower than 44. Moreover, an increase of the Al amount in Al-ITQ-21 induced the generation of two different kinds of acidic protons, i.e., Brønsted acid sites. The acidic protons are preferentially generated on O1 by occupying T1 positions with Al when the Al concentration of Al-ITQ-21 is low and are successively generated on O3 by occupying T2 positions with Al when the Al concentration increases. It was reported that n-heptane conversion over investigated Al-ITQ-21 samples proceeds by parallel isomerization and cracking reactions. As the Al amount in the materials increased, the selectivity for cracking was lower while the isomerisation selectivity rose. The catalytic activities for both isomerization and cracking of n-heptane for acidic protons bonded to O3 atoms in Al-ITQ-21 were higher than those for acidic protons at O1 atoms [309].

4.4.3 Tin-containing zeolites

Tin-containing zeolite materials were included in the present review to demonstrate the possibilities offered by the Lewis acidity in zeolites. The presence of Sn in the framework of crystalline microporous solids generates Lewis acidity since the σ^* orbitals of the Sn–O cluster can accept the electron density of the substrate and thus enable the onset of the catalytic process. Sn-containing zeolites have shown to be exceptionally active and selective Lewis-acid catalysts. They are arguably one of the best water-resistant heterogeneous catalysts for liquid-phase catalysis. Sn-containing zeolites are employed in reactions of oxygenated reactants, which are of particular importance in fine chemistry and biomass valorization processes (e.g. Baeyer-Villiger (BV) oxidation, Meerwein-Ponndorf-Verley

(MPV) reaction, Diels-Alder reaction, aldol condensation, ring-opening of epoxides [310–315]), whereas the most important chemicals that can be produced using Sn-zeolites are glucose isomers and epimers, 5-(hydroxymethyl)furfural (5-HMF), lactates, levulinates, ϵ -caprolactones, nopol, catechol, γ -valerolactone, etc.

Similar to the other heteroatoms-containing zeolitic materials, various types of active sites may be generated when Sn is introduced into zeolite framework. Closed sites correspond to Sn incorporated into the framework as a fully coordinated distorted tetrahedron ($\text{Sn}(\text{SiO})_4$). In contrast, open sites refer to partially hydrolyzed tin located within the zeolite framework ($(\text{SiO})_3\text{SnOH}$, Figure 24) [316]. It was found that the interconversion between open and closed Sn sites can take place and might have an impact on the catalyst's reactivity [317]. In the reaction of glucose isomerization to fructose, glucose epimerization to mannose, BV oxidation as well as in MPV reduction, the open Sn sites were proposed as the active sites [312,316,318] while in ethanol dehydration to

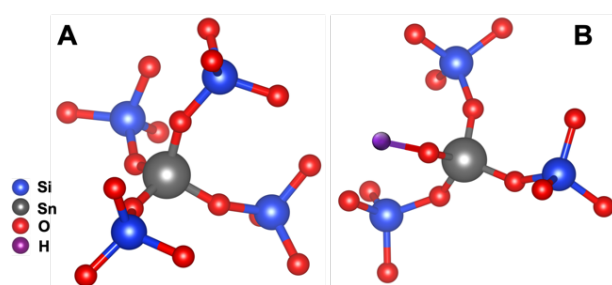


Figure 24. Examples of Sn sites in Sn-BEA zeolite: (A) tetrahedral closed Sn site and (B) a partially hydroxylated open Sn site according to the definition in [316].

diethylether the closed sites seem to be the most relevant for the reaction [319]. It should be noted that generally, under ambient conditions, Sn sites possess distorted octahedral coordination since they are hydrated with two water molecules [320]. In addition, extra-framework SnO_2 moieties can be deposited on the material or within the zeolite pores. There is an interesting example of glucose isomerization where extra-framework SnO_2 clusters located within the zeolite Beta channels act as catalytically active sites, whereas bulk SnO_2 displays any activity [320,321].

The first attempt to introduce Sn into a zeolite framework concerns the addition of SnCl_4 to the silicalite-1 synthesis mixture as early as in 1976 [322]. Later on, both *in situ* and post-synthesis approaches have been attempted to introduce tin efficiently in a zeolite [323–328]. Still, not until the work of Mal et al. was confirmed the embedding of Sn in the zeolite framework [329]. In the latter study, SnCl_4 was directly added to TEOS, water, and TPAOH were subsequently admixed. The unit cell volumes of the prepared materials increased with the tin content in the sample. Further, the T–O–T lattice vibrations wavenumbers are shifted towards lower values in the samples of higher Sn content. The obtained Sn-MFI material was a comparably active catalyst to TS-1 in the phenol hydroxylation reaction, whereas for the ethylbenzene oxidation it showed almost two times higher turnover number than did TS-1 [330]. This research group also successfully obtained Sn-Beta zeolite. Yet, Al was present both in the reaction mixture and in the end products. These Sn-Beta materials were found to be functioning catalysts in the acetylation of 1,3,5-trimethylbenzene (1,3,5-TMB) with acetyl chloride and in the m-cresol and 1,3,5-TMB oxidation with H_2O_2 where their activity depended on the amount of Al in the sample [331]. A giant leap in the field occurred with the work of Corma et al. where was reported direct preparation of highly crystalline Al-free as well as defect-free Sn-Beta zeolite of Si/Sn ratio 125 in the fluoride-containing system using dealuminated nanosized zeolite Beta seeds [310]. ^{119}Sn MAS NMR indicated the presence of

tetrahedrally coordinated Sn, suggesting that Sn is built into the zeolite framework. The material showed a remarkable selectivity in BV oxidation of dihydrocarvone, a molecule containing ketone group along with a double bond, which is prone to react with an oxidizing agent forming a range of products. Sn-Beta yielded the target lactone circumventing the double bond oxidation. This work paved the way for a plethora of studies both in terms of incorporating Sn into various zeolite lattices and exploring the catalytic activity of Sn-zeolites in numerous reactions. A selection of these studies is presented in the following section.

In situ insertion of Sn into the zeolite framework connotes the presence of the Sn species in the starting reaction mixture before zeolite material is formed. A rather long synthesis period of Sn-zeolites, as well as the usage of fluorides in many systems, represent the most significant impediments to their large-scale production. For instance, the synthesis in the work of Corma takes 20 days at 140 °C in a tumbling oven [332]. The data suggest that the zeolite crystallization kinetics is retarded when Sn is present in the initial synthesis mixture [333]. An extensive study of Sn-Beta crystallization in the fluoride medium found that it is a function of the type and quantity of tin source added to the initial reaction mixture [334]. Increasing the tin loading required a longer period to obtain a material of high crystallinity, e.g., at Si/Sn = 100 with SnCl₄·5H₂O it took 60 days to reach fully crystalline material. Further, zeolite Sn-Beta crystals grew larger as the Sn amount increased, whereas the pyramidal faces shrank, and the pinacoidal ones became the dominant crystal feature. No matter the Si/Sn ratio, all of the crystals analyzed by SEM wavelength dispersive spectrometry exhibit Sn zoning with Sn located in the rim of the crystals, as displayed in Figure 25. In the reaction of conversion of dihydroxyacetone to methyl lactate the Sn-Beta of Si/Sn = 150 exhibited the highest activity for the samples, which are prepared for a rather short time, yet show high crystallinity [334]. Clearly, the addition of Sn to the zeolite synthesis mixture substantially alters the crystallization process. Thus various resourceful approaches were scrutinized in order to achieve the Sn anchoring to zeolite structure and control of the end product properties at the same time trying to reduce the preparation period.

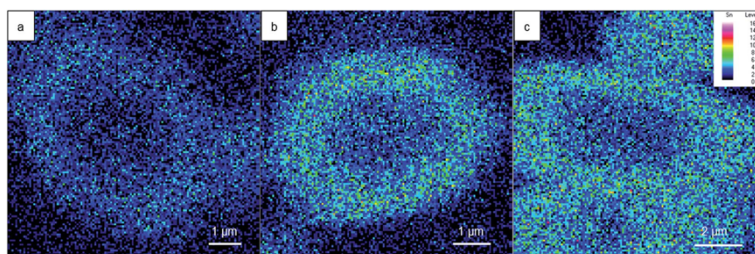


Figure 25. Sn distribution based on SEM wavelength dispersive spectrometry analysis of the cross-sections of Sn-Beta zeolites with Si/Sn ratios of (a) 400, (b) 200, and (c) 100. Reproduced from Ref. [334] with permission from The Royal Society of Chemistry.

Nearly identical reaction mixture as in Corma's work yielded Sn-Beta zeolite material of Si/Sn = 96 (140 °C, 40 days, static conditions) [321]. When added to a 10 wt% glucose water solution, the Sn-Beta produced a mixture containing glucose (46 wt%), fructose (31 wt%), and mannose (9 wt%). The same reactivity was observed after three repeated cycles, as well as in the case of 45 wt% glucose solution. Noteworthy, the material was active at pH = 2. Under the same conditions, any isomerisation activity was found neither for bulk SnO₂ nor SnCl₄·5H₂O suggesting that in the studied process, the active species are the Sn sites integrated within the zeolite framework [321].

A relatively short synthesis time of Sn-containing zeolite Beta (Si/Sn = 63) was achieved by the interzeolite conversion of ITQ-1 (all-silica MWW-type zeolite) in the presence of dealuminated zeolite Beta seeds, TEOH and NH₄F [311]. Here solely isolated tetrahedral Sn

was observed by XPS and UV/Vis spectroscopy. The high catalytic activity of the material in the Baeyer-Villiger oxidation of 2-adamantanone with H_2O_2 was attributed to rather high Sn framework content and small crystal size. The hydrothermal treatment of the NaOH-TPAOH- SiO_2 system with an added solution of SnCl_4 and EDTA with citrate buffer represents another efficient approach for the *in situ* insertion of Sn in the zeolite framework [336]. Al was added to some of the reaction mixtures, and thus Sn-MFI materials of Si/Sn ranging from 122 to 69 and Sn-Al-MFI materials having Si/Sn \approx 90 and Si/Al in the range 240–80 were prepared. Based on the XPS and UV/Vis data, the authors conclude that in the studied series of the samples, Sn occupies only tetrahedral positions within the zeolite framework. IR spectra of pyridine adsorbed on the materials reveal the presence of Lewis sites in the Sn-MFI materials and both the Brønsted and Lewis acid sites in Sn-Al-MFI samples, as corroborated by ^{31}P NMR spectra of adsorbed TMPO probe molecule. Both types of materials are comparably active catalysts in the conversion of 1,3-dihydroxyacetone to methyl lactate, the BV oxidation of cyclopentanone, and the aldol condensation reaction between furfural and acetone which indicate that Brønsted acid sites are beneficial in these reactions. Still, there is an optimal Al amount, which is advantageous for achieving desired product selectivity.

Sn introduced by *in situ* synthesis into a series of porous materials (SBA-15, Beta, and MFI-type) was evaluated for its catalytic activity in the epichlorohydrin epoxide ring-opening. Sn-Beta by far exceeded Sn-SBA while Sn-MFI performed slightly inferiorly. Besides, the Sn-Beta zeolite performed similarly after three cycles [315]. Worth reporting, the Zr- and Hf-containing Beta zeolites exhibit certain activity in the studied reaction, but 6 and 7 times less than does Sn-Beta. The *in situ* preparation of nanosized Sn-zeolites was the extension of this work in terms of the substrate size. Namely, nanosized Sn-MFI (Si/Sn = 200) and Sn-Beta (Si/Sn = 170) exceeded the catalytic activity of corresponding Sn-zeolite materials with larger crystals in the reactions of 1,2-epoxyhexane with methanol and 1,2-epoxyoctane with ethanol, respectively [337,338].

A series of Sn-Al-MOR samples with Si/Sn in the range ∞ –143 and Si/Al = 12–9 was prepared in the presence of 1-butyl-3-methylimidazolium bromide. UV/Vis spectra indicated the insertion of Sn in the zeolite framework, although the Si/Sn ratio as low as 455 was obtained for the initial system with the lowest Sn quantity. The MOR materials originating from the systems with higher initial Sn content presented six-coordinated tin species or small SnO_2 clusters beside the framework Sn atoms. In the toluene alkylation with tert-butyl alcohol reaction, the p-tert-butyltoluene selectivity is higher for Sn-Al-MOR catalysts than that for Al-MOR of Si/Al = 9. Moreover, MOR catalyst having Si/Sn = 182 retained its catalytic activity upon five consecutive cycles [339].

Sn-CHA was prepared using TEOS, $\text{SnCl}_4 \cdot 5\text{H}_2\text{O}$, and TMADAOH in the presence of H_2O_2 . The ethanol released from TEOS and the excess water in the solution were evaporated until $\text{H}_2\text{O}/\text{SiO}_2 = 3$. The almost dry powder was dispersed in water and again dehydrated until reaching the $\text{H}_2\text{O}/\text{SiO}_2$ ratio of 3, mixed with HF, and heated at 150 °C (48 h, rotation). If the dehydration steps are omitted, any crystalline material is formed up to 10 days of hydrothermal treatment [340]. ^{119}Sn NMR data (Figure 26) combined with DFT models suggest that the closed Sn sites in dehydrated material become hydrated hydrolysed open sites upon the exposure to a water-containing environment. Thus prepared Sn-CHA displays significant catalytic activity in the reactions of MPV reductions of propionaldehyde, Oppenauer oxidation of ethanol, and glucose isomerization. Still, Sn-Beta is a more active catalyst, especially in the isomerization of glucose, where the turnover rates are four orders of magnitude higher than on Sn-CHA. The observed performance of Sn-CHA is attributed to the distinctive transport limitations in these materials.

As already mentioned, the properties of Sn-containing zeolites are susceptible to the Sn source and the mode it is added to the reaction mixture. Some of the proposed synthetic routes

concern where the bonds Si–O–Sn exist prior to the hydrothermal treatment as achieved by milling or preparing xerogels [323,341]. Further, one should bear in mind that Na in the zeolite MFI synthesis mixture may limit the quantity of Sn built into the framework and that at pH below 12, sodium stannate impurity gets formed on the surface of the crystals [342]. Indeed, numerous parameters affect Sn and Si behavior under hydrothermal conditions, and thus it is necessary to continue pursuing the goal to produce (new) materials of improved properties/performance.

An alternative avenue to Sn-containing zeolite catalysts is the post-synthesis tin incorporation. Different Sn compounds in solid, solution, or vapor form were explored to introduce Sn in zeolite structures. The post-synthesis treatment can be executed with conventional laboratory equipment and usually requires shorter treatment time with respect to the *in situ* synthesis. The degree of introduced Sn, as well as its location, are related to zeolite framework type, presence of defect sites, and the tin source, i.e., susceptibility/availability of Sn atoms to react with the zeolite. In the following section are going to be addressed different methods developed to conduct post-synthesis stannation of zeolites, the types of generated Sn sites as well as the catalytic efficiency of the prepared materials.

A series of nanosized dealuminated commercial zeolite Beta samples were exposed to SnCl₄ vapors at 200–600 °C. The samples treated at 400 and 500 °C present the lowest Si/Sn ratio of 35 and 36, respectively. Herein, Sn occupies tetrahedral framework positions according to the ¹¹⁹Sn MAS NMR results. Further, the IR spectrum of the adsorbed pyridine indicates the presence of Lewis acid sites solely. The decreased intensity of the silanol nests band at 3500 cm⁻¹ in the IR spectrum of the Sn-Beta samples together with the decrease of the Q³ resonance at -103 ppm in the corresponding ²⁹Si MAS NMR spectra supports the conclusion that the mechanism of the Sn incorporation occurs through the reaction with SiOH groups in the hydroxyl nests, thus healing the framework defects [343]. The nanosized Sn-Beta obtained herein outperforms the conventional Sn-Beta prepared in fluoride medium in the Baeyer-Villiger oxidation of 2-adamantanone. The same research group applied the modification procedure by SnCl₄ vapors on the zeolite Beta prepared via a seeded synthesis route in the caustic medium [344]. The Sn was found to be exclusively in tetrahedral positions, and the mechanism of Sn incorporation was attributed to the healing of silanol nests defect sites as supported by the IR spectra analysis shown in Figure 26. The material outperformed Sn-Beta obtained by the fluoride-assisted method in the BV oxidation of 2-adamantanone.

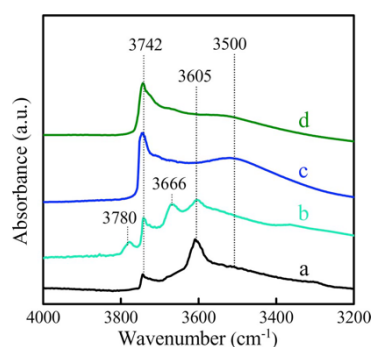


Figure 26. FT-IR spectra in the hydroxyl stretching vibration region for (a) parent zeolite H-Beta and its derivatives: (b) zeolite Beta calcined at 823 K for 30 min; (c) calcined zeolite Beta treated with HNO₃; and (d) Sn-Beta (Si/Sn = 83) prepared from the calcined and HNO₃ treated zeolite Beta (Reproduced with permission from reference [344]).

Noteworthy, the post-synthesis obtained Sn-Beta showed slightly higher catalytic activity than the *in situ* synthesized F-Sn-Beta in the conversion of dihydroxyacetone to ethyl lactate.

At the same time, bulk SnO₂ acted with lower conversion and yielded a small quantity of ethyl lactate [344].

Commercial TEA-Beta zeolite was dealuminated with HNO₃ to reach Si/Al > 1000 [345]. This material was subsequently treated with SnCl₄ solution, and thus Sn-Beta materials having 0.5 and 2 wt.% of tin were prepared. The interaction of Sn and silanol groups of the zeolite defect sites is evidenced by the ²⁹Si CP MAS NMR spectra of the materials. The tin-containing materials displayed a reduced intensity of Q³ species compared to the dealuminated samples. The IR spectra of the Sn-containing zeolites showed a decreased intensity of silanol bands corroborating the interaction of Sn with the silanol nests. According to the IR analysis of the samples with adsorbed probe molecules, additional Lewis acid sites are generated upon the Sn treatment. The Meerwein-Ponndorf-Verley reduction of cyclohexanone takes place on both catalysts. A higher conversion was achieved on the sample having a larger amount of Sn. Likewise, in the case of the reduction of 4-methoxybenzaldehyde with 2-butanol to 4-methoxybenzylalcohol followed by its etherification, the 2 wt% Sn-Beta material shows higher conversion degree. However, the catalysts deactivate when the MPV process is followed by etherification, arguably due to the water adsorption on Lewis acid sites. Considering that the turnover number per Sn atom is higher for the material with less Sn, the authors conclude that the active sites in all studied reactions are isolated tetrahedral Sn atoms incorporated into the zeolite framework [345].

Hammond et al. obtained materials comprising 5 and 10 wt% of Sn by grinding dealuminated zeolite Beta with tin(II) acetate, followed by calcination at 550 °C [346]. The IR band of silanol nests in these samples diminished, whereas the UV/Vis spectra provide evidence of the presence of tetrahedral Sn. Employed as catalysts in BV oxidation of cyclohexanone with H₂O₂ into ε-caprolactone, the samples present high selectivity. On the other hand, SnO₂ deposited on dealuminated zeolite Beta as well as pristine zeolite Beta treated with Sn(II) acetate were utterly inactive. These results confirm that isolated, tetrahedral Sn built into the zeolite framework is the active site herein [346].

Subjecting the commercial zeolite Y (Si/Al = 6) to dealumination by nitric acid resulted in 90% of Al removed and substantial reduction of material's crystallinity [347]. Two post-synthesis routes were undertaken in order to introduce Sn into zeolite framework: 1) refluxing with SnCl₄ in isopropanol and 2) adding trimethylamine to the SnCl₄ solution in acetone and dichloromethane. The obtained materials comprised 1–2.2 wt% of tin. The features in the UV/Vis spectra of the samples prepared in isopropanol show the presence of Sn with coordination number higher than four implying there are extra-framework Sn species together with SnO₂ domains. On the other hand, the UV/Vis spectra of the trimethylamine-derived zeolite suggest a low abundance of extra-framework Sn species. Besides Lewis acid sites, which should originate from Sn, a noteworthy quantity of Brønsted acid sites was observed and ascribed to Al, which remained after the dealumination. Such samples were poor catalysts with poor selectivity in methyl lactate synthesis from glucose solutions in methanol. Namely, a variety of products was formed due to several reactions pathways through which the glucose undergoes because both Brønsted and Lewis acid sites take part in the processes. However, the trimethylamine-derived materials that were ion-exchanged with the alkali cations exhibited switched products' selectivities with methyl lactate being the main product and thus suggesting the retro-aldol reaction pathways become dominant. The Na⁺ and K⁺ have double-action – suppressing of the Brønsted sites and enhancing the catalytic activity of Sn species in retro-aldol reaction through the interaction with the Sn sites [347]. The promotion effect of Na⁺ and K⁺ on the epimerization and retro-aldol reactions was observed on Sn-Beta zeolites as well [312,348].

In order to obtain Sn-MWW zeolite material, as-prepared B-MWW zeolite was deboronated with nitric acid and subsequently treated with SnCl₄ and hexamethyleneimine [349]. Samples

with Si/Sn ratio of 52 and 54 were obtained. XRD and UV/Vis data confirmed that Sn occupies the zeolite framework sites. When assessed as catalysts in the conversion of dihydroxyacetone into lactic acid, Sn-MWW zeolites were more efficient than Ti- and B-MWW counterparts. Further, in the conversion of glucose, fructose, and sucrose, the Sn-MWW zeolites yield the highest amount of desired product methyl lactate, comparable to Sn-Beta performance reported in the literature [350].

Lari et al. investigated a series of materials: Sn-MFI materials synthesized in OH medium, Sn-MFI and Sn-Beta synthesized with the assistance of fluoride ions and Sn-Beta, Sn-MFI, Sn-FAU as well as Sn-MOR prepared by post-synthesis modification with SnSO₄ in basic solutions [351]. Generally, the post-synthesis treatment with Sn notably reduced the crystallinity of all samples with respect to parent zeolites. In each of the studied materials, there are Lewis acid sites present and the UV/Vis spectra provided information on the respective Sn coordination – the coordination number 6 is dominant in the MFI prepared in the OH medium, while in the F-containing medium and by a post-synthesis system more tetrahedral Sn is formed. In Sn-FAU and Sn-MOR was observed that Sn mostly resides in tetrahedral positions. Based on their catalytic performance, in the isomerization of dihydroxyacetone in water and methanol and in that of xylose in water, the authors concluded that Sn incorporated into zeolite framework during hydrothermal synthesis is generating materials with higher hydrophobicity and improved catalytic activity [351]. The investigation by van der Graaff et al. confirmed the findings that the zeolite materials with Sn introduced by post-synthesis modification are more prone to deactivation, tin leaching, and structural degradation than the Sn-zeolites obtained by *in situ* routes [352].

5 Summary and outlook

Acid sites in zeolites are related to Al and heteroatoms present within the material, and their nature and strength are a function of the number, coordination, and framework position of these atoms. Depending on the structure type, aluminium atoms have shown a preference for certain T positions within the framework. Furthermore, in some zeolite crystals has been observed a gradient of Al concentration throughout the volume of the crystal. A range of experimental techniques (NMR, IR, XPS, EDX, ICP, ...) is available to examine zeolite acid sites providing information on the local environment of Al atoms, connectivity between Si and Al, the nature and position of hydroxyl groups together with their spatial proximity and interactions. Monitoring the interactions with probe molecules (CO, NH₃, CH₃CN, pyridine, 2,6-lutidine, 2,4,6-collidine, trimethylphosphine oxide, etc.) enables the assessment of the acid sites' nature and strength as well their location with respect to zeolite channel system and within 6-membered rings, and consequently the accessibility to molecules of various sizes. In addition, the theoretical calculations are frequently employed either to predict the acidic properties of a particular material or to complement and clarify the experimental findings.

In general, there are two principally different approaches for introducing and controlling the Al sites within the zeolite materials – *in situ* and post-synthesis methods. *In situ* route includes the incorporation of Al into the growing zeolite skeleton. The critical factors determining the level of Al incorporation and distribution in a particular framework are the composition of the synthesis systems and the structure-directing agent(s) employed. On the other hand, the post-synthesis concept involves the incorporation of Al in the already formed zeolite framework by treatment in gas or liquid phase with a very reactive Al compound. Aluminium incorporated in this way is preferentially embedded in the framework vacancies or replaces T atoms of lower stability. Both framework and extra-framework Al species are usually generated by the post-synthesis modification of zeolite materials with Al. The Al can be incorporated in the defect sites during the crystallization of (alumino)silicate zeolites. Alternatively, Al can isomorphously substitute T sites that remain vacant upon the hydrolysis of heteroatoms (most

common are B and Ge). Sometimes multi-step procedures such as several cycles of aluminations followed by hydrochloric acid treatment or partial T atom removal prior to the aluminations are beneficial for preparing materials with Al in the framework tetrahedral positions. Besides, the Al incorporation in some materials can be more efficient in the case when the treatment temperature is increased, or the OSDA is not completely eliminated.

The preparation of zeolite materials of tailored acidic properties by performing one-step synthesis (*in situ* control of acid sites) has many advantages: it is an integrated process, the reproducibility degree is usually higher since there are fewer steps to be undertaken, low energy consumption, less waste produced and the material's production costs are low. As already mentioned, the post-synthesis zeolite modification by Al is not as selective for building Al into the tetrahedral positions as in the case of *in situ* methods. Moreover, this approach requires several steps, more waste remediation, as well as higher energy and solvent consumption. However, these two axes of zeolite materials preparation are complementary, not exclusive. Namely, the post-synthesis treatment by Al allowed the preparation of a number of materials possessing properties that could not have been obtained by the *in situ* procedure and vice versa. Thus, it is necessary to continue research in both directions in order to be able to meet the demand on zeolite production to deliver materials of desired size and morphology, with a controlled fraction of structural defects in terms of silanols and/or extraframework species and with Al or other heteroatoms incorporated in any T position in any quantity.

Designing zeolite materials in terms of their acid site distribution can be achieved at several levels of acid sites position: the occupation of crystallographically non-equivalent sites, the paired sites arrangement, the location with respect to the channel system, the presence of framework defect sites as well as the extra-framework species. In addition, the number and strength of acid sites are controllable too. In total, there are almost 250 approved zeolite framework types. Yet, a small portion (less than 5 %) is produced at large scales and used in various industrial processes where their acidic character and porosity represent the basis of their performance. In general, the focus of the studies of engineering zeolites' acidic properties is on the industrially relevant materials as well as on the ones that have the potential to be used for commercial purposes, most often because of their pores' dimensions. Intensive studies have been conducted on MFI-, MOR-, BEA-, FER-, CHA- and FAU-type materials, and in these frameworks, the Al quantity, location, and acid sites strength can be controlled to a great extent. There are three main reasons these materials to be in the focus of academic and applied researchers: 1) important industrial processes are based on them, and any improvement may have significant practical consequences; 2) they proved the ability to undergo modifications (Si/Al ratio, particle size, ...) and thus to be adapted to different applications; and 3) their preparation and post-synthesis modification is optimized. A number of zeolites offer promises for practical applications, however, the preparation conditions limit their uses. For instance, CON-, *SFV-, RTH-, STW-, OKO-type materials, etc., are mostly prepared in the presence of a specific OSDA in a relatively narrow range of chemical compositions of the synthesis mixture. For this reason, the degree of acid site control in these materials is rather low and is limited to preparing and modifying a few representative materials. Hence, the ability to synthesize less common zeolite framework types materials of broader chemical composition range is going to allow for engineering of their acidity as well. This overview presents a comprehensive picture of the analysis and control of active sites in aluminum-containing zeolites. The presented findings indicate that further studies need to be conducted in order to achieve complete control over tailoring the acidic properties of any zeolite material. This goal can be accomplished by preparing new zeolite materials with unknown framework topologies and acidic properties different from the now available zeolites. A good example in this respect is MWW-type zeolite [353]. Modifying the acidic

properties of well-known zeolites by *in situ* and/or post-synthesis methods is also an avenue that proved efficiency and will continue to be explored. Furthermore, engineering the acidity of zeolites can be realized by the incorporation of heteroatoms into zeolite framework. In the present review, this concept is illustrated by highlighting the example of Sn-zeolites that bear Lewis acidity and have particularly disclosed new opportunities in biomass valorization as well as in the production of certain groups of commodities. In addition, there are multiple-step reactions where both Brønsted and Lewis sites are the operating features that represent another direction for developing zeolite-based processes aiming to enhance the prospects to attain sustainable solutions in the energy transition period.

This survey is expected to provide guidelines for the preparation of zeolite materials by design in terms of their acidity (number, strength, and position) and consequently developing more efficient acid zeolite catalysts in already existing as well as in the new processes.

Acknowledgments

This work has been supported in part by Croatian Science Foundation under the project UIP-2019-04-4977 and the CARNOT-ESP project 3DNANOZET 5281. V.V. acknowledges the support from the Industrial Chair ANR-TOTAL “Nanoclean Energy”.

References

- [1] M. Thommes, K. Kaneko, A.V. Neimark, J.P. Olivier, F. Rodriguez-Reinoso, J. Rouquerol, K.S.W. Sing, Physisorption of gases, with special reference to the evaluation of surface area and pore size distribution (IUPAC Technical Report), *Pure Appl. Chem.* 87 (2015) 1051-1069. <https://doi.org/10.1515/pac-2014-1117>
- [2] D.S. Coombs, A. Alberti, T. Armbruster, G. Artioli, C. Colella, E. Galli, J.D. Grice, F. Liebau, J.A. Mandarino, H. Minato, E.H. Nickel, E. Passaglia, D.R. Peacor, S. Quartieri, R. Rinaldi, M. Ross, R.A. Sheppard, E. Tillmans, G. Vezzalini, Recommended nomenclature for zeolite minerals; report of the Subcommittee on Zeolites of the International Mineralogical Association, Commission on New Minerals and Mineral Names, *Can. Mineral.* 35 (1997) 1571-1606.
- [3] <http://www.hypotheticalzeolites.net> (accessed January 27, 2020)
- [4] <http://www.iza-online.org> (accessed January 27, 2020)
- [5] S. Sircar, A.L. Myers, Gas separation by zeolites, in: S.M. Auerbach, K.A. Carrado, P.K. Dutta (Eds.), *Handbook of Zeolite Science and Technology*, Marcel Dekker Inc., New York, 2003, pp. 1063-1104.
- [6] J. B. Nagy, P. Bodart, I. Hannus, I. Kiricsi, *Synthesis and use of zeolitic microporous materials*, DecaGen, Szeged-Szõreg, 1998.
- [7] E.T.C. Vogt, B.M. Weckhuysen, Fluid catalytic cracking: recent developments on the grand old lady of zeolite catalysis, *Chem. Soc. Rev.* 44 (2015) 7342-7370. <https://doi.org/10.1039/C5CS00376H>
- [8] P. Tian, Y. Wei, M. Ye, Z. Liu, Methanol to olefins (MTO): from fundamentals to commercialization, *ACS Catal.* 5 (2015) 1922-1938. <https://doi.org/10.1021/acscatal.5b00007>
- [9] <https://www.uop.com/processing-solutions/petrochemicals/olefins/#ethylene> (accessed January 19 2020)
- [10] C. Paolucci, J. Di Iorio, F.H. Ribeiro, R. Gounder, W.F. Schneider, Catalysis science of NOx selective catalytic reduction with ammonia over Cu-SSZ-13 and Cu-SAPO-34, in: C. Song (Ed.), *Adv. Catal.* Vol. 59, Academic Press, 2016, pp 1-107.
- [11] <http://www.marketresearchstore.com/news/global-zeolite-market-140> (accessed January 16, 2020)

- [12] <https://www.grandviewresearch.com/press-release/global-zeolite-market> (accessed January 19, 2020)
- [13] L.R. Aramburo, E. de Smit, B. Arstad, M.M. van Schooneveld, L. Sommer, A. Juhin, T. Yokosawa, H.W. Zandbergen, U. Olsbye, F.M.F. de Groot, B.M. Weckhuysen, X-ray Imaging of Zeolite Particles at the Nanoscale: Influence of Steaming on the State of Aluminum and the Methanol-To-Olefin Reaction, *Angew. Chem. Int. Ed.* 51 (2012) 3616-3619. <https://doi.org/10.1002/anie.201109026>
- [14] M. Lozinska, E. Mangano, A. Greenaway, R. Fletcher, S. Thompson, C. Murray, S. Brandani, P.A. Wright, Cation control of molecular sieving by flexible Li-containing zeolite RHO, *J. Phys. Chem. C* 120 (2016) 19652-19662. <https://doi.org/10.1021/acs.jpcc.6b04837>
- [15] J. Milovanović, R. Luque, R. Tschentscher, A.A. Romero, H. Li, K. Shih, N. Rajić, Study on the pyrolysis products of two different hardwood lignins in the presence of NiO contained-zeolites, *Biomass Bioenerg.* 103 (2017) 29-34. <https://doi.org/10.1016/j.biombioe.2017.05.007>
- [16] I. Graça, M.C. Bacariza, A. Fernandes, D. Chadwick, Desilicated NaY zeolites impregnated with magnesium as catalysts for glucose isomerisation into fructose, *Appl. Catal. B-Environ.* 224 (2018) 660-670. <https://doi.org/10.1016/j.apcatb.2017.11.009>
- [17] IUPAC. Compendium of Chemical Terminology, 2nd ed. (the "Gold Book"). Compiled by A.D. McNaught and A. Wilkinson. Blackwell Scientific Publications, Oxford (1997). XML on-line corrected version: <http://goldbook.iupac.org> (2006-) created by M. Nic, J. Jirat, B. Kosata; updates compiled by A. Jenkins. ISBN 0-9678550-9-8. <https://doi.org/10.1351/goldbook>.
- [18] M. Boronat, A. Corma, Factors controlling the acidity of zeolites, *Catal. Lett.* 145 (2015) 162-172. <https://doi.org/10.1007/s10562-014-1438-7>
- [19] Z. Wang, Y. Jiang, O. Lafon, J Trébosc, K. D. Kim, C. Stampfl, A. Baiker, J.-P. Amoureux, J. Huang, Brønsted acid sites based on penta-coordinated aluminum species, *Nature Comm.* 7 (2016) 13820. <https://doi.org/10.1038/ncomms13820>
- [20] G. Busca, Acidity and basicity of zeolites: a fundamental approach, *Micropor. Mesopor. Mater.* 254 (2017) 3-16. <https://doi.org/10.1016/j.micromeso.2017.04.007>
- [21] T.K. Phung, G. Busca, On the Lewis acidity of protonic zeolites, *Appl. Catal. A Gen.* 504 (2015) 151-157. <https://doi.org/10.1016/j.apcata.2014.11.031>
- [22] J.A. Rabo, G.J. Gajda, D. Barthomeuf, E. Derouane, W. Hoelderich (Eds.), in: *Guidelines for Mastering the Properties of Molecular Sieves*, NATO ASI Series, Plenum Press, New York, 1990, B-221, 273-297.
- [23] E.G. Derouane, J.C. Védrine, R. Ramos Pinto, P.M. Borges, L. Costa, M.A.N.D.A. Lemos, F. Lemos, F. Ramôa Ribeiro, the acidity of zeolites: concepts, measurements and relation to catalysis: a review on experimental and theoretical methods for the study of zeolite acidity, *Catal. Rev.* 55 (2013) 454-515. <https://doi.org/10.1080/01614940.2013.822266>
- [24] G.L. Woolery, G.H. Kuehl, H.C. Timken, A.W. Chester, J.C. Vartuli, On the nature of framework Brønsted and Lewis acid sites in ZSM-5, *Zeolites* 19 (1997) 288-296. [https://doi.org/10.1016/S0144-2449\(97\)00086-9](https://doi.org/10.1016/S0144-2449(97)00086-9)
- [25] A. Corma, E. Herrero, A. Martinez, J. Prieto, Influence of the method of preparation of ultrastable Y zeolites on extraframework aluminium and the activity and selectivity during the cracking of gas oil, *Prepr. Am. Chem. Soc. Div. Petrol. Chem.* 32 (1987) 639-646.

- [26] A. Omega, Jeroen A. van Bokhoven, R. Prins, Flexible aluminum coordination in aluminosilicates. Structure of zeolite H-USY and amorphous silica-alumina, *J. Phys. Chem. B* 107 (2003) 8854-8860. <https://doi.org/10.1021/jp030094+>
- [27] A. Corma, Inorganic solid acids and their use in acid-catalyzed hydrocarbon reactions, *Chem. Rev.* 95 (1995) 559-614. <https://doi.org/10.1021/cr00035a006>
- [28] M. Guisnet, Influence of zeolite composition on catalytic activity, in D.C. Sherrington, A.P. Kybett (Eds.), *Supported Catalysts and Their Applications*, The proceedings of the 4th International Symposium on Supported Reagents and Catalysts in Chemistry held on 2-6 July 2000 at the University of St Andrews, UK, The Royal Society of Chemistry 2001, Cambridge UK, 55-67.
- [29] J. Sommer, M. Hachoumy, F. Garin, D. Barthomeuf, Zeolite Y-catalyzed versus superacid-catalyzed protium-deuterium exchange in alkanes, *J. Am. Chem. Soc.* 116 1994 5491-5492. <https://doi.org/10.1021/ja00091a072>
- [30] T. Xu, E. J. Munson, J.F. Haw, Toward a systematic chemistry of organic reactions in zeolites: in situ NMR studies of ketones, *J. Am. Chem. Soc.* 116 (1994) 1962-1972. <https://doi.org/10.1021/ja00084a041>
- [31] J. Sauer, Acidic sites in heterogeneous catalysis: structure, properties and activity, *J. Mol. Catal.* 54 (1989) 312-323. [https://doi.org/10.1016/0304-5102\(89\)80149-X](https://doi.org/10.1016/0304-5102(89)80149-X)
- [32] J.F. Haw, Zeolite acid strength and reaction mechanisms in catalysis, *Phys Chem Chem Phys* 4 (2002) 5431-5441. <https://doi.org/10.1039/B206483A>
- [33] J.A. Rabo, M.W. Schoonover, Early discoveries in zeolite chemistry and catalysis at Union Carbide, and follow-up in industrial catalysis, *Appl. Catal. A Gen.* 222 (2001) 261-275. [https://doi.org/10.1016/S0926-860X\(01\)00840-7](https://doi.org/10.1016/S0926-860X(01)00840-7)
- [34] E. Kassab, K. Seiti, M. Allavena, Determination of structure and acidity scales in zeolite systems by ab initio and pseudopotential calculations, *J. Phys. Chem.* 92 (1988) 6705-6709. <https://doi.org/10.1021/j100334a043>
- [35] D. Barthomeuf, Framework induced basicity in zeolites, *Micropor. Mesopor. Mater.* 66 (2003) 1-14. <https://doi.org/10.1016/j.micromeso.2003.08.006>
- [36] D.H. Dompas, W.J. Mortier, C.H. Kenter, M.J.G. Janssen, J.P. Verduijn, The influence of framework-gallium in zeolites: electronegativity and infrared spectroscopic study, *J. Catal.* 129 (1991) 19-24. [https://doi.org/10.1016/0021-9517\(91\)90004-N](https://doi.org/10.1016/0021-9517(91)90004-N)
- [37] M. Guisnet, J.-P. Gilson, Introduction to zeolite science and technology, in: M. Guisnet, J.-P. Gilson (Eds.) *Zeolites for cleaner technologies*, Imperial College Press, London, 2002, pp. 1-28.
- [38] N. Danilina, F. Krumeich, S.A. Castelanelli, J.A. van Bokhoven, Where are the active sites in zeolites? Origin of aluminum zoning in ZSM-5, *J. Phys. Chem. C* 114 (2010) 6640-6645. <https://doi.org/10.1021/jp1006044>
- [39] Z. Ristanović, J.P. Hofmann, U. Deka, T.U. Schüllli, M. Rohnke, A.M. Beale, B.M. Weckhuysen, Intergrowth structure and aluminium zoning of a zeolite ZSM-5 crystal as resolved by synchrotron-based micro X-Ray diffraction imaging, *Angew. Chem. Int. Ed.* 52 (2013) 13382-13386. <http://dx.doi.org/10.1002/anie.201306370>.
- [40] J. Dědeček, Z. Sobalík, B. Wichterlová, Siting and distribution of framework aluminium atoms in silicon-rich zeolites and impact on catalysis, *Catal. Rev. Sci. Eng.* 54 (2012) 135-223. <https://doi.org/10.1080/01614940.2012.632662>
- [41] J. Dědeček, D. Kaucky, B. Wichterlová, Al distribution in ZSM-5, *Chem. Commun.* (2001) 970-971. <https://doi.org/10.1039/B009589N>
- [42] S. Sklenak, J. Dědeček, C. Li, B. Wichterlová, V. Gbov, M. Sierka, J. Sauer, Aluminum siting in silicon-rich zeolite frameworks: a combined high-resolution ²⁷Al NMR

- spectroscopy and quantum mechanics/molecular mechanics study of ZSM-5, *Angew. Chem. Int. Ed.* 46 (2007) 7286-7289. <https://doi.org/10.1002/anie.200702628>
- [43] O.H. Han, C.S. Kim, S.B. Hong, Direct evidence for the nonrandom nature of Al substitution in zeolite ZSM-5: an investigation by ^{27}Al MAS and MQ MAS NMR, *Angew. Chem. Int. Ed.* 4 (2002) 469-472. [https://doi.org/10.1002/1521-3773\(20020201\)41:3<469::AID-ANIE469>3.0.CO;2-K](https://doi.org/10.1002/1521-3773(20020201)41:3<469::AID-ANIE469>3.0.CO;2-K)
- [44] D.E. Perea, I. Arslan, J. Liu, Z. Ristanović, L. Kovarik, B.W. Arey, J.A. Lercher, S.R. Bare, B.M. Weckhuysen, Determining the location and nearest neighbours of aluminium in zeolites with atom probe tomography, *Nat. Commun.* 6 (2015) 7589. DOI: 10.1038/ncomms8589
- [45] P.A. Wright, *Microporous Framework Solids*, RSC Publishing, Cambridge, 2008.
- [46] J.A. van Bokhoven, C. Lamberti, Structure of aluminum, iron, and other heteroatoms in zeolites by X-ray absorption spectroscopy, *Coord. Chem. Rev.* 277-278 (2014) 275-290.
- [47] A. Vjunov, J.L. Fulton, T. Huthwelker, S. Pin, D. Mei, G.K. Schenter, N. Govind, D.M. Camaioni, J.Z. Hu, J.A. Lercher, Quantitatively probing the Al distribution in zeolites, *J. Am. Chem. Soc.* 136 (2014) 8296-8306. <https://doi.org/10.1021/ja501361v>
- [48] A. Vjunov, M. Wang, N. Govind, T. Huthwelker, H. Shi, D. Mei, J.L. Fulton, J.A. Lercher, Tracking the chemical transformations at the Brønsted acid site upon water-induced deprotonation in a zeolite pore, *Chem. Mater.* 29 (2017) 9030-9042.
- [49] L.R. Aramburo, Y. Liu, T. Tyliszczak, F.M.F. de Groot, J.C. Andrews, B.M. Weckhuysen, 3D nanoscale chemical imaging of the distribution of aluminum coordination environments in zeolites with soft X-ray microscopy, *ChemPhysChem* 14 (2013) 496-499.
- [50] D. Freude, J. Kärger, NMR techniques, in: F. Schüth, K.S.W. Sing and J. Weitkamp (eds.): *Handbook of Porous Solids*, Wiley-VCH, Weinheim, 2002, vol. 1, p. 465-504.
- [51] M. Haouas, F. Taulelle, C. Martineau, Recent advances in application of ^{27}Al NMR spectroscopy to materials science, *Prog. Nucl. Mag. Reson. Sp.* 94-95 (2016) 11-36. <https://doi.org/10.1016/j.pnmrs.2016.01.003>
- [52] R. Anwender, C. Palm, O. Groeger, G. Engelhardt, Formation of Lewis acidic support materials via chemisorption of trimethylaluminum on mesoporous silicate MCM-41, *Organometallics* 17 (1998) 2027-2036. <https://doi.org/10.1021/om9710632>
- [53] Z. Zhao, S. Xu, M.Y. Hu, X. Bao, C.H.F. Peden, J. Hu, investigation of aluminum site changes of dehydrated zeolite H-Beta during a rehydration process by high-field solid-state NMR, *J. Phys. Chem. C* 119 (2015) 1410-1417. <https://doi.org/10.1021/jp509982r>
- [54] P. Bräuer, O. Situmorang, P. Ling Ng, C. D'Agostino, Effect of Al content on the strength of terminal silanol species in ZSM-5 zeolite catalysts: a quantitative DRIFTS study without the use of molar extinction coefficients, *Phys. Chem. Chem. Phys.* 20 (2018) 4250-4262. <https://doi.org/10.1039/C7CP07826A>
- [55] S. Hayashi, N. Kojima, Acid properties of H-type mordenite studied by solid-state NMR, *Micropor. Mesopor. Mater.* 141 (2011) 49-55. <https://doi.org/10.1016/j.micromeso.2009.11.006>
- [56] C.A. Fyfe, G.C. Gobbi, J. Klinowski, J.M. Thomas, S. Ramdas, Resolving crystallographically distinct tetrahedral sites in silicalite and ZSM-5 by solid-state NMR, *Nature* 296 (1982) 530.
- [57] M. Hunger, Solid-State NMR Spectroscopy, in: A.W. Chester. E.G. Derouane (Eds.), *Zeolite Characterization and Catalysis*, Springer, Heidelberg, 2009, pp. 65-105.

- [58] J. Huang, Y. Jiang, M.V.R. Reddy, B. Thomas, E. Romanova, M. Hunger Characterization and acidic properties of aluminum-exchanged zeolites X and Y, *J. Phys. Chem. C* 112 (2008) 3811-3818. <https://doi.org/10.1021/jp7103616>
- [59] Z. Yu, A. Zheng, Q. Wang, L. Chen, J. Xu, J. P. Amoureux, F. Deng, Insights into the dealumination of zeolite HY revealed by sensitivity-enhanced ^{27}Al DQ-MAS NMR spectroscopy at high field, *Angew. Chem., Int. Ed.* 49 (2010) 8657-8661. <https://doi.org/10.1002/anie.201004007>
- [60] K. Barbera, F. Bonino, S. Bordiga, T. V. W. Janssen, P. Beato, Structure–deactivation relationship for ZSM-5 catalysts governed by framework defects, *J. Catal.* 280 (2011) 196-205. <https://doi.org/10.1016/j.jcat.2011.03.016>
- [61] Z. Qin, L. Lakiss, L. Tosheva, J.-P. Gilson, A. Vicente, C. Fernandez, V. Valtchev, Comparative study of nano-ZSM-5 catalysts synthesized in OH^- and F^- media, *Adv. Funct. Mater.* 24 (2014) 257-264. <https://doi.org/10.1002/adfm.201301541>
- [62] A. Vimont, F. Thibault-Starzyk, M. Daturi, Analysing and understanding the active site by IR spectroscopy, *Chem. Soc. Rev.* 39 (2010) 4928-4950. <https://doi.org/10.1039/B919543M>
- [63] T. Barzetti, E. Selli, D. Moscotti, L. Forni, *J. Chem. Soc., Faraday Trans.* 92 (1996) 1401-1407. <https://doi.org/10.1039/FT9969201401>
- [64] G.T. Palomino, M.R.L. Carayol, C.O. Arean, Thermodynamics of hydrogen adsorption on the zeolite Ca-Y, *Catal. Today* 138 (2008) 249-252. <https://doi.org/10.1016/j.cattod.2008.05.021>
- [65] L.M. Kustov, V.B. Kazansky, Infrared spectroscopic study of the interaction of cations in zeolites with simple molecular probes. Part 1.—Adsorption of molecular hydrogen on alkaline forms of zeolites as a test for localization sites, *J. Chem. Soc., Faraday Trans.* 87 (1991) 2675-2678. <https://doi.org/10.1039/FT9918702675>
- [66] F. Geobaldo, C. Lamberti, G. Ricchiardi, S. Bordiga, A. Zecchina, G. Turnes Palomino, C. Otero Arean, N_2 adsorption at 77 K on H-Mordenite and alkali-metal-exchanged mordenites: an IR study, *J Phys Chem* 99 (1995) 11167-11177. <https://doi.org/10.1021/j100028a018>
- [67] R. Shigeishi, B. H. Chiche, F. Fajula, CO adsorption on superacid sites on dealuminated mazzite, *Micropor. Mesopor. Mater.* 43 (2001) 211-226. [https://doi.org/10.1016/S1387-1811\(00\)00365-6](https://doi.org/10.1016/S1387-1811(00)00365-6)
- [68] S. Bordiga, C. Lamberti, F. Geobaldo, A. Zecchina, G. Turnes Palomino, C. Otero Arean, Fourier-transform infrared study of CO adsorbed at 77 K on H-mordenite and alkali-metal-exchanged mordenites, *Langmuir* 112 (1995) 527-533. <https://doi.org/10.1021/la00002a027>
- [69] A.S. Medin, V.Yu. Borovkov, V.B. Kazansky, A.G. Pelmentschikov, G.M. Zhidomirov, On the unusual mechanism of Lewis acidity manifestation in HZSM-5 zeolites, *Zeolites* 10 (1990) 668-673. [https://doi.org/10.1016/0144-2449\(90\)90077-5](https://doi.org/10.1016/0144-2449(90)90077-5)
- [70] B. Wichterlová, Z. Tvarůžková, Z. Sobalík, P. Sarv, Determination and properties of acid sites in H-ferrierite: A comparison of ferrierite and MFI structures, *Micropor. Mesopor. Mater.* 24 (1998) 223-233. [https://doi.org/10.1016/S1387-1811\(98\)00167-X](https://doi.org/10.1016/S1387-1811(98)00167-X)
- [71] A. Zecchina, L. Marchese, C. Bordiga, C. Pazè, E. Gianotti, Vibrational spectroscopy of NH_4^+ ions in zeolitic materials: an IR study, *J. Phys. Chem. B* 101 (1997) 10128-10135. <https://doi.org/10.1021/jp9717554>
- [72] F. Yin, A.L. Blumenfeld, V. Gruver, J.J. Fripiat, NH_3 as a probe molecule for NMR and IR Study of zeolite catalyst acidity, *J. Phys. Chem. B* 101 (1997) 1824-1830. <https://doi.org/10.1021/jp9618542>

- [73] B.V. Liengme, W.K. Hall, Studies of hydrogen held by solids. Part 11.—Interaction of simple olefins and pyridine with decationated zeolites, *Trans. Faraday Soc.* 62 (1966) 3229-3243. <https://doi.org/10.1039/TF9666203229>
- [74] T. Armaroli, M. Bevilacqua, M. Trombetta, A. Gutiérrez Alejandro, J. Ramírez, B. Notari, R.J. Willey, G. Busca, A study of the external and internal sites of MFI-type zeolitic materials through the FT-IR investigation of the adsorption of nitriles, *Appl. Catal. A* 216 (2001) 59-71. [https://doi.org/10.1016/S0926-860X\(01\)00543-9](https://doi.org/10.1016/S0926-860X(01)00543-9)
- [75] T. Onfroy, G. Clet, M. Houalla, Quantitative IR characterization of the acidity of various oxide catalysts, *Micropor. Mesopor. Mater.* 82 (2005) 99-104. <https://doi.org/10.1016/j.micromeso.2005.02.020>
- [76] F. Thibault-Starzyk, A. Vimont, J.-P. Gilson, 2D-COS IR study of coking in xylene isomerisation on H-MFI zeolite, *Catal. Today* 70 (2001) 227-241. [https://doi.org/10.1016/S0920-5861\(01\)00420-5](https://doi.org/10.1016/S0920-5861(01)00420-5)
- [77] N.S. Nesterenko, F. Thibault-Starzyk, V. Montouillout, V.V. Yuschenko, C. Fernandez, J.-P. Gilson, F. Fajula, I.I. Ivanova, The use of the consecutive adsorption of pyridine bases and carbon monoxide in the IR spectroscopic study of the accessibility of acid sites in microporous/mesoporous materials, *Kinet. Catal.* 47 (2006) 40-48. <https://doi.org/10.1134/S0023158406010071>
- [78] K. Góra-Marek, K. Tarach, M. Choi, 2,6-di-tert-butylpyridine sorption approach to quantify the external acidity in hierarchical zeolites, *J. Phys. Chem. C* 118 (2014) 12266-12274. <https://doi.org/10.1021/jp501928k>
- [79] S. Bordiga, C. Lamberti, F. Bonino, A. Travert, F. Thibault-Starzyk, Probing zeolites by vibrational spectroscopies, *Chem. Soc. Rev.* 44 (2015) 7262-7341. <https://doi.org/10.1039/C5CS00396B>
- [80] N.S. Nesterenko, F. Thibault-Starzyk, V. Montouillout, V.V. Yuschenko, C. Fernandez, J.-P. Gilson, F. Fajula, I.I. Ivanova, Accessibility of the acid sites in dealuminated small-pore mordenites studied by FTIR of co-adsorbed alkylpyridines and CO, *Micropor. Mesopor. Mater.* 71 (2004) 157-166. <https://doi.org/10.1016/j.micromeso.2004.03.028>
- [81] K. Hadjiivanov, Identification and characterization of surface hydroxyl groups by infrared spectroscopy, in: F.C. Jentoft (Ed.), *Advances in Catalysis*, Volume 57, 2014, pp. 99-318.
- [82] J.C. Lavalley, Infrared spectrometric studies of the surface basicity of metal oxides and zeolites using adsorbed probe molecules, *Catal. Today* 27 (1996) 377-401. [https://doi.org/10.1016/0920-5861\(95\)00161-1](https://doi.org/10.1016/0920-5861(95)00161-1)
- [83] A. Zheng, S.-B. Liu, F. Deng, ³¹P NMR chemical shifts of phosphorus probes as reliable and practical acidity scales for solid and liquid catalysts, *Chem. Rev.* 117 (2017) 12475-12531. <https://doi.org/10.1021/acs.chemrev.7b00289>
- [84] J.H. Lunsford, Characterization of acidity in zeolites and related oxides using trimethylphosphine as a probe, *Top. Catal.* 4 (1997) 91-98. <https://doi.org/10.1023/A:1019171702160>
- [85] Q. Zhao, W.-H. Chen, S.-J. Huang, Y.-C. Wu, H.-K. Lee, S.-B. Liu, Discernment and quantification of internal and external acid sites on zeolites, *J. Phys. Chem. B*, 106 (2002) 4462-4469. <https://doi.org/10.1021/jp015574k>
- [86] L. Peng, Y. Liu, N. Kim, J.E. Readman, C.P. Grey, Detection of Brønsted acid sites in zeolite HY with high-field ¹⁷O-MAS-NMR techniques, *Nat. Mater.* 4 (2005) 216-219. <https://doi.org/10.1038/nmat1332>
- [87] W.R. Gunther, V.K. Michaelis, R.G. Griffin, Y. Román-Leshkov, Interrogating the Lewis acidity of metal sites in Beta zeolites with ¹⁵N pyridine adsorption coupled with

- MAS NMR spectroscopy, *J. Phys. Chem. C* 120 (2016) 28533-28544. <https://doi.org/10.1021/acs.jpcc.6b07811>
- [88] B. Louis, A. Vicente, C. Fernandez, V. Valtchev, Crystal size–acid sites relationship study of nano- and micrometer-sized zeolite crystals, *J. Phys. Chem. C* 115 (2011) 18603-18610. <https://doi.org/10.1021/jp204234d>
- [89] R. Osuga, T. Yokoi, K. Doitomi, H. Hirao, J.N. Kondo, Infrared investigation of dynamic behavior of Brønsted acid sites on zeolites at high temperatures, *J. Phys. Chem. C* 121 (2017) 25411-25420. <https://doi.org/10.1021/acs.jpcc.7b09846>
- [90] T. Kubota, R. Osuga, T. Yokoi, J.N. Kondo, Consideration of acid strength of a single OH group on zeolites by isotope exchange reaction with ethane at high temperatures, *Top. Catal.* 60 (2017) 1496-1505. <https://doi.org/10.1007/s11244-017-0834-9>
- [91] J.E. Schmidt, L. Peng, A. Lucini Paioni, H.L. Ehren, W. Guo, B. Mazumder, D.A. Matthijs de Winter, Ö. Attila, D. Fu, A. Dutta Chowdhury, K. Houben, M. Baldus, J.D. Poplawsky, B.M. Weckhuysen, Isolating clusters of light elements in molecular sieves with atom probe tomography, *J. Am. Chem. Soc.* 140 (2018) 9154-9158. <https://doi.org/10.1021/jacs.8b04494>
- [92] M.E.Z. Velthoen, S. Nab, B.M. Weckhuysen, Probing acid sites in solid catalysts with pyridine UV-Vis spectroscopy, *Phys. Chem. Chem. Phys.* 20 (2018) 21647-21659. <https://doi.org/10.1039/C8CP03991G>
- [93] I.L.C. Buurmans, J. Ruiz-Martínez, W.V. Knowles, D. van der Beek, J.A. Bergwerff, E.T.C. Vogt, B.M. Weckhuysen, Catalytic activity in individual cracking catalyst particles imaged throughout different life stages by selective staining, *Nat. Chem.* 3 (2011) 862-867. <https://doi.org/10.1038/nchem.1148>
- [94] I.L.C. Buurmans, J. Ruiz-Martínez, S.L. van Leeuwen, D. van der Beek, J.A. Bergwerff, W.V. Knowles, E.T.C. Vogt, B.M. Weckhuysen, Staining of fluid-catalytic-cracking catalysts: localising Brønsted Acidity within a single catalyst particle, *Chem. Eur. J.* 18 (2012) 1094-1101. <https://doi.org/10.1002/chem.201102949>
- [95] J.L. Falconer, J.A. Schwarz, Temperature-programmed desorption and reaction: applications to supported catalysts, *Catal. Rev.-Sci. Eng.* 25 (1983) 141-227. <https://doi.org/10.1080/01614948308079666>
- [96] D.J. Parrillo, A.T. Adamo, G.T. Kokotailo, R.J. Gorte, Amine adsorption in H-ZSM-5, *Appl. Catal.* 67 (1990) 107-118. [https://doi.org/10.1016/S0166-9834\(00\)84435-8](https://doi.org/10.1016/S0166-9834(00)84435-8)
- [97] A.I. Biaglow, D.J. Parrillo, G.T. Kokotailo, R.J. Gorte, A study of dealuminated faujasites, *J. Catal.* 148 (1994) 213-223. <https://doi.org/10.1006/jcat.1994.1203>
- [98] H.G. Karge, V. Dondur, Investigation of the distribution of acidity in zeolites by temperature-programmed desorption of probe molecules. I. Dealuminated mordenites, *J. Phys. Chem.* 94 (1990) 765-772. <https://doi.org/10.1021/j100365a047>
- [99] M. Niwa, N. Katada, New method for the temperature-programmed desorption (TPD) of ammonia experiment for characterization of zeolite acidity: a review, *Chem. Rec.* 13 (2013) 432-455. <https://doi.org/10.1002/tcr.201300009>
- [100] D. Esquivel, A.J. Cruz-Cabeza, C. Jiménez-Sanchidrián, F.J. Romero-Salguero, Local environment and acidity in alkaline and alkaline-earth exchanged β zeolite: Structural analysis and catalytic properties, *Micropor. Mesopor. Mater.* 142 (2011) 672-679. <https://doi.org/10.1016/j.micromeso.2011.01.018>
- [101] R. J. Cvetanovic, Y. Amenomiya, Application of a temperature-programmed desorption technique to catalyst studies, *Adv. Catal.* 17 (1967) 103-149. [https://doi.org/10.1016/S0360-0564\(08\)60686-0](https://doi.org/10.1016/S0360-0564(08)60686-0)
- [102] M. Niwa, N. Katada, K. Okumura, Characterization and Design of Zeolite Catalysts – Solid Acidity, Shape Selectivity and Loading Properties, Springer Series in Materials Science, 141, Heidelberg, 2010.

- [103] M. Hunger, Catalytically active sites: generation and characterization, in: J. Čejka, A. Corma, S. Zones (Eds.), *Zeolites and Catalysis, Synthesis Reactions and Applications*, Wiley-VCH, Weinheim, 2010, pp. 493-546.
- [104] N. Katada, Analysis and interpretation of acidic nature of aluminosilicates, *Molecular Catal.* 458 (2018) 116-126. <https://doi.org/10.1016/j.mcat.2017.12.024>
- [105] N. Katada, K. Nouno, J.K. Lee, J. Shin, S.B. Hong, M. Niwa, Acidic properties of cage-based, small-pore zeolites with different framework topologies and their silicoaluminophosphate analogues, *J. Phys. Chem. C* 115 (2011) 22505-22513. <https://doi.org/10.1021/jp207894n>
- [106] A. Auroux, Acidity and basicity: determination by adsorption microcalorimetry, in: H.G. Karge, J. Weitkamp (Eds.), *Molecular Sieves*, vol. 6, Springer-Verlag, Berlin Heidelberg, 2006, pp. 45-152.
- [107] D.T. Chen, L. Zhang, C. Yi, J.A. Dumesic, Methylamine synthesis over solid acid catalysts: Microcalorimetric and infrared spectroscopic studies of adsorbed species, *J. Catal.* 146 (1994) 257-267. [https://doi.org/10.1016/0021-9517\(94\)90029-9](https://doi.org/10.1016/0021-9517(94)90029-9)
- [108] V. Dondur, V. Rakić, Lj. Damjanović, A. Auroux, Comparative study of the active sites in zeolites by different probe molecules, *J. Serb. Chem. Soc.* 70 (2005) 457-474.
- [109] A. Auroux, Microcalorimetry Methods to study the acidity and reactivity of zeolites, pillared clays and mesoporous materials, *Top. Catal.* 19 (2002) 205-213. <https://doi.org/10.1023/A:1015367708955>
- [110] Lj. Damjanović, A. Auroux, Determination of acid/base properties by temperature programmed desorption (TPD) and adsorption calorimetry, in: A.W. Chester. E.G. Derouane (Eds.), *Zeolite Characterization and Catalysis*, Springer, Heidelberg, 2009, pp. 107-167.
- [111] O.A. Abdelrahman, K.P. Vinter, L. Ren, D. Xu, R.J. Gorte, M. Tsapatsis, P.J. Dauenhauer, Simple quantification of zeolite acid site density by reactive gas chromatography, *Catal. Sci. Technol.* 7 (2017) 3831-3841. <https://doi.org/10.1039/C7CY01068K>
- [112] J. Dědeček, L. Čapek, P. Sazama, Z. Sobalík, B. Wichterlová, Control of metal ion species in zeolites by distribution of aluminium in the framework: From structural analysis to performance under real conditions of SCR-NO_x and NO, N₂O decomposition, *Appl. Catal. A: Gen.* 391 (2011) 244-253. <https://doi.org/10.1016/j.apcata.2010.06.026>
- [113] J.R. Di Iorio, C.T. Nimlos, R. Gounder, Introducing catalytic diversity into single-site chabazite zeolites of fixed composition via synthetic control of active site proximity, *ACS Catal.* 7 (2017) 6663-6674. <https://doi.org/10.1021/acscatal.7b01273>
- [114] L. Grajciar, C.O. Areán, A. Pulido, P. Nachtigall, Periodic DFT investigation of the effect of aluminium content on the properties of the acid zeolite H-FER, *Phys. Chem. Chem. Phys.* 12 (2010) 1497-1506. <https://doi.org/10.1039/B917969K>
- [115] A. Janda, A.T. Bell, Effects of Si/Al ratio on the distribution of framework Al and on the rates of alkane monomolecular cracking and dehydrogenation in H-MFI, *J. Am. Chem. Soc.* 135 (2013) 19193-19207. <https://doi.org/10.1021/ja4081937>
- [116] T. Demuth, J. Hafner, L. Benco, H. Toulhoat, Structural and acidic properties of mordenite. An ab initio density-functional study *J. Phys. Chem. B* 104 (2000) 4593-4607. <https://doi.org/10.1021/jp993843p>
- [117] G. Sastre, V. Fornes, A. Corma, On the preferential location of Al and proton siting in zeolites: a computational and infrared study, *J. Phys. Chem. B* 106 (2002) 701-708. <https://doi.org/10.1021/jp013189p>

- [118] V. Van Speybroeck, K. Hemelsoet, L. Joos, M. Waroquier, R.G. Bellb, C.R.A. Catlow, Advances in theory and their application within the field of zeolite chemistry, *Chem. Soc. Rev.* 44 (2015) 7044-7111. <https://doi.org/10.1039/C5CS00029G>
- [119] R. Bulanek, K. Frolich, P. Cicmanec, D. Nachtigallova, A. Pulido, P. Nachtigall, Combined experimental and theoretical investigations of heterogeneous dual cation sites in Cu,M-FER zeolites, *J. Phys. Chem. C* 115 (2011) 13312-13321. <https://doi.org/10.1021/jp200293y>
- [120] K. Suzuki, G. Sastre, N. Katada, M. Niwa, Ammonia IRMS-TPD measurements and DFT calculation on acidic hydroxyl groups in CHA-type zeolites, *Phys. Chem. Chem. Phys.* 9 (2007) 5980-5987. <https://doi.org/10.1039/B711961E>
- [121] K. Suzuki, T. Noda, G. Sastre, N. Katada, M. Niwa, Periodic density functional calculation on the Brønsted acidity of modified Y-type zeolite, *J. Phys. Chem. C* 113 (2009) 5672-5680. <https://doi.org/10.1021/jp8104562>
- [122] A.J. O'Malley, A.J. Logsdail, A.A. Sokola, C.R.A. Catlow, Modelling metal centres, acid sites and reaction mechanisms in microporous catalysts, *Faraday Discuss.* 188 (2016) 235-255. <https://doi.org/10.1039/C6FD00010J>
- [123] N. Katada, K. Suzuki, T. Noda, G. Sastre, M. Niwa, Correlation between Brønsted acid strength and local structure in zeolites, *J. Phys. Chem. C* 113 (2009) 19208-19217. <https://doi.org/10.1021/jp903788n>
- [124] H. Kawakami, S. Yoshida, T. Yonezawa, A quantum-chemical approach to the generation of solid acidity in composite metal oxides, *J. Chem. Soc., Faraday Trans. 2* 80 (1984) 205-217. <https://doi.org/10.1039/F29848000205>
- [125] M. Brändle, J. Sauer, Acidity differences between inorganic solids induced by their framework structure. A combined quantum mechanics/molecular mechanics ab initio study on zeolites, *J. Am. Chem. Soc.* 120 (1998) 1556-1570. <https://doi.org/10.1021/ja9729037>
- [126] A.J. Jones, E. Iglesia, The strength of Brønsted acid sites in microporous aluminosilicates *ACS Catal.* 5 (2015) 5741-5755. <https://doi.org/10.1021/acscatal.5b01133>
- [127] M. Rybicki, J. Sauer, Acid strength of zeolitic Brønsted sites - dependence on dielectric properties, *Catal. Today* 323 (2019) 86-93. <https://doi.org/10.1016/j.cattod.2018.04.031>
- [128] M. Boronat, A. Corma, What is measured when measuring acidity in zeolites with probe molecules?, *ACS Catal.* 9 (2019) 1539-1548. <https://doi.org/10.1021/acscatal.8b04317>
- [129] A.A. Lucasa, I. Derycke, Ph. Lambin, J.-P. Vigneron, L. Leherste, M. Elanany, J.-M. André, A.V. Larin, D.P. Vercauteren, Confinement in molecular sieves: The pioneering physical concepts, *J. Mol. Catal. A Chem.* 305 (2009) 16-23. <https://doi.org/10.1016/j.molcata.2009.02.040>
- [130] R.L. Martin, T.F. Willems, L.C. Lin, J. Kim, J.A. Swisher, B. Smit, M. Haranczyk, Similarity-driven discovery of zeolite materials for adsorption-based separations, *ChemPhysChem* 13 (2012) 3595-3597. <https://doi.org/10.1002/cphc.201200554>
- [131] Y.G. Kolyagin, A.V. Yakimov, S. Tolborg, P.N.R. Vennestrøm, I.I. Ivanova, Direct observation of tin in different T-sites of Sn-BEA by one- and two-dimensional ¹¹⁹Sn MAS NMR spectroscopy, *J. Phys. Chem. Lett.* 9 (2018) 3738-3743. <https://doi.org/10.1021/acs.jpcclett.8b01415>
- [132] S. Svelle, C. Tuma, X. Rozanska, T. Kerber, J. Sauer, Quantum chemical modeling of zeolite-catalyzed methylation reactions: toward chemical accuracy for barriers, *J. Am. Chem. Soc.* 13 (2009) 816-825. <https://doi.org/10.1021/ja807695p>

- [133] J. Van der Mynsbrugge, A. Janda, S. Mallikarjun Sharada, L.-C. Lin, V. Van Speybroeck, M. Head-Gordon, A.T. Bell, Theoretical analysis of the influence of pore geometry on monomolecular cracking and dehydrogenation of n-butane in Brønsted acidic zeolites, *ACS Catal.* 7 (2017) 2685-2697. <https://doi.org/10.1021/acscatal.6b03646>
- [134] A.J. Jones, S.I. Zones, E. Iglesia, Implications of transition state confinement within small voids for acid catalysis, *J. Phys. Chem. C* 118 (2014) 17787-17800. <https://doi.org/10.1021/jp5050095>
- [135] H. Fang, A. Zheng, J. Xu, S. Li, Y. Chu, L. Chen, F. Deng, Theoretical Investigation of the Effects of the Zeolite Framework on the Stability of Carbenium Ions, *J. Phys. Chem. C* 115 (2011) 7429–7439. <https://doi.org/10.1021/jp1097316>
- [136] L. Grajciar, PbS clusters embedded in sodalite zeolite cavities of different compositions: unraveling the structural evolution and optical properties using ab initio calculations, *J. Phys. Chem. C* 120 (2016) 27050-27065. <https://doi.org/10.1021/acs.jpcc.6b09423>
- [137] S.A. Zygmunt, L.A. Curtiss, P. Zapol, L.E. Iton, Ab initio and density functional study of the activation barrier for ethane cracking in cluster models of zeolite HZSM-5, *J. Phys. Chem. B* 104 (2000) 1944–1949, <http://dx.doi.org/10.1021/jp993194h>.
- [138] E.M. Gallego, M. T. Portilla, C. Paris, A. León-Escamilla, M. Boronat, M. Moliner, A. Corma, “Ab initio” synthesis of zeolites for preestablished catalytic reactions, *Science* 355 (2017) 1051-1054. <https://doi.org/10.1126/science.aal0121>
- [139] L. Grajciar, C.J. Heard, A.A. Bondarenko, M.V. Polynski, J. Meeprasert, E.A. Pidko, P. Nachtigall, Towards operando computational modeling in heterogeneous catalysis, *Chem. Soc. Rev.* 47 (2018) 8307-8348. <https://doi.org/10.1039/C8CS00398J>
- [140] J. Sauer, Brønsted activity of two-dimensional zeolites compared to bulk materials, *Faraday Discuss.* 188 (2016) 227-234. <https://doi.org/10.1039/C5FD00207A>
- [141] D.W. Breck, *Zeolite Molecular Sieves, Structure, Chemistry and Use*, Wiley, New York, 1974.
- [142] E.R. Cooper, C.D. Andrews, P.S. Wheatley, P.B. Webb, P. Wormald, R.E. Morris, Ionic liquids and eutectic mixtures as solvent and template in synthesis of zeolite analogues, *Nature* 430 (2004) 1012-1016. <https://doi.org/10.1038/nature02860>
- [143] Q. Huo, S. Feng, R. Xu, First syntheses of pentasil-type silica zeolites from non-aqueous systems, *J. Chem. Soc. Chem. Commun.* (1988) 1486-1487. <https://doi.org/10.1039/C39880001486>
- [144] M.A. Camblor, P.A. Barrett, M.-J. Díaz-Cabañas, L.A. Villaescusa, M. Puche, T. Boix, E.Perez, H. Koller, High silica zeolites with three-dimensional systems of large pore channels, *Micropor. Mesopor. Mater.* 48 (2001) 11-22. [https://doi.org/10.1016/S1387-1811\(01\)00325-0](https://doi.org/10.1016/S1387-1811(01)00325-0)
- [145] H. Kessler, Synthesis of high-silica zeolites and phosphate-based materials in the presence of fluoride, in: H. Robson (Ed.), *Verified Synthesis of Zeolitic Materials*, Elsevier, 2001, pp. 25-26.
- [146] S.I. Zones, S.-J. Hwang, A novel approach to borosilicate zeolite synthesis in the presence of fluoride, *Micropor. Mesopor. Mater.* 146 (2011) 48-56. <https://doi.org/10.1016/j.micromeso.2011.05.034>
- [147] V.M. Georgieva, E.L. Bruce, M.C. Verbraeken, A.R. Scott, W.J. Casteel Jr., S. Brandani, P.A. Wright, Triggered gate opening and breathing effects during selective CO₂ adsorption by merlinoite zeolite, *J. Am. Chem. Soc.* 141 (2019) 12744-12759. <https://doi.org/10.1021/jacs.9b05539>

- [148] M.D. Oleksiak, J.D. Rimer, Synthesis of zeolites in the absence of organic structure-directing agents: factors governing crystal selection and polymorphism, *Rev. Chem. Eng.* 30 (2014) 1-49. <https://doi.org/10.1515/revce-2013-0020>
- [149] H. Lee, S.I. Zones, M.E. Davis, A combustion-free methodology for synthesizing zeolites and zeolite-like materials, *Nature* 425 (2003) 385-388. <https://doi.org/10.1038/nature01980>
- [150] H. Gies, B. Marler, The structure-controlling role of organic templates for the synthesis of porosils in the system SiO₂/template/H₂O, *Zeolites* 12 (1992) 42-49. [https://doi.org/10.1016/0144-2449\(92\)90008-D](https://doi.org/10.1016/0144-2449(92)90008-D)
- [151] C.T.G. Knight, R.J. Bales, S.D. Kinrade, The structure of silicate anions in aqueous alkaline solutions, *Angew. Chem. Int. Ed.* 46 (2007) 8148-8152. <https://doi.org/10.1002/anie.200702986>
- [152] G. Harvey, L.S. Dent Glaser, Structure and properties of aluminosilicate solutions and gels, in: M.L. Ocelli, H.E. Robson (Eds.), *Zeolite Synthesis, Symposium Series 398*, American Chemical Society, 1989, Washington D.C., pp. 49-65.
- [153] A.T. Bell, Applications of NMR spectroscopy to the study of zeolite synthesis, in M.L. Ocelli, H.E. Robson (Eds.), *Zeolite Synthesis, Symposium Series 398*, American Chemical Society, 1989, Washington D.C., pp. 66-82.
- [154] S. Bosnar, M. Dutour Sikirić, V. Smrečki, J. Bronić, S. Šegota, V. Strasser, T. Antonić Jelić, A. Palčić, B. Subotić, Controlled aggregation of core(amorphous silica)@shell(TPA⁺-polysilicate) nanoparticles at room temperature by selective removal of TPA⁺ ions from the nanoparticle shell, *Inorg. Chem. Front.* 6 (2019) 1639-1653. <https://doi.org/10.1039/C9QI00200F>
- [155] M. Smaïhi, O. Barida, V. Valtchev, Investigation of the crystallization stages of LTA-type zeolite by complementary characterization techniques, *Eur. J. Inorg. Chem.* (2003) 4370-4377. <https://doi.org/10.1002/ejic.200300154>
- [156] A. Navrotsky, O. Trofymuk, A.A. Levchenko, Thermochemistry of microporous and mesoporous materials, *Chem. Rev.* 9 (2009) 3885-3902. <https://doi.org/10.1021/cr800495t>
- [157] B.M. Lok, T.R. Cannan, C.A. Messina, The role of organic molecules in molecular sieve synthesis, *Zeolites* 3 (1983) 282-291. [https://doi.org/10.1016/0144-2449\(83\)90169-0](https://doi.org/10.1016/0144-2449(83)90169-0)
- [158] V.P. Shiralkar, A. Clearfield, Synthesis of the molecular sieve ZSM-5 without the aid of templates, *Zeolites* 9 (1989) 363-370. [https://doi.org/10.1016/0144-2449\(89\)90089-4](https://doi.org/10.1016/0144-2449(89)90089-4)
- [159] F.Y. Dai, M. Susuki, H. Takahashi, Y. Saito, Crystallization of pentasil zeolite in the absence of organic templates, in M.L. Ocelli, H.E. Robson (Eds.), *Zeolite Synthesis, Symposium Series 398*, American Chemical Society, 1989, Washington D.C., pp. 244-256.
- [160] G. Bellusi, G. Perego, A. Carati, U. Cornaro, V. Fattore, 5-1 SBU based zeolites from wholly inorganic systems, *Stud. Surf. Sci. Catal.* 37 (1988) 37-44. [https://doi.org/10.1016/S0167-2991\(09\)60580-2](https://doi.org/10.1016/S0167-2991(09)60580-2)
- [161] S.D. Kim, S.H. Noh, K.H. Seong, W.J. Kim, Compositional and kinetic study on the rapid crystallization of ZSM-5 in the absence of organic template under stirring, *Micropor. Mesopor. Mater.* 72 (2004) 185-192. <https://doi.org/10.1016/j.micromeso.2004.04.024>
- [162] K. Honda, M. Itakura, Y. Matsuura, A. Onda, Y. Ide, M. Sadakane, T. Sano, Role of structural similarity between starting zeolite and product zeolite in the interzeolite conversion process, *J. Nanosci. Nanotechnol.* 13 (2013) 3020-3026. <https://doi.org/10.1166/jnn.2013.7356>

- [163] Q. Yu, Q. Zhang, J. Liu, C. Li, Q. Cui, Inductive effect of various seeds on the organic template-free synthesis of zeolite ZSM-5, *CrystEngComm* 15 (2013) 7680-7687. <https://doi.org/10.1039/C3CE40784E>
- [164] Y. Kamimura, K. Iyoki, S.P. Elangovan, K. Itabashi, A. Shimojima, T. Okubo, OSDA-free synthesis of MTW-type zeolite from sodium aluminosilicate gels with zeolite beta seeds, *Micropor. Mesopor. Mater.* 163 (2012) 282-290. <https://doi.org/10.1016/j.micromeso.2012.07.014>
- [165] Z. Liu, K. Okabe, C. Anand, Y. Yonezawa, J. Zhu, H. Yamada, A. Endo, Y. Yanaba, T. Yoshikawa, K. Ohara, T. Okubo, T. Wakihara, Continuous flow synthesis of ZSM-5 zeolite on the order of seconds, *PNAS* 113 (2016) 14267-14271. <https://doi.org/10.1073/pnas.1615872113>
- [166] S. Goel, S.I. Zones, E. Iglesia, Synthesis of zeolites via interzeolite transformations without organic structure-directing agents, *Chem. Mater.* 27 (2015) 2056-2066. <https://doi.org/10.1021/cm504510f>
- [167] M. Taramasso, G. Perego, B. Notari, Preparation of porous crystalline synthetic material comprised of silicon and titanium oxides, US patent 4 410 501 (1983).
- [168] R. de Ruiter, J.C. Jansen, H. van Bekkum, On the incorporation mechanism of B and Al in MFI-type zeolite frameworks, *Zeolites* 12 (1992) 56-62. [https://doi.org/10.1016/0144-2449\(92\)90011-D](https://doi.org/10.1016/0144-2449(92)90011-D)
- [169] J. Patarin, H. Kessler, J.L. Guth, Iron distribution in iron MFI-type zeolite samples synthesized in fluoride medium: Influence of the synthesis procedure, *Zeolites* 10 (1990) 674-679. [https://doi.org/10.1016/0144-2449\(90\)90078-6](https://doi.org/10.1016/0144-2449(90)90078-6)
- [170] K. Kanie, M. Sakaguchi, F. Muto, M. Horie, M. Nakaya, T. Yokoi, A. Muramatsu, Mechanochemically assisted hydrothermal synthesis of Sn-substituted MFI-type silicates, *Sci. Technol. Adv. Mat.* 19 (2018) 545-553. <https://doi.org/10.1080/14686996.2018.1497404>
- [171] J. Kornatowski, M. Sychev, V. Goncharuk, W.H. Baur, New molecular sieve - vanadium silicalite KVS-5, *Stud. Surf. Sci. Catal.* 65 (1991) 581-590. [https://doi.org/10.1016/S0167-2991\(08\)62942-0](https://doi.org/10.1016/S0167-2991(08)62942-0)
- [172] G. Giordano, A. Katović, E. Szymkowiak-Janiszewka, S. Kowalak, Synthesis and properties of the MFI zincosilicalite, *Collect. Czech. Chem. Commun.* 68 (2003) 1149-1162. <https://doi.org/10.1135/cccc20031149>
- [173] S.V. Awate, P.N. Joshi, V.P. Shiralkar, A.N. Kotasthane, Synthesis and characterization of gallosilicate pentasil (MFI) framework zeolites, *J. Incl. Phenom.* 13 (1992) 207-218. <https://doi.org/10.1007/BF01042779>
- [174] A. Bhaumik, R. Kumar, A new As³⁺-silicate molecular sieve with MFI structure, *Chem. Commun.* (1995) 869-870. <https://doi.org/10.1039/C39950000869>
- [175] N. Novak Tušar, N. Zabukovec Logar, I. Arcon, F. Thibault-Starzyk, A. Ristić, N. Rajić, V. Kaučić, Manganese-containing silica-based microporous molecular sieve MnS-1: synthesis and characterization, *Chem. Mater.* 15 (2003) 4745-4750. <https://doi.org/10.1021/cm031091c>
- [176] T. Yokoi, H. Mochizuki, S. Namba, J.N. Kondo, T. Tatsumi, Control of the Al distribution in the framework of ZSM-5 Zeolite and its evaluation by solid-state NMR technique and catalytic properties, *J. Phys. Chem. C* 119 (2015) 15303-15315. <https://doi.org/10.1021/acs.jpcc.5b03289>
- [177] V. Pashkova, S. Sklenak, P. Klein, M. Urbanova, J. Dědeček, Location of framework Al atoms in the channels of ZSM-5: effect of the (hydrothermal) synthesis, *Chem. Eur. J.* 22, (2016) 3937-3941. <https://doi.org/10.1002/chem.201503758>

- [178] T. Yokoi, H. Mochizuki, T. Biliget, Y. Wang, T. Tatsumi, Unique Al distribution in the MFI framework and its impact on catalytic properties, *Chem. Lett.* 4 (2017) 798-800. <https://doi.org/10.1246/cl.170156>
- [179] T. Biliget, Y. Wang, T. Nishitoba, R. Otomo, S. Park, H. Mochizuki, J.N. Kondo, T. Tatsumi, T. Yokoi, Al distribution and catalytic performance of ZSM-5 zeolites synthesized with various alcohols, *J. Catal.* 353 (2017) 1-10. <https://doi.org/10.1016/j.jcat.2017.06.026>
- [180] S. Park, T. Biliget, Y. Wang, T. Nishitoba, J.N. Kondo, T. Yokoi, Acidic and catalytic properties of ZSM-5 zeolites with different Al distributions, *Catal. Today* 303 (2018) 64-70. <https://doi.org/10.1016/j.cattod.2017.07.022>
- [181] H. Liu, H. Wang, A.-H. Xing, J.-H. Cheng, Effect of Al distribution in MFI framework channels on the catalytic performance of ethane and ethylene aromatization, *J. Phys. Chem. C* 123 (2019) 15637-15647. <https://doi.org/10.1021/acs.jpcc.9b03507>
- [182] M. Bernauer, E. Tabor, V. Pashkova, D. Kaucký, Z. Sobalík, B. Wichterlová, J. Dedecek, Proton proximity – new key parameter controlling adsorption, desorption and activity in propene oligomerization over H-ZSM-5 zeolites, *J. Catal.* 344 (2016) 157-172. <http://dx.doi.org/10.1016/j.jcat.2016.09.025>
- [183] V. Pashkova, P. Klein, J. Dedecek, V. Tokarová, B. Wichterlová, Incorporation of Al at ZSM-5 hydrothermal synthesis. Tuning of Al pairs in the framework, *Micropor. Mesopor. Mater.* 202 (2015) 138-146. <http://dx.doi.org/10.1016/j.micromeso.2014.09.056>
- [184] K. Gołabek, E. Tabor, V. Pashkova, J. Dedecek, K. Tarach, K. Góra-Marek, The proximity of aluminium atoms influences the reaction pathway of ethanol transformation over zeolite ZSM-5, *Comm. Chem.* 3 (2020) 25. <https://doi.org/10.1038/s42004-020-0268-3>
- [185] T. Liang, J. Chen, Z. Qin, J. Li, P. Wang, S. Wang, G. Wang, M. Dong, W. Fan, J. Wang, Conversion of methanol to olefins over H-ZSM-5 zeolite: reaction pathway is related to the framework aluminum siting, *ACS Catal.* 6 (2016) 7311-7325. <https://doi.org/10.1021/acscatal.6b01771>
- [186] J. Shao, T. Fu, Q. Ma, Z. Ma, C. Zhang, Z. Li, Controllable synthesis of nano-ZSM-5 catalysts with large amount and high strength of acid sites for conversion of methanol to hydrocarbons, *Micropor. Mesopor. Mater.* 273 (2019) 122-132. <https://doi.org/10.1016/j.micromeso.2018.07.007>
- [187] A. Palčić, V.V. Ordonsky, Z. Qin, V. Georgieva, V. Valtchev, Tuning zeolite properties for a highly efficient synthesis of propylene from methanol, *Chem. Eur. J.* 24 (2018) 13136-13149. <https://doi.org/10.1002/chem.201803136>
- [188] Z. Wu, K. Zhao, Y. Zhang, T. Pan, S. Ge, Y. Ju, T. Li, T. Dou, Synthesis and consequence of aggregated nanosized ZSM-5 zeolite crystals for methanol to propylene reaction, *Ind. Eng. Chem. Res.* 58 (2019) 10737-10749. <https://doi.org/10.1021/acs.iecr.9b00502>
- [189] X. Zhu, L. Wu, P.C.M.M. Magusin, B. Mezari, E.J.M. Hensen, On the synthesis of highly acidic nanolayered ZSM-5, *J. Catal.* 327 (2015) 10-21. <http://dx.doi.org/10.1016/j.jcat.2015.04.011>
- [190] G. Perego, G. Bellussi, R. Millini, A. Alberti, S. Zanardi, B-containing molecular sieves crystallized in the presence of ethylenediamine. Part I: Crystal structure of as-synthesized B-FER, *Micropor. Mesopor. Mater.* 56 (2002) 193-202. [https://doi.org/10.1016/S1387-1811\(02\)00485-7](https://doi.org/10.1016/S1387-1811(02)00485-7)

- [191] N.E. Jacob, P.N. Joshi, A.A. Shaikh, V.P. Shiralkar, Crystallization of gallium analog of zeolite Nu-23/ferrierite, *Zeolites* 13 (1993) 430-434. [https://doi.org/10.1016/0144-2449\(93\)90116-K](https://doi.org/10.1016/0144-2449(93)90116-K)
- [192] R.K. Ahedi, A.N. Kotasthane, Synthesis of FER titanosilicates from a non-aqueous alkali-free seeded system, *J. Mater. Chem.* 8 (1998) 1685-1686. <https://doi.org/10.1039/A803170C>
- [193] E. Catizzone, M. Magliori, S. van Daele, T. Mineva, V. Valtchev, G. Giordano, New synthesis routes and catalytic applications of ferrierite crystals. Part 1: 1,8-Diaminooctane as a new OSDA, *Micropor. Mesopor. Mater.* 296 (2020) 109987. <https://doi.org/10.1016/j.micromeso.2019.109987>
- [194] X. Ju, F. Tian, Y. Wang, F. Fan, Z. Feng, C. Li, A novel synthetic strategy of Fe-ZSM-35 with pure framework Fe species and its formation mechanism, *Inorg. Chem. Front.* 5 (2018) 2031-2037. <https://doi.org/10.1039/C8QI00432C>
- [195] E. Catizzone, M. Magliori, S. van Daele, T. Mineva, V. Valtchev, G. Giordano, New synthesis routes and catalytic applications of ferrierite crystals. Part 2: The effect of OSDA type on zeolite properties and catalysis, *Micropor. Mesopor. Mater.* 296 (2020) 109988. <https://doi.org/10.1016/j.micromeso.2019.109988>
- [196] R. Szostak, *Handbook of Molecular Sieves*, Van Nostrand Reinhold, New York, 1992.
- [197] D. Seddon, T.V. Whittam, EPA 0 055 529 (1985).
- [198] A. Petushkov, H.-X. Li, W. E. Cormier, Small crystal ferrierite and method of making the same, WO 2014/074492 A1 (2014).
- [199] S.J. Weigel, J.C. Gabriel, E. Gutiérrez-Puebla, A. Monge-Bravo, N.J. Henson, L.M. Bull, A.K. Cheetham, Structure-directing effects in zeolite synthesis: a single-crystal X-ray diffraction, ²⁹Si MAS NMR, and computational study of the competitive formation of siliceous ferrierite and dodecasil-3C (ZSM-39), *J. Am. Chem. Soc.* 118 (1996) 2427-2435. <https://doi.org/10.1021/ja952418g>
- [200] A.B. Pinar, L. Gómez-Hortigüela, J. Pérez-Pariente, Cooperative structure directing role of the cage-forming tetramethylammonium cation and the bulkier benzylmethylpyrrolidinium in the synthesis of zeolite ferrierite, *Chem. Mater.* 19 (2007) 5617-5626. <https://doi.org/10.1021/cm071753o>
- [201] V.J. Margarit, M.R. Díaz-Rey, M.T. Navarro, C. Martínez, A. Corma, Direct synthesis of nano-ferrierite along the 10-ring-channel direction boosts their catalytic behavior, *Angew. Chem. Int. Ed.* 57 (2018) 3459-3463. <https://doi.org/10.1002/anie.201711418>
- [202] Y. Suzuki, T. Wakihara, K. Itabashi, M. Ogura, T. Okubo, Cooperative effect of sodium and potassium cations on synthesis of ferrierite, *Top. Catal.* 52 (2009) 67-74. <https://doi.org/10.1007/s11244-008-9136-6>
- [203] A.B. Pinar, L. Gómez-Hortigüela, L.B. McCusker, J. Pérez-Pariente, Controlling the aluminum distribution in the zeolite ferrierite via the organic structure directing agent, *Chem. Mater.* 25 (2013) 3654-3661. <https://doi.org/10.1021/cm4018024>
- [204] A.B. Pinar, R. Verel, J. Pérez-Pariente, J.A. van Bokhoven, Direct evidence of the effect of synthesis conditions on aluminum siting in zeolite ferrierite: A ²⁷Al MQ MAS NMR study, *Micropor. Mesopor. Mater.* 193 (2014) 111-114. <http://dx.doi.org/10.1016/j.micromeso.2014.03.016>
- [205] Y. Román-Leshkov, M. Moliner, M.E. Davis, Impact of controlling the site distribution of Al atoms on catalytic properties in ferrierite-type zeolites, *J. Phys. Chem. C* 115 (2011) 1096-1102. <https://doi.org/10.1021/jp106247g>
- [206] J. Kim, H. Ham, H.S. Jung, Y. Wang, Y. He, N. Tsubaki, S.J. Cho, G.Y. Hana, J.W. Bae, Dimethyl ether carbonylation to methyl acetate over highly crystalline zeolite seed-derived ferrierite, *Catal. Sci. Technol.* 8 (2018) 3060-3072. <https://doi.org/10.1039/C8CY00329G>

- [207] E. Catizzone, S. Van Daele, M. Bianco, A. Di Michele, A. Aloise, M. Migliori, V. Valtchev, G. Giordano, Catalytic application of ferrierite nanocrystals in vapour-phase dehydration of methanol to dimethyl ether, *Appl. Catal. B Environ.* 243 (2019) 273-282. <https://doi.org/10.1016/j.apcatb.2018.10.060>
- [208] H. Robson (Ed.), *Verified Synthesis of Zeolitic Materials*, Elsevier, 2001.
- [209] S.I. Zones, Preparation of molecular sieves using a structure directing agent and an N,N,N-triethyl benzylquaternary ammonium cation, US patent 2008007565 (2008).
- [210] M.A. Cambor, L.A. Villaescusa, M.J. Díaz-Cabañas, Synthesis of all-silica and high-silica molecular sieves in fluoride media, *Top. Catal.* 9 (1999) 59-76. <https://doi.org/10.1023/A:1019154304344>
- [211] N. Martín, M. Moliner, A. Corma, High yield synthesis of high-silica chabazite by combining the role of zeolite precursors and tetraethylammonium: SCR of NO_x, *Chem. Commun.* 51 (2015) 9965-9968. <https://doi.org/10.1039/C5CC02670A>
- [212] Z. Liu, T. Wakihara, K. Oshima, D. Nishioka, Y. Hotta, S.P. Elangovan, Y. Yanaba, T. Yoshikawa, W. Chaikittisilp, T. Matsuo, T. Takewaki, T. Okubo, Widening synthesis bottlenecks: realization of ultrafast and continuous-flow synthesis of high-silica zeolite SSZ-13 for NO_x removal, *Angew. Chem. Int. Ed.* 54 (2015) 5683-5687. <https://doi.org/10.1002/anie.201501160>
- [213] L. Regli, S. Bordiga, C. Lamberti, K.P. Lillerud, S.I. Zones, A. Zecchina, Effect of boron substitution in chabazite framework: IR studies on the acidity properties and reactivity towards methanol *J. Phys. Chem. C* 111 (2007) 2992-2999. <https://doi.org/10.1021/jp064048w>
- [214] S. Zanardi, M. Bellettato, S. Guidetti, E. Montanari, W. O'Neil Parker Jr., Incorporation of germanium and boron in zeolite chabazite, *Micropor. Mesopor. Mater.* 168 (2013) 164-170. <http://dx.doi.org/10.1016/j.micromeso.2012.10.004>
- [215] M.J. Dusselier, M.E. Davis, Processes for preparing zincoaluminosilicates with AEI, CHA, and GME topologies and compositions derived therefrom, US patent US2018/0154342A1 (2018).
- [216] M. Feyen, U. Mueller, X. Bao, W. Zhang, D. De Vos, H. Gies, F.-S. Xiao, T. Yokoi, U. Kolb, B. Marler, T. Wang, T. De Baerdemaeker, C. Shi, X. Pan, X. Meng, A zeolitic material having framework type cha and comprising a transition metal and one or more of potassium and cesium, WO2019024909-A1 (2019).
- [217] Q. Yue, J. Zhang, M. Shamzhy, M. Opanasenko, Seeded growth of isomorphously substituted chabazites in proton-form, *Micropor. Mesopor. Mater.* 280 (2019) 331-336. <https://doi.org/10.1016/j.micromeso.2019.02.017>
- [218] M. Lusardi, T. T. Chen, M.J. Kale, J.H. Kang, M. Neurock, M.E. Davis, Carbonylation of dimethyl ether to methyl acetate over SSZ-13, *ACS Catal.* 10 (2020) 842-851. <https://doi.org/10.1021/acscatal.9b04307>
- [219] J.R. Di Iorio, R. Gounder, Controlling the isolation and pairing of aluminum in chabazite zeolites using mixtures of organic and inorganic structure-directing agents, *Chem. Mater.* 28 (2016) 2236-2247. <https://doi.org/10.1021/acs.chemmater.6b00181>
- [220] J.R. Di Iorio, S. Li, C.B. Jones, C.T. Nimlos, Y. Wang, E. Kunkes, V. Vattipalli, S. Prasad, A. Moini, W.F. Schneider, R. Gounder, Cooperative and competitive occlusion of organic and inorganic structure directing agents within chabazite zeolites influences their aluminum arrangement, *J. Am. Chem. Soc.* 142 (2020) 4807-4819. <https://doi.org/10.1021/jacs.9b13817>
- [221] J. Devos, M.L. Bols, D. Plessers, C. Van Goethem, J. Won Seo, S.-J. Hwang, B.F. Sels, Michiel Dusselier, Synthesis-structure-activity relations in Fe-CHA for C-H activation: control of Al-distribution by interzeolite conversion, *Chem. Mater.* 32 (2020) 273-285. <https://doi.org/10.1021/acs.chemmater.9b03738>

- [222] T. Nishitoba, N. Yoshida, J.N Kondo, T. Yokoi, Control of Al distribution in the CHA-type aluminosilicate zeolites and its impact on the hydrothermal stability and catalytic properties, *Ind. Eng. Chem. Res.* 57 (2018) 3914-3922.
- [223] L. Zeng, Z. Yu, Z. Sun, Y. Han, Y. Xu, J. Wu, Z. Liang, Z. Wang, Fast synthesis of SSZ-13 zeolite by steam-assisted crystallization method, *Micropor. Mesopor. Mater.* 293 (2020) 109789. <https://doi.org/10.1016/j.micromeso.2019.109789>
- [224] Y. Li, Y. Zhang, A. Lan, H. Bian, R. Liu, X. Li, P. Han, T. Dou, Synthesis of SSZ-13 zeolite with zeolite L-added synthesis gel absent from additional aluminum source, *Micropor. Mesopor. Mater.* 279 (2019) 1-9. <https://doi.org/10.1016/j.micromeso.2018.11.038>
- [225] Z.C. Zhao, Y.D. Xing, S.H. Li, X.J. Meng, F.S. Xiao, R. McGuire, A.-N. Parvulescu, U. Muller, W.P. Zhang, Mapping Al distributions in SSZ-13 zeolites from ²³Na solid-state NMR spectroscopy and DFT calculations, *J. Phys. Chem. C* 122 (2018) 9973-9979. <https://doi.org/10.1021/acs.jpcc.8b01423>
- [226] B. Liu, X. Zhao, W. Mao, H. Chen, L. Han, K. Zhu, X. Zhou, Pickering emulsion mediated crystallization of hierarchical zeolite SSZ-13 with enhanced NH₃ selective catalytic reduction performance, *Micropor. Mesopor. Mater.* 285 (2019) 202-214. <https://doi.org/10.1016/j.micromeso.2019.05.004>
- [227] A. Alberti, Location of Brønsted sites in mordenite, *Zeolites* 19 (1997) 411-415. [https://doi.org/10.1016/S0144-2449\(97\)00114-0](https://doi.org/10.1016/S0144-2449(97)00114-0)
- [228] K. Itabashi, T. Fukushima, K. Igawa, Synthesis and characteristic properties of siliceous mordenite, *Zeolites* 6 (1986) 30-34. [https://doi.org/10.1016/0144-2449\(86\)90008-4](https://doi.org/10.1016/0144-2449(86)90008-4)
- [229] A.A. Shaikh, P.N. Joshi, N.E. Jacob, V.P. Shiralkar, Direct hydrothermal crystallization of high-silica large-pore mordenite, *Zeolites* 13 (1993) 511-517. [https://doi.org/10.1016/0144-2449\(93\)90227-T](https://doi.org/10.1016/0144-2449(93)90227-T)
- [230] H. Sasaki, Y. Oumi, K. Itabashi, B. Lu, T. Teranishi, T. Sano, Direct hydrothermal synthesis and stabilization of high-silica mordenite (Si:Al = 25) using tetraethylammonium and fluoride ions, *J. Mater. Chem.*, 2003, 13, 1173-1179. <https://doi.org/10.1039/B212519F>
- [231] T. Sano, S. Wakabayashi, Y. Oumi, T. Uozumi, Synthesis of large mordenite crystals in the presence of aliphatic alcohol, *Micropor. Mesopor. Mater.* 46 (2001) 67-74. [https://doi.org/10.1016/S1387-1811\(01\)00285-2](https://doi.org/10.1016/S1387-1811(01)00285-2)
- [232] Z. Ma, J. Xie, J. Zhang, W. Zhang, Y. Zhou, J. Wang, Mordenite zeolite with ultrahigh SiO₂/Al₂O₃ ratio directly synthesized from ionic liquid-assisted dry-gel-conversion, *Micropor. Mesopor. Mater.* 224 (2016) 17-25. <https://doi.org/10.1016/j.micromeso.2015.11.007>
- [233] T.R. Gaffney, R. Pierantozzi, M.R. Seger, Isomorphous substitution of boron in mordenite and zeolite Y, in M.L. Ocelli, H.E. Robson (Eds.), *Zeolite Synthesis, Symposium Series 398*, American Chemical Society, 1989, Washington D.C., pp. 374-392.
- [234] G.J. Kim, B.R. Cho, J.H. Kim, Structure modification of mordenite through isomorphous Ti substitution: Characterization and catalytic properties, *Catal. Lett.*, 22 (1993) 259-270. <https://doi.org/10.1007/BF00810372>
- [235] G. Giordano, A. Katović, D. Caputo, Synthesis and adsorption properties of iron containing BEA and MOR type zeolites, *Stud. Surf. Sci. Catal.* 140 (2001) 307-314. [https://doi.org/10.1016/S0167-2991\(01\)80159-2](https://doi.org/10.1016/S0167-2991(01)80159-2)
- [236] M. Dong, J. Wang, Y. Sun, Synthesis of zincosilicate mordenite using citric acid as complexing agent, *Micropor. Mesopor. Mater.* 43 (2001) 237-243. [https://doi.org/10.1016/S1387-1811\(01\)00211-6](https://doi.org/10.1016/S1387-1811(01)00211-6)

- [237] M.J. Eapen, K.S.N. Reddy, P.N. Joshi, V.P. Shiralkar, Synthesis of a gallosilicate analogue of high silica, large port mordenite, *J. Incl. Phenom.* 14 (1992) 119-129. <https://doi.org/10.1007/BF01029659>
- [238] Y. Li, Z. Zhou, J. Qin, Z. Liu, H. Huang, G. Liu, W. Wu, Preparation of tin-doped mordenite by multistep pH template-free method for the tert-alkylation of toluene, *Rev. Roum. Chim.* 64 (2019) 485-492. Doi: 10.33224/rch.2019.64.6.03
- [239] L. Li, Q. Wang, H. Liu, T. Sun, D. Fan, M. Yang, P. Tian, Z. Liu, Preparation of spherical mordenite zeolite assemblies with excellent catalytic performance for dimethyl ether carbonylation, *ACS Appl. Mater. Interfaces* 10 (2018) 32239-32246. <https://doi.org/10.1021/acsami.8b11823>
- [240] O.V. Shvets, K.M. Konyshva, M.V. Shamzhy, M.V. Opanasenko, P.S. Yaremov, C. Xiao, X. Zou, J. Čejka, Mordenite nanorods and nanosheets prepared in presence of gemini type surfactants, *Catal. Today* 324 (2019) 115-122. <https://doi.org/10.1016/j.cattod.2018.10.043>
- [241] S. Wang, B. He, R. Tian, C. Sun, R. Dai, X. Li, X. Wu, X. An, X. Xie, Synthesis and catalytic performance of hierarchically structured MOR zeolites by a dual-functional templating approach, *J. Coll. Interf. Sci.* 527 (2018) 339-345. <https://doi.org/10.1016/j.jcis.2018.05.053>
- [242] M. Liu, W. Jia, J. Li, Y. Wang, S. Ma, H. Chen, Z. Zhu, Catalytic properties of hierarchical mordenite nanosheets synthesized by self-assembly between subnanocrystals and organic templates, *Catal. Lett.* 146 (2016) 249-254. <https://doi.org/10.1007/s10562-015-1632-2>
- [243] X. Wang, R. Li, C. Yu, L. Zhang, C. Xu, H. Zhou, Dimethyl ether carbonylation over nanosheet-assembled hierarchical mordenite, *Micropor. Mesopor. Mater.* 274 (2019) 227-235. <https://doi.org/10.1016/j.micromeso.2018.07.048>
- [244] J.M. Newsam, M.M.J. Treacy, W.T. Koetsier, C.B. de Gruyter, Structural characterization of zeolite Beta, *Proc. R. Soc. London A* 420 (1988) 375-405. <https://doi.org/10.1098/rspa.1988.0131>
- [245] M. Tong, D. Zhang, W. Fan, J. Xu, L. Zhu, W. Guo, W. Yan, J. Yu, S. Qiu, J. Wang, F. Deng, R. Xu, Synthesis of chiral polymorph A-enriched zeolite Beta with an extremely concentrated fluoride route, *Sci. Reports* 5 (2015) 11521. <https://doi.org/10.1038/srep11521>
- [246] A. Corma, M. Moliner, Á. Cantín, M. J. Díaz-Cabañas, J. L. Jordá, D. Zhang, J. Sun, K. Jansson, S. Hovmöller, X. Zou, Synthesis and structure of polymorph B of zeolite beta, *Chem. Mater.* 20 (2008) 3218-3223. <https://doi.org/10.1021/cm8002244>
- [247] A. Corma, M.T. Navarro, F. Rey, J. Rius, S. Valencia, Pure polymorph C of zeolite Beta synthesized by using framework isomorphous substitution as a structure-directing mechanism, *Angew. Chem. Int. Ed.* 40 (2001) 2277-2280. [https://doi.org/10.1002/1521-3773\(20010618\)40:12<2277::AID-ANIE2277>3.0.CO;2-O](https://doi.org/10.1002/1521-3773(20010618)40:12<2277::AID-ANIE2277>3.0.CO;2-O)
- [248] A. Cantin, A. Corma, M.J. Díaz-Cabañas, J. L. Jorda, M. Moliner, F. Rey, Synthesis and characterization of the all-silica pure polymorph C and an enriched polymorph B intergrowth of zeolite beta, *Angew. Chem., Int. Ed.* 45 (2006) 8013-8015. <https://doi.org/10.1002/anie.200603027>
- [249] O. Larlus, V.P. Valtchev, Control of the morphology of all-silica BEA-type zeolite synthesized in basic media, *Chem. Mater.* 17 (2005) 881-886. <https://doi.org/10.1021/cm048799r>
- [250] A. Corma, M.E. Domine, S. Valencia, Water-resistant solid Lewis acid catalysts: Meerwein-Ponndorf-Verley and Oppenauer reactions catalyzed by tin-beta zeolite, *J. Catal.* 215 (2003) 294-304. [https://doi.org/10.1016/S0021-9517\(03\)00014-9](https://doi.org/10.1016/S0021-9517(03)00014-9)

- [251] S.I. Zones, Low-aluminum boron beta, US patent 5166111A (1992).
- [252] J.D. Lewis, S. Van de Vyver, A.J. Crisci, W.R. Gunther, V.K. Michaelis, R.G. Griffin, Y. Román-Leshkov, A continuous flow strategy for the coupled transfer hydrogenation and etherification of 5-(Hydroxymethyl)furfural using Lewis acid zeolites, *ChemSusChem* 7 (2014) 2255-2265. <https://doi.org/10.1002/cssc.201402100>
- [253] A. Corma, L.T. Nemeth, M. Renz, S. Valencia, Sn-zeolite beta as a heterogeneous chemoselective catalyst for Baeyer-Villiger oxidations, *Nature* 412 (2001) 423-425. <https://doi.org/10.1038/35086546>
- [254] R. de Ruite, K. Pamin, A.P.M. Kentgens, J.C. Jansen, H. van Bekkum, Synthesis of molecular sieve [B]-BEA and modification of the boron site, *Zeolites* 13 (1993) 611-621. [https://doi.org/10.1016/0144-2449\(93\)90132-M](https://doi.org/10.1016/0144-2449(93)90132-M)
- [255] M.A. Cambor, M. Costantini, A. Corma, L. Gilbert, P. Esteve, A. Martínez, S. Valencia, Synthesis and catalytic activity of aluminium-free zeolite Ti-β oxidation catalysts, *Chem. Commun.* (1996) 1339-1340. <https://doi.org/10.1039/CC9960001339>
- [256] T. Takewaki, L. Beck, M.E. Davis, Synthesis of CIT-6, a zincosilicate with the *BEA topology, *Top. Catal.* 9 (1999) 35-42. <https://doi.org/10.1023/A:1019150203436>
- [257] G.G. Juttu, R.F. Lobo, Framework modification of microporous silicates via gas-phase treatment with ZrCl₄, *Catal. Lett.* 62 (1999) 99-106. <https://doi.org/10.1023/A:1019047022166>
- [258] R.L. Wadlinger, G.T. Kerr, E. J. Rosinski, Catalytic composition of a crystalline zeolite, US patent 3,308,069 (1967).
- [259] P. Caultet, J. Hazm, J.L. Guth, J.F. Joly, J. Lynch, F. Raatz, Synthesis of zeolite Beta from nonalkaline fluoride aqueous aluminosilicate gels, *Zeolites* 12 (1992) 240-250. [https://doi.org/10.1016/S0144-2449\(05\)80290-8](https://doi.org/10.1016/S0144-2449(05)80290-8)
- [260] A. Abraham, S.-H. Lee, C.-H. Shin, S.B. Hong, R. Prins, J.A. van Bokhoven, Influence of framework silicon to aluminium ratio on aluminium coordination and distribution in zeolite Beta investigated by ²⁷Al MAS and ²⁷Al MQ MAS NMR, *Phys. Chem. Chem. Phys.* 6 (2004) 3031-3036. <https://doi.org/10.1039/B401235F>
- [261] X. Zhao, L. Wang, J. Li, S. Xu, W. Zhang, Y. Wei, X. Guo, P. Tian, Z. Liu, Investigation of methanol conversion over high-Si beta zeolites and the reaction mechanism of their high propene selectivity, *Catal. Sci. Technol.* 7 (2017) 5882-5892. <https://doi.org/10.1039/C7CY01804E>
- [262] S. Prodingler, H. Shi, H. Wang, M.A. Derewinski, J.A. Lercher, Impact of structural defects and hydronium ion concentration on the stability of zeolite BEA in aqueous phase, *Appl. Catal. B* 237 (2018) 996-1002. <https://doi.org/10.1016/j.apcatb.2018.06.065>
- [263] R. Martínez-Franco, C. Paris, M.E. Martínez-Armero, C. Martínez, M. Moliner, A. Corma, High-silica nanocrystalline Beta zeolites: efficient synthesis and catalytic application, *Chem. Sci.* 7 (2016) 102-108. <https://doi.org/10.1039/C5SC03019F>
- [264] E.M. Gallego, C. Paris, M.R. Díaz-Rey, M.E. Martínez-Armero, J. Martínez-Triguero, C. Martínez, M. Moliner, A. Corma, Simple organic structure directing agents for synthesizing nanocrystalline zeolites, *Chem. Sci.* 8 (2017) 8138-8149. <https://doi.org/10.1039/C7SC02858J>
- [265] P. Sazama, E. Tabor, P. Klein, B. Wichterlova, S. Sklenak, L. Mokrzycki, V. Pashkkova, M. Ogura, J. Dedecek, Al-rich beta zeolites. Distribution of Al atoms in the framework and related protonic and metal-ion species, *J. Catal.* 333 (2016) 102-114. <https://doi.org/10.1016/j.jcat.2015.10.010>
- [266] S.F. Rastegar, G. Sadovska, R. Pilar, J. Moravkova, D. Kaucky, L. Brabec, J. Pastvova, P. Sazama, Analysis of decisive structural parameters of zeolites for

- alkylation of benzene with ethylene, *Appl. Catal. A* 591 (2020) 117379. <https://doi.org/10.1016/j.apcata.2019.117379>
- [267] R. Barakov, N. Shcherban, P. Yaremov, I. Bezverkhyy, V. Tsyryna, M. Opanasenko, Hierarchical Beta zeolites obtained in concentrated reaction mixtures as catalysts in tetrahydropyranlation of alcohols, *Appl. Catal. A* 594 (2020) 117380. <https://doi.org/10.1016/j.apcata.2019.117380>
- [268] S. Ferdov, K. Tsuchiya, N. Tsunoji, T. Sano, Comparative study between high-silica faujasites (FAU) from organic-free system and the commercial zeolite Y, *Micropor. Mesopor. Mater.* 276 (2019) 154-159. <https://doi.org/10.1016/j.micromeso.2018.09.036>
- [269] C. Venkatesan, H. Park, J. Kim, S. Lee, R. Ryoo, Facile synthesis of mesoporous zeolite Y using seed gel and amphiphilic organosilane, *Micropor. Mesopor. Mater.* 288 (2019) 109579. <https://doi.org/10.1016/j.micromeso.2019.109579>
- [270] D.M. Bibby, N.B. Milestone, L.P. Aldridge, Silicalite-2, a silica analogue of the aluminosilicate zeolite ZSM-11, *Nature* 280 (1979) 664-665. <https://doi.org/10.1038/280664a0>
- [271] S. Wang, P. Wang, Z. Qin, Y.-Y. Chen, M. Dong, J. Li, K. Zhang, P. Liu, J. Wang, W. Fan, Relation of catalytic performance to the aluminum siting of acidic zeolites in the conversion of methanol to olefins, viewed via a comparison between ZSM-5 and ZSM-11, *ACS Catal.* 8 (2018) 5485-5505. <https://doi.org/10.1021/acscatal.8b01054>
- [272] S. Wang, L. Zhang, S. Li, Z. Qin, D. Shi, S. He, K. Yuan, P. Wang, T.-S. Zhao, S. Fan, M. Dong, J. Li, W. Fan, J. Wang, Tuning the siting of aluminum in ZSM-11 zeolite and regulating its catalytic performance in the conversion of methanol to olefins, *J. Catal.* 377 (2019) 81-97. <https://doi.org/10.1016/j.jcat.2019.07.028>
- [273] M. Liu, T. Yokoi, M. Yoshioka, H. Imai, J.N. Kondo, T. Tatsumi, Differences in Al distribution and acidic properties between RTH-type zeolites synthesized with OSDAs and without OSDAs, *Phys. Chem. Chem. Phys.* 16 (2014) 4155-4164. <https://doi.org/10.1039/C3CP54297A>
- [274] R. Ransom, R. Moulton, D.F. Shantz, The structure directing agent isomer used in SSZ-39 synthesis impacts the zeolite activity towards selective catalytic reduction of nitric oxides, *J. Catal.* 382 (2020) 339-346. <https://doi.org/10.1016/j.jcat.2019.12.038>
- [275] Y. Chen, C. Li, X. Chen, Y. Liu, C. Liang, Synthesis of ZSM-23 zeolite with dual structure directing agents for hydroisomerization of n-hexadecane, *Micropor. Mesopor. Mater.* 268 (2018) 216-224. <https://doi.org/10.1016/j.micromeso.2018.04.033>
- [276] P. Vinaches, A. Rojas, A.E.V. de Alencar, E. Rodríguez-Castellón, T.P. Braga, S.B.C. Pergher, Introduction of Al into the HPM-1 framework by in situ generated seeds as an alternative methodology, *Appl. Sci.* 8 (2018) 1634. <https://doi.org/10.3390/app8091634>
- [277] M.W. Anderson, J. Klinowski, L. Xinsheng, Alumination of highly siliceous zeolites, *J. Chem. Soc. Chem. Commun.* (1984) 1596-1597. <https://doi.org/10.1039/C39840001596>
- [278] C.D. Chang, C. T.-W. Chu, J.N. Miale, R.F. Bridger, R.B. Calvert, Aluminum insertion into high silica zeolite frameworks. 1. Reaction with aluminum halides, *J. Am. Chem. Soc.* 106 (1984) 8143-8146. <https://doi.org/10.1021/ja00338a023>
- [279] J. Ma, Y. Kang, N. Ma, W. Hao, Y. Wang, R. Li, A high acid mesoporous USY zeolite prepared by alumination, *Mater. Sci. Poland*, 31 (2013) 19-24. <https://doi.org/10.2478/s13536-012-0061-9>

- [280] C. Yang, Q. Xu, Aluminated zeolites β and their properties Part 1.—Alumination of zeolites β , *J. Chem. Soc. Faraday Trans.* 93 (1997) 1675-1680. <https://doi.org/10.1039/A606807C>
- [281] J. Zhang, L. Zhou, X. Li, Modification of Beta-zeolite by dealumination and realumination, *Stud. Surf. Sci. Catal.* 135 (2001) 213-220. [https://doi.org/10.1016/S0167-2991\(01\)81427-0](https://doi.org/10.1016/S0167-2991(01)81427-0)
- [282] A. Omegna, M. Haouas, G. Pirngruber, R. Prins, Alumination of siliceous zeolites, *Stud. Surf. Sci. Catal.* 135 (2001) 215-222. [https://doi.org/10.1016/S0167-2991\(01\)81433-6](https://doi.org/10.1016/S0167-2991(01)81433-6)
- [283] A. Omegna, M. Haouas, G. Pirngruber, R. Prins, Grafting of aluminium on dealuminated H-BEA using alkoxides, *Stud. Surf. Sci. Catal.* 142 (2002) 31-38. [https://doi.org/10.1016/S0167-2991\(02\)80008-8](https://doi.org/10.1016/S0167-2991(02)80008-8)
- [284] J. Ding, J. Hu, Y. Guan, H. Wu, M.-y. He, Aluminated hierarchical silicalite-2 particles: Catalyst with remarkably increased lifetime for methanol to hydrocarbons, *Catal. Comm.* 86 (2016) 139-142. <https://doi.org/10.1016/j.catcom.2016.08.023>
- [285] S.P. Sree, J. Dendooven, T.I. Korányi, G. Vanbutsele, K. Houthoofd, D. Deduytsche, C. Detavernier, J.A. Martens, Aluminium atomic layer deposition applied to mesoporous zeolites for acid catalytic activity enhancement, *Catal. Sci. Technol.* 1 (2011) 218-221. <https://doi.org/10.1039/C0CY00056F>
- [286] <https://www.forgenano.com/uncategorized/atomic-layer-deposition/> (accessed January 27, 2020)
- [287] Y. Wu, Z. Lu, L. Emdadi, S.C. Oh, J. Wang, Y. Lei, H. Chen, D.T. Tran, I.C. Lee, D. Liu, Tuning external surface of unit-cell thick pillared MFI and MWW zeolites by atomic layer deposition and its consequences on acid-catalyzed reactions, *J. Catal.* 337 (2016) 177-187. <https://doi.org/10.1016/j.jcat.2016.01.031>
- [288] E. Verheyen, S.P. Sree, K. Thomas, J. Dendooven, M. De Prins, G. Vanbutsele, E. Breynaert, J.-P. Gilson, C.E.A. Kirschhock, C. Detavernier, J.A. Martens, Catalytic activation of OKO zeolite with intersecting pores of 10- and 12-membered rings using atomic layer deposition of aluminium, *Chem. Commun.* 50 (2014) 4610-4612. <https://doi.org/10.1039/C3CC49028A>
- [289] M. De Prins, E. Verheyen, G. Vanbutsele, S.P. Sree, K. Thomas, J.-P. Gilson, J. Vleugels, C.E.A. Kirschhock, J.A. Martens, Catalytic activation of all-silica COK-14 zeolite through alumination and particle size reduction using wet ball milling, *Catal. Today* 334 (2019) 3-12. <https://doi.org/10.1016/j.cattod.2019.03.016>
- [290] L. Tosheva, N. Mahé, V. Valtchev, One-pot template extraction and alumination of BEC-type zeolite, *Stud. Surf. Sci. Catal.* 170 (2007) 616-621. [https://doi.org/10.1016/S0167-2991\(07\)80899-8](https://doi.org/10.1016/S0167-2991(07)80899-8)
- [291] F. Gao, M. Jaber, K. Bozhilov, A. Vicente, C. Fernandez, V. Valtchev, Framework stabilization of Ge-rich zeolites via postsynthesis alumination, *J. Am. Chem. Soc.* 131 (2009) 16580-16586. <https://doi.org/10.1021/ja904458y>
- [292] V. Valtchev, G. Majano, S. Mintova, J. Pérez-Ramírez, Tailored crystalline microporous materials by post-synthesis modification, *Chem. Soc. Rev.* 42 (2013) 263-290. <https://doi.org/10.1039/C2CS35196J>
- [293] M.V. Shamzhy, M.V. Opanasenko, F.S. de O. Ramos, L. Brabec, M. Horáček, M. Navarro-Rojas, R.E. Morris, H. de O. Pastore, J. Čejka, Post-synthesis incorporation of Al into germanosilicate ITH zeolites: the influence of treatment conditions on the acidic properties and catalytic behavior in tetrahydropyranlation, *Catal. Sci. Technol.* 5 (2015) 2973-2984. <https://doi.org/10.1039/C4CY01594K>

- [294] Y. Zhou, S.A. Kadam, M. Shamzhy, J. Čejka, M. Opanasenko, Isorecticular UTL-derived zeolites as model materials for probing pore size–activity relationship, *ACS Catal.* 9 (2019) 5136-5146. <https://doi.org/10.1021/acscatal.9b00950>
- [295] M. Mazur, V. Kasneryk, J. Přeč, F. Brivio, C. Ochoa-Hernández, A. Mayoral, M. Kubů, J. Čejka, Zeolite framework functionalisation by tuneable incorporation of various metals into the IPC-2 zeolite, *Inorg. Chem. Front.* 5 (2018) 2746-2755. <https://doi.org/10.1039/C8QI00732B>
- [296] Y. Zhou, N. Žilková, M. Shamzhy, Y. Avadhut, M. Hartmann, J. Čejka, M. Opanasenko, Novel approach towards Al-rich AFI for catalytic application, *Appl. Catal. A* 577 (2019) 62-68. <https://doi.org/10.1016/j.apcata.2019.03.015>
- [297] S. Senapati, J. Zimdars, J. Ren, H. Koller, Post-synthetic modifications of as-made zeolite frameworks near the structure-directing agents, *J. Mater. Chem. A* 2 (2014) 10470-10484. <https://doi.org/10.1039/C4TA00656A>
- [298] S.I. Zones, C.Y. Chen, A. Benin, S.-J. Hwang, Opportunities for selective catalysis within discrete portions of zeolites: The case for SSZ-57LP, *J. Catal.* 308 (2013) 213-225. <https://doi.org/10.1016/j.jcat.2013.07.028>
- [299] S.I. Zones, A. Benin, S.-J. Hwang, D. Xie, S. Elomari, M.-F. Hsieh, Studies of aluminum reinsertion into borosilicate zeolites with intersecting channels of 10- and 12-ring channel systems, *J. Am. Chem. Soc.* 136 (2014) 1462-1471. <https://doi.org/10.1021/ja4100194>
- [300] R. von Ballhnoos, W.M. Meier, Zoned aluminium distribution in synthetic zeolite ZSM-5, *Nature* 289 (1981) 782-783. <https://doi.org/10.1038/289782a0>
- [301] R. Althoff, B. Schulz-Dobrick, F. Schüth, K. Unger, Controlling the spatial distribution of aluminum in ZSM-5 crystals, *Micropor. Mater.* 1 (1993) 207-218. [https://doi.org/10.1016/0927-6513\(93\)80079-A](https://doi.org/10.1016/0927-6513(93)80079-A)
- [302] T. Li, F. Krumeich, M. Chen, Z. Ma, J.A. van Bokhoven, Defining aluminum-zoning during synthesis of ZSM-5 zeolites, *Phys. Chem. Chem. Phys.* 22 (2020) 734-739. <https://doi.org/10.1039/C9CP05423E>
- [303] K.P. Schröder, J. Sauer, M. Leslie, C.R.A. Catlow, Siting of Al and bridging hydroxyl groups in ZSM-5: A computer simulation study, *Zeolites* 12 (1992) 20-23. [https://doi.org/10.1016/0144-2449\(92\)90004-9](https://doi.org/10.1016/0144-2449(92)90004-9)
- [304] C. Li, A. Vidal-Moya, P.J. Miguel, J. Dedecek, M. Boronat, A. Corma, Selective introduction of acid sites in different confined positions in ZSM-5 and its catalytic implications, *ACS Catal.* 8 (2018) 7688-7697. <https://doi.org/10.1021/acscatal.8b02112>
- [305] Y.G. Hur, P.M. Kester, C.T. Nimlos, Y.R. Cho, J.T. Miller, R. Gounder, Influence of tetrapropylammonium and ethylenediamine structure-directing agents on the framework Al distribution in B–Al–MFI zeolites, *Ind. Eng. Chem. Res.* 58 (2019) 11849-11860. <https://doi.org/10.1021/acs.iecr.9b01726>
- [306] M.H.M. Ahmed, O. Muraza, A. Galadima, M. Yoshioka, Z.H. Yamani, T. Yokoi, Choreographing boron-aluminum acidity and hierarchical porosity in *BEA zeolite by in-situ hydrothermal synthesis for a highly selective methanol to propylene catalyst, *Micropor. Mesopor. Mater.* 273 (2019) 249-255. <https://doi.org/10.1016/j.micromeso.2018.06.036>
- [307] Y. Kunitake, M. Yoshioka, J.N. Kondo, T. Yokoi, Development of AEI-type boroaluminosilicate zeolites, and their acidic and catalytic properties in ethene conversion reaction, *Appl. Catal. A* 568 (2018) 123-129. <https://doi.org/10.1016/j.apcata.2018.08.024>

- [308] M. Yoshioka, T. Yokoi, T. Tatsumi, Development of the CON-type aluminosilicate zeolite and its catalytic application for the MTO reaction, *ACS Catal.* 5 (2015) 4268-4275. <https://doi.org/10.1021/acscatal.5b00692>
- [309] A. Miyaji, T. Koyama, K. Motokura, T. Yashima, R. Koide, J.K. Reddy, S. Yamaguchi, T. Baba, Identification and catalytic behavior of brønsted acid sites on Al-containing ITQ-21, *J. Phys. Chem. C* 117 (2013) 18074-18083. <https://doi.org/10.1021/jp404970k>
- [310] A. Corma, L.T. Nemeth, M. Renz, S. Valencia, Sn-zeolite beta as a heterogeneous chemoselective catalyst for Baeyer–Villiger oxidations, *Nature* 412 (2001) 423-425. <https://doi.org/10.1038/35086546>
- [311] J. Dijkmans, W. Schutyser, M. Dusselier, B.F. Sels, Sn β -zeolite catalyzed oxidation-reduction cascade chemistry with biomass-derived molecules, *Chem. Commun.* 52 (2016) 6712-6715. <https://doi.org/10.1039/C6CC00199H>
- [312] R. Bermejo-Deval, M. Orazov, R. Gounder, S.-J. Hwang, M.E. Davis, Active sites in Sn-beta for glucose isomerization to fructose and epimerization to mannose, *ACS Catal.* 4 (2014) 2288-2297. <https://doi.org/10.1021/cs500466j>
- [313] J.J. Pacheco, M.E. Davis, Synthesis of terephthalic acid via Diels-Alder reactions with ethylene and oxidized variants of 5-hydroxymethylfurfural, *Proc. Natl. Acad. Sci. U.S.A.* 111 (2014) 8363-8367. <https://doi.org/10.1073/pnas.1408345111>
- [314] M. Su, W. Li, T. Zhang, H.S. Xin, S. Li, W. Fan, L. Ma, Production of liquid fuel intermediates from furfural via aldol condensation over Lewis acid zeolite catalysts, *Catal. Sci. Technol.* 7 (2017) 3555-3561. <https://doi.org/10.1039/C7CY01028A>
- [315] N. Deshpande, A. Parulkar, R. Joshi, B. Diep, A. Kulkarni, N.A. Brunelli, Epoxide ring opening with alcohols using heterogeneous Lewis acid catalysts: Regioselectivity and mechanism, *J. Catal.* 370 (2019) 46-54. <https://doi.org/10.1016/j.jcat.2018.11.038>
- [316] M. Boronat, P. Concepcion, A. Corma, M. Renz, S. Valencia, Determination of the catalytically active oxidation Lewis acid sites in Sn-beta zeolites, and their optimisation by the combination of theoretical and experimental studies, *J. Catal.* 234 (2005) 111–118, <https://doi.org/10.1016/j.jcat.2005.05.023>
- [317] R. Bermejo-Deval, R.S. Assary, E. Nikolla, M. Moliner, Y. Román-Leshkova, S.-J. Hwang, A. Palsdottir, D. Silverman, R.F. Lobo, L.A. Curtiss, M.E. Davis, Metalloenzyme-like catalyzed isomerizations of sugars by Lewis acid zeolites, *Proc. Natl. Acad. Sci. U. S. A.* 109 (2012) 9727-9732. <https://doi.org/10.1073/pnas.1206708109>
- [318] H.Y. Luo, D.F. Consoli, W.R. Gunther, Y. Román-Leshkov, Investigation of the reaction kinetics of isolated Lewis acid sites in Beta zeolites for the Meerwein–Ponndorf–Verley reduction of methyl levulinate to γ -valerolactone, *J. Catal.* 320 (2014) 198-207. <https://doi.org/10.1016/j.jcat.2014.10.010>
- [319] B.C. Bukowski, J.S. Bates, R. Gounder, J. Greeley, First principles, microkinetic, and experimental analysis of Lewis acid site speciation during ethanol dehydration on Sn-Beta zeolites, *J. Catal.* 365 (2018) 261-276. <https://doi.org/10.1016/j.jcat.2018.07.012>
- [320] R. Bermejo-Deval, R. Gounder, M.E. Davis, Framework and extraframework tin sites in zeolite beta react glucose differently, *ACS Catal.* 2 (2012) 2705-2713. <https://doi.org/10.1021/cs300474x>
- [321] M. Moliner, Y. Román-Leshkov, M.E. Davis, Tin-containing zeolites are highly active catalysts for the isomerization of glucose in water, *Proc. Natl. Acad. Sci. U. S. A.* 107 (2010) 6164-6168. <https://doi.org/10.1073/pnas.1002358107>
- [322] F.G. Dwyer, E.E. Jenkins, Crystalline silicates and method of preparing the same, US patent 3941871A (1976).

- [323] N. Knudsen, E. Krogh Andersen, I.G. Krogh Andersen, E. Skou, Tin-mordenites, syntheses and ionic conductivity, *Solid State Ionics* 35 (1989) 51-55. [https://doi.org/10.1016/0167-2738\(89\)90011-8](https://doi.org/10.1016/0167-2738(89)90011-8)
- [324] R.M. Dessau, E.W. Valyocsik, J.C. Vartuli, Tin-containing microporous crystalline materials and their use as dehydrogenation, dehydrocyclization and reforming catalysts, US patent 4990710A (1991).
- [325] D.E.W. Vaughan, S.B. Rice, Tin substitution into zeolite frameworks, US patent 4933161A (1990).
- [326] M. Costantini, J.L. Guth, A. Lopez, J.M. Popa, Zéolithes à base de silice et d'oxydes d'éléments tétravalents, leur procédé de synthèse et leur application, European patent 0466545A1 (1992).
- [327] V. Valtchev, Isomorphous substitution of Si(IV) for Fe(III), Cr(III), Ti(IV) and Sn(IV) in MFI type zeolites, *Anniv. Univ. Sofia* 83 (1990) 87.
- [328] G.W. Skeels, D.M. Chapman, E.M. Flanigen, Substitution of Sn in place of Al in the framework of molecular sieve via treatment with fluoride salts, US patent 5401488A (1995).
- [329] N.K. Mal, V. Ramaswamy, S. Ganapathy, A.V. Ramaswamy, Synthesis and characterization of crystalline, tin-silicate molecular sieves with MFI structure, *J. Chem. Soc., Chem. Commun.* (1994) 1933-1934. <https://doi.org/10.1039/C39940001933>
- [330] N.K. Mal, A.V. Ramaswamy, Oxidation of ethylbenzene over Ti-, V- and Sn-containing silicalites with MFI structure, *Appl. Catal. A* 143 (1996) 75-85. [https://doi.org/10.1016/0926-860X\(96\)00071-3](https://doi.org/10.1016/0926-860X(96)00071-3)
- [331] N.K. Mal, A.V. Ramaswamy, Synthesis and catalytic properties of large-pore Sn- β and Al-free Sn- β molecular sieves, *Chem. Commun.* (1997) 425-426. <https://doi.org/10.1039/A607038H>
- [332] M. Renz, T. Blasco, A. Corma, V. Fornés, R. Jensen, L. Nemeth, Selective and Shape-Selective Baeyer–Villiger Oxidations of Aromatic Aldehydes and Cyclic Ketones with Sn-Beta Zeolites and H₂O₂, *Chem. Eur. J.* 8 (2002) 4708-4717. [https://doi.org/10.1002/1521-3765\(20021018\)8:20<4708::AID-CHEM4708>3.0.CO;2-U](https://doi.org/10.1002/1521-3765(20021018)8:20<4708::AID-CHEM4708>3.0.CO;2-U)
- [333] R. van Grieken, C. Martos, M. Sánchez-Sánchez, D.P.Serrano, J.A.Melero, J. Iglesias, A.G.Cubero, Synthesis of Sn–silicalite from hydrothermal conversion of SiO₂–SnO₂ xerogels, *Micropor. Mesopor. Mater.* 19 (2009) 176-185. <https://doi.org/10.1016/j.micromeso.2008.10.020>
- [334] S. Tolborg, A. Katerinopoulou, D.D. Falcone, I. Sádaba, C.M. Osmundsen, R.J. Davis, E. Taarning, P. Fristrup, M.S. Holm, Incorporation of tin affects crystallization, morphology, and crystal composition of Sn-Beta, *J. Mater. Chem. A* 2 (2014) 20252-20262. <https://doi.org/10.1039/C4TA05119J>
- [335] Z. Zhu, H. Xu, J. Jiang, Y. Guan, P. Wu, Sn-Beta zeolite hydrothermally synthesized via interzeolite transformation as efficient Lewis acid catalyst, *J. Catal.* 352 (2017) 1-12. <https://doi.org/10.1016/j.jcat.2017.04.031>
- [336] E. Yuan, W. Dai, G. Wu, N. Guan, M. Hunger, L. Li, Facile synthesis of Sn-containing MFI zeolites as versatile solid acid catalysts, *Micropor. Mesopor. Mater.* 270 (2018) 265-273. <https://doi.org/10.1016/j.micromeso.2018.05.032>
- [337] A. Parulkar, R. Joshi, N. Deshpande, N.A. Brunelli, Synthesis and catalytic testing of Lewis acidic nano-MFI zeolites for the epoxide ring opening reaction with alcohol, *Appl. Catal. A* 566 (2018) 25-32. <https://doi.org/10.1016/j.apcata.2018.08.018>

- [338] A. Parulkar, A.P. Spanos, N. Deshpande, N.A. Brunelli, Synthesis and catalytic testing of Lewis acidic nano zeolite Beta for epoxide ring opening with alcohols, *Appl. Catal. A* 577 (2019) 28-34. <https://doi.org/10.1016/j.apcata.2019.03.009>
- [339] F. Cheng, Z. Zhou, J. Qin, D. Li, J. Wang, W. Wu, Framework-substituted Sn-MOR zeolite prepared by multiple pH-adjusting co-hydrolysis as efficient catalyst for tert-butylation of toluene, *Rus. J. Phys. Chem. A* 92 (2018) 2640-2646. <https://doi.org/10.1134/S0036024418130095>
- [340] J.W. Harris, W.-C. Liao, J.R. Di Iorio, A.M. Henry, T.-C. Ong, A. Comas-Vives, C. Copéret, R. Gounder, Molecular structure and confining environment of Sn sites in single-site chabazite zeolites, *Chem. Mater.* 29 (2017) 8824-8837. <https://doi.org/10.1021/acs.chemmater.7b03209>
- [341] T. Iida, A. Takagaki, S. Kohara, T. Okubo, T. Wakihara, Sn-Beta zeolite catalysts with high Sn contents prepared from Sn-Si mixed oxide composites, *ChemNanoMat* 1 (2015) 155-158. <https://doi.org/10.1002/cnma.201500038>
- [342] N. Garcia Vargas, S. Stevenson, D.F. Shantz, Synthesis and characterization of tin(IV) MFI: Sodium inhibits the synthesis of phase pure materials, *Micropor. Mesopor. Mater.* 152 (2012) 37-49. <https://doi.org/10.1016/j.micromeso.2011.11.036>
- [343] P. Li, G. Liu, H. Wu, Y. Liu, J. Jiang, P. Wu, Postsynthesis and selective oxidation properties of nanosized Sn-beta zeolite, *J. Phys. Chem. C* 115 (2011) 3663-3670. <https://doi.org/10.1021/jp1076966>
- [344] Z. Zhu, H. Xu, J. Jiang, Y. Guan, P. Wu, Sn-Beta zeolite derived from a precursor synthesized via an organotemplate-free route as efficient Lewis acid catalyst, *Appl. Catal. A* 556 (2018) 52-63. <https://doi.org/10.1016/j.apcata.2018.02.017>
- [345] N.O. Popovych, P.I. Kyriienko, Y. Millot, L. Valentin, . Gurgul, R.P. Socha, J. Żukrowski, S.O. Soloviev, S. Dzwigaj, Sn-BEA zeolites prepared by two-step postsynthesis method: Physicochemical properties and catalytic activity in processes based on MPV reduction, *Micropor. Mesopor. Mater.* 268 (2018) 178-188. <https://doi.org/10.1016/j.micromeso.2018.04.026>
- [346] C. Hammond, S. Conrad, I. Hermans, Simple and scalable preparation of highly active Lewis acidic Sn-β, *Angew. Chem. Int. Ed.* 51 (2012) 11736-11739. <https://doi.org/10.1002/anie.201206193>
- [347] J. Iglesias, J. Moreno, G. Morales, J.A. Melero, P. Juárez, M. López-Granados, Rafael Mariscal, I. Martínez-Salazar, Sn-Al-USY for the valorization of glucose to methyl lactate: switching from hydrolytic to retro-aldol activity by alkaline ion exchange, *Green Chem.* 21 (2019) 5876-5885. <https://doi.org/10.1039/C9GC02609F>
- [348] S.G. Elliot, S. Tolborg, R. Madsen, E. Taarning, S. Meier, Effects of alkali and counter ions in Sn-Beta catalyzed carbohydrate conversion, *ChemSusChem* 11 (2018) 1198-1203. <https://doi.org/10.1002/cssc.201702413>
- [349] Q. Guo, F. Fan, E.A. Pidko, W.N.P. van der Graaff, Z. Feng, C. Li, E.J.M. Hensen, Highly active and recyclable Sn-MWW zeolite catalyst for sugar conversion to methyl lactate and lactic acid, *ChemSusChem* 6 (2013) 1352-1356. <http://dx.doi.org/10.1002/cssc.201300160>
- [350] M. S. Holm, S. Saravanamurugan, E. Taarning, Conversion of sugars to lactic acid derivatives using heterogeneous zeotype catalysts, *Science* 328 (2010) 602-605. <https://doi.org/10.1126/science.1183990>
- [351] G.M. Lari, P.Y. Dapsens, D. Scholz, S. Mitchell, C. Mondelli, J. Pérez-Ramírez, Deactivation mechanisms of tin-zeolites in biomass conversions, *Green Chem.* 18 (2016) 1249–1260, <https://doi.org/10.1039/C5GC02147B>.
- [352] W.N.P. van der Graaff, C.H.L. Tempelman, F.C. Hendriks, J. Ruiz-Martinez, S. Bals, B.M. Weckhuysen, E.A. Pidko, E.J.M. Hensen, Deactivation of Sn-Beta during

- carbohydrate conversion, *App. Catal. A* 564 (2018) 113-122.
<https://doi.org/10.1016/j.apcata.2018.07.023>
- [353] A. Corma, V. Fornes, S.B. Pergher, T.L.M. Maesen, J.G. Buglass, Delaminated zeolite precursors as selective acidic catalysts, *Nature* 396 (1998) 353-356.
<https://doi.org/10.1038/24592>